DISSERTATION

Flood Susceptibility Modeling in the uMhlatuzana River Catchment using Computer Vision-Based Deep Learning Techniques

Student:
Jonas CHIRINDZA (1900596)

Supervisor(s):
Prof. Ritesh AJOODHA
Prof. Jasper KNIGHT

UNIVERSITY OF THE WITWATERSRAND, JOHANNESBURG

submitted to
the Faculty of Science, in fulfilment of the requirements for the degree of Master of Science in Computer Sciences

in the

Explainable AI Lab
School of Computer Science and Applied Mathematics

October 29, 2024

Declaration of Authorship

I, Jonas Chirindza (1900596), declare that this dissertation titled, “Flood Susceptibility Modeling in the uMhlatuzana River Catchment using Computer Vision-Based Deep Learning Techniques” represents my own work. All sources of information and contributions from others have been appropriately acknowledged and referenced. This dissertation has not been previously submitted for any degree or examination at any other institution. I understand that unauthorized use of another’s work or the submission of work without proper acknowledgment will be treated as plagiarism. This declaration is a true representation of my academic efforts and adherence to ethical standards in research.

Signed:

Date: **October 29, 2024**

Abstract

In this study, covolutional neural networks (CNN) models are employed for flood susceptibility modeling in the uMhalatuzana River catchment in KwaZulu-Natal, South Africa. The CNN models, including 1D-CNN, 2D-CNN, and 3D-CNN, pro- vide a detailed assessment of flood vulnerability in the region. The models use di- verse spatial information, such as topography, land use, and hydrological features, to estimate the likelihood of flooding in different areas of the catchment. The flood susceptibility maps within the uMhalatuzana River catchment, classified into five risk zones namely, 'very low', 'low', 'moderate', 'high' and 'very high' susceptibility zone, serve as proactive instruments for risk mitigation and disaster management.

The 1D-CNN model displays strong overall performance in flood susceptibility modeling, evident in key metrics such as accuracy, precision, recall, area under curve (AUC) score, and F1-score. The results suggest that the model effectively captures patterns in the input data, emphasizing its potential for flood susceptibility modeling. Moreover, the 2D-CNN model outperforms the 1D-CNN, achieving higher values when evaluated using various performance metrics. Finally, the 3D-CNN model outperformed both the 1D-CNN and 2D-CNN, emphasizing its predictive abilities in flood susceptibility modelling.

The flood susceptibility maps produced by the 1D-CNN model, shows that most of the study area exhibits very low flood susceptibility (96.4%), with localized ar- eas of higher susceptibility, particularly in the very high-risk category (2.53%). The 2D-CNN model demonstrates a more diverse risk distribution, with a substantial portion having very low susceptibility (74.19%) and significant areas of higher risk, notably in the very high-risk category (10.93%). The 3D-CNN model emphasizes a spatial pattern where a large portion has very low susceptibility (84.10%), but with a concentration of high and very high-risk areas, comprising 12.34% of the total area. Finally, the consistent identification of higher risk susceptibility areas enhances the robustness of the assessments.

The models' high accuracy and detailed risk assessments provide valuable tools for decision-makers, urban planners, and emergency response teams in the uMhalatuzana River catchment. The precision of the models facilitates informed strate- gies for flood risk management, including targeted interventions such as improved drainage systems and early warning systems.

Acknowledgements

I stand at the culmination of an arduous yet immensely rewarding journey, and I am profoundly grateful for the support and guidance that have shaped this endeavor.

I would like to extend my deepest appreciation to my esteemed supervisors, Professor Ritesh Ajoodha and Professor Jasper Knight. Your wisdom, encouragement, and unwavering commitment to excellence have been the bedrock upon which this dissertation stands. Your mentorship has not only enriched my academic understanding but has also inspired me to reach for new heights.

To God, the source of all strength and inspiration, I offer my heartfelt gratitude. In moments of doubt and challenge, your grace has been my guiding light. Your presence has been felt in the quiet hours of research, the moments of breakthrough, and the joy of accomplishment. I am profoundly thankful for the unwavering faith that sustained me throughout this journey.

I am also indebted to my family and friends whose support has been a constant source of strength. Your understanding, patience, and encouragement have made this academic pursuit not only possible but also meaningful.

To my fellow researchers and colleagues who shared this intellectual voyage, thank you for the camaraderie, discussions, and the collective pursuit of knowledge. The exchange of ideas has been instrumental in shaping the depth and breadth of this work.

This dissertation is a testament to the collaborative spirit that exists within the academic community, and I am honored to be a part of it. Everyone mentioned here has played a unique role in the tapestry of this research, and for that, I am eternally grateful.

To my beloved parents, who may not be here in body but remain forever in my heart. Your enduring love and wisdom have been my guiding light throughout this journey. Though you cannot witness this moment firsthand, your legacy lives on in every word penned.

"1 Corinthians 13:7 - Love bears all things, believes all things, hopes all things, endures all things."

Contents

List of Figures

List of Tables

Chapter 1

Introduction

Floods are an often-occurring weather event that affects a large number of people worldwide. According to the definition by Bankoff and Lee [1986], flooding happens when water overflows into dry areas usually caused by various weather phenomena like heavy rainfall. The destructive impact of floods is due to various factors. Firstly, the speed and force with which floodwaters move can cause damage to infrastructure and communities. Moreover, once the floodwaters recede from an area they leave behind a layer of mud and debris which adds to the damage and makes recovery efforts more challenging [Doswell *et al.* 1996].

Over the years flooding has caused damage worldwide. It has led to loss of lives, economic setbacks, degradation of agricultural land and damage to residential buildings [Douben 2006]. As shown in Figure 1, South Africa has also faced its share of flooding with more than 120 catastrophic events occurring between 1959 and 2019 [Busayo *et al.* 2022]. Most of these floods took place in KwaZulu-Natal and Gauteng provinces resulting in loss of lives, destruction of livelihoods and extensive property damage. Additionally, Brown *et al.* [2017] emphasized that the vulnerability and risks posed by flooding are likely to remain as a threat, despite the mitigation efforts, risk reduction measures, development initiatives and the implementation of strategies aimed at reducing poverty caused by flood disasters.

Figure 1: KwaZulu-Natal flood disaster [Makhaya 2022].

Flood risk estimation has always relied on physical models such as hydrological, hydraulic, and GIS based [Zhao and Hendon 2009]. These models can accurately predict the likelihood of flooding. However, implementing these models requires knowledge of the geology, topography, morphology and hydrology specific to the study area [Al-Sabhan *et al.* 2003]. Consequently, their development is time consuming and expensive due to lack of spatial data. Despite advancements in resources, these models still have limitations in their ability to accurately simulate flooding and provide reliable quantitative data, for risk assessment and resilience management.

Flooding in South Africa is a problem with significant impact on the environment, economy and society [Busayo *et al.* 2022]. This study aims to tackle this issue by exploring the potential of a cutting-edge deep learning model called a convolutional neural network (CNN) as an alternative method for predicting floods. The use of CNNs as proposed in this study offers an innovative approach to flood modeling. This deep learning model has shown exceptional results in addressing environmental challenges [Nikoobakht *et al.* 2022; Fang *et al.* 2020]. Consequently, applying CNNs to predict floods can potentially provide a robust and data driven approach for assessing and forecasting flood events, in South Africa.

Accurately predicting floods plays an important role in assessing and mitigating flood risks. Using machine learning is an effective approach to enhance flood vulnerability prediction, resulting in improved accuracy [Furquim *et al.* 2016]. Effective use of machine learning can pave the way for the development of flood warning and prediction systems. These systems have the potential to offer insights and information about areas prone to flooding especially during heavy rainfall or stormy conditions. Having timely and accurate forecasts is crucial as it enables proactive measures to be taken in response.

The benefits of using machine learning for predicting floods go beyond response to disasters. It can also assist communities in flood areas and stakeholders involved in land planning to make well informed decisions that proactively reduce the impact of flooding. This improves safety and resilience and contributes to sustainable land use planning ensuring that flood vulnerable regions are utilized in ways that minimize the risk and consequences of flooding. Furthermore, machine learning techniques show potential in improving the ability to predict and mitigate floods ultimately enhancing community resilience and promoting sustainable land management practices.

To achieve the purpose of this research, the following research questions are explored:

1. What are the critical predictors of flood vulnerability among the topographical, geological, morphological, and hydrological factors within the uMhlatuzana River catchment?
2. How accurate, robust, and reliable is the proposed convolutional neural network (CNN) modeling process in predicting flood vulnerability?

Prioritizing the creation of accurate and efficient flood susceptibility models is essential. Such models contribute significantly to mitigating flood impacts and bolstering the resilience of communities and infrastructure in flood-prone areas [Mosavi *et al.* 2018a]. This study focuses on leveraging convolutional neural networks (CNNs) for flood susceptibility modeling and prediction. Moreover, it emphasizes the significance of incorporating morphological, geological, topographical, and hydrological indicators within the uMhlatuzana River catchment area to enhance the precision of flood prediction models.

The above aim(s) of this research are guided by the following objectives:

- To identify the key predictors of flood vulnerability using frequency ratio (FR) and information gain ratio (IGR).
- To generate flood vulnerability maps for the uMhlatuzana River catchment using the proposed CNN models.

By addressing these objectives, this study is expected to make the following contributions:

- Developing models that can be integrated into real-time monitoring systems, offering timely alerts and practical insights for regions susceptible to flooding.
- Developing methodologies to quantify the uncertainties associated with flood susceptibility models.
- Adding to the existing knowledge about using machine learning in flood susceptibility modeling in the context of South Africa.
- Highlighting the importance and effectiveness of deep learning techniques in enhancing flood prediction and risk management, which aligns with the global need to build resilience against climate related issues.

This dissertation is structured as follows: Chapter 2 presents relevant literature that served as the foundation for the selection of flood prediction models and flood conditioning factors in this study. Chapter 3 outlines the research methodology used to model flood vulnerability in the uMhlatuzana River catchment. Chapter 4 presents the experimental results of this study. Chapter 5 provides a discussion of the experimental results obtained in this study. Finally, Chapter 6 concludes with remarks on the study's conclusions, research limitations, and future research directions.

Chapter 2

Related Work

This chapter discusses the existing literature on flood modelling approaches and applications.

2.1 Methodological Framework

This study has adopted the methodological framework employed in previous studies that have used different machine learning models in flood assessment and predictive modeling [Yamazaki *et al.* 2011; Sharif *et al.* 2014; Tehrany *et al.* 2015; Huang *et al.* 2019; Fang *et al.* 2021; Zhou *et al.* 2021]. The methodological framework employs machine learning and deep learning techniques to integrate meteorological, geological, hydrological, and topographical variables, thereby enhancing the accuracy and reliability of flood prediction models. It leverages advanced techniques to process and integrate diverse data sources, emphasizing the importance of input data selection, data preprocessing, and feature engineering to optimize the use of meteorological, geological, hydrological, and topographical variables in flood prediction modeling.

The framework emphasizes the critical role of the selection and integration of diverse data sources, including meteorological data such as rainfall; geological data including soil and lithology types; hydrological such as topographic wetness index (TWI); and topographical data such as elevation, slope, and land cover. For instance, Yamazaki *et al.* [2011] emphasized the significance of physically based descriptions of floodplain inundation dynamics in a global river routing model, highlighting the relevance of hydrological and topographical data for flood prediction modeling.

The integration of machine learning and deep learning models presents an avenue for enhanced flood prediction accuracy. Machine learning and deep learning techniques have been increasingly explored to capture and predict flooding processes, reducing the burden on physical modeling and enabling rapid and accurate flood prediction [Tehrany *et al.* 2013; Mojaddadi *et al.* 2017; Mosavi *et al.* 2018a; Bui *et al.* 2019; Islam *et al.* 2021]. These models have been found to be effective in capturing the complex relationships between meteorological, geological, hydrological, and topographical variables, thus enhancing the accuracy of flood prediction.

The methodological framework provides a comprehensive understanding of the multifaceted factors influencing flood prediction models. It establishes the foundation for the subsequent studies, methodologies, and critical evaluations of existing flood prediction models. The integration of meteorological, geological, hydrological, and topographical elements with machine learning and deep learning techniques creates a robust framework for advancing flood prediction capabilities.

2.2 Flood Dynamics and Impact

The impacts of floods are multifaceted and have significant implications for various aspects of human life and the environment. Floods can have effects on human health, traffic flows, public risk perception, property values, agriculture, and infrastructure [Du *et al.* 2010; Douben 2006; Evans *et al.* 2020]. Du *et al.* [2010] revealed that floods can have effects on human health, such as illnesses, disabilities, mental health problems and diseases linked to poverty. Evans *et al.* [2020], further emphasize the disruptive effects of flooding on traffic flows, revealing that as the severity of flooding increases, the disruption and impacts on traffic flows also increase, and that these effects are expected to be worse due to climate change.

Floods have been proven to cause loss of life every year and damage the economy and environment [Douben 2006]. This emphasizes the importance of mapping flood hazards and planning for disasters [Ullah and Zhang 2020]. Understanding relationships between the intensity of a flood event and the corresponding level of vulnerability is essential for evaluating the effects of flood hazards and risks on the population [Nederhoff *et al.* 2023]. Direct and indirect impacts of floods have been identified, where direct impacts occur due to contact, with the floodwaters while indirect impacts results from socio-economic disruptions [Ur Tariq *et al.* 2020].

The effects of flooding on agriculture can vary depending on how crops or land use activities can handle water as well as the frequency, duration, depth and timing of the event [Pourali *et al.* 2016]. Understanding the factors that influence floodplain managers' perceptions and decision-making provides insights into the complexities of managing flood risks within communities [Tyler *et al.* 2021]. It has been observed that flood disasters have impacts on cities highlighting the need for risk assessment and disaster planning [Shi *et al.* 2019]. The value of having information about flood risks is important in developing plans that enhance urban flood resilience [Afriyanie *et al.* 2022].

Floods have negative effects on the public causing both tangible and intangible damages [Chaerani *et al.* 2020]. This emphasizes the importance of having flood protection plans in place. The uncertainty surrounding flood coverage and its impact on decision-making when it comes to implementing flood prevention measures has been highlighted by presenting the effect of the uncertainty derived from the lack of data on the estimation of peak discharge, based upon which the flooded areas are identified [Yannopoulos *et al.* 2015]. This emphasizes the difficulties faced in areas where there is inadequate data about water levels in river basins.

2.3 Data Sources in Flood Susceptibility Modeling

Flood susceptibility modeling is a crucial aspect of flood risk assessment and management, involving the use of various data sources and analytical techniques to predict floods. The selection of data sources is important in ensuring the accuracy and reliability of the flood susceptibility models. Several studies [Tehrany *et al.* 2013; Mojaddadi *et al.* 2017; Chapi *et al.* 2017; Chowdhuri *et al.* 2020; Islam *et al.* 2021] have emphasized the importance of different data sources that can be used in flood susceptibility modeling. These data sources include past flood events and influencing factors such as distance from rivers, aspect, elevation, slope, rainfall, topographic wetness index, curvature, sediment transport index, vegetation cover, land use patterns, stream intensity, topographic ruggedness index, soil, land use, and lithology.

These data sources are crucial for flood susceptibility modeling as they provide valuable information about various factors that influence the likelihood and severity of flooding in a particular area [Lee *et al.* 2017; Pham *et al.* 2020]. The significance of collecting and using data sources for flood susceptibility mapping has been further highlighted by Lee *et al.* [2017], emphasizing that the incorporation of these data sources into flood susceptibility models can allow a comprehensive and multidimensional analysis, improving the accuracy and reliability of predictions.

The unique characteristics of each study area drive the choice of flood factors. What proves significant in one locale may have little impact in another. For instance, the flow of water from high-elevated to low-elevated areas can significantly affect flood dynamics. In high-elevated regions, the reduced rate of water infiltration con- tributes to flooding in low-lying areas [Tehrany *et al.* 2013]. As technology advances, the integration of these factors into spatial databases becomes increasingly essential for effective flood prediction and risk management strategies.

2.4 Integrated Approaches in Flood Susceptibility Modeling

2.4.1 Hydrological and Hydraulic Models

Historically, flood susceptibility modeling has utilized conventional methods such as hydrological and hydraulic models [Nunes Correia *et al.* 1998; Ramírez *et al.* 2000]. While hydrological and hydraulic models are essential for flood susceptibility modeling, they have limitations. One of the primary constraints is the lack of spatial data, especially in data-sparse areas [Sözer *et al.* 2018]. Moreover, the complexity and heterogeneity of natural hydrological processes pose challenges in accurately representing them through models [Feng and Beighley 2020].

Furthermore, basins with hydrological modifications also present challenges in modeling, particularly when there is limited data about basin characteristics [Jouma and Dadaser-Celik 2021]. The reason behind this challenge lies in the availability of historical records pertaining to hydrological modifications. This scarcity prevents the representation of the original baseline conditions prior to these modifications taking place thereby impeding the calibration and validation processes of hydrological models.

The spatial and temporal scales of application are critical considerations in hydrological and hydraulic models for flood modeling due to the inherent complexity of hydrological processes and the varying spatial patterns of flood events [Harter *et al.* 2004]. Hydrological models, such as the soil and water management system (SWAT) or the hydrological modeling system (HEC-HMS), operate at watershed scales, simulating the movement of water over large areas to capture the integrated response of the entire basin [Wood *et al.* 2011; Fanta and Sime 2022]. To accurately represent surface runoff and river flow these models rely on information about topography, land use and soil properties.

On the other hand, hydraulic models, like the flood modelling system (FMS) or river analysis system (RAS), operate at finer spatial scales, focusing on localized river channels and urban areas to simulate the intricacies of flow dynamics and inundation patterns [Verzano 2009; Wang *et al.* 2018a]. Additionally, balancing spatial and temporal scales of application is crucial for capturing both the large-scale watershed interactions and the detailed local features, ensuring a comprehensive understanding of flood susceptibility and facilitating effective flood risk management strategies.

2.4.2 Remote Sensing and GIS Integration

Remote sensing and GIS integration has become a crucial approach in flood susceptibility modeling and has has been considered by various studies [Brivio *et al.* 2002; Dano *et al.* 2019; Munawar *et al.* 2022]. These studies have demonstrated that the integration of remote sensing and GIS techniques is effective in assessing flood hazard impacts on urban areas, infrastructure, and agricultural areas, as well as in evaluating flood vulnerability and predicting flood-prone areas. Furthermore, the combination of remote sensing and GIS has been utilized to analyze and provide results on flood vulnerability required for prompt and effective decision-making on floods [Olatunji *et al.* 2023].

Remote sensing data and GIS tools play important roles in flood susceptibility modeling, offering several important advantages [Roy and Sarker 2016; Psomiadis *et al.* 2021]. Remote sensing provides detailed and up-to-date information about land cover, topography, and hydrological features through satellite imagery and LiDAR data [Wedajo 2017; Munawar *et al.* 2022]. This data enables the extraction of precise parameters relevant to flood modeling, enhancing the accuracy of susceptibility assessments. GIS tools serve as a powerful platform for organizing, analyzing, and visualizing spatial data. They facilitate the integration of diverse datasets, allowing the incorporation of information about land use changes, river networks, and elevation into comprehensive flood models [Samela *et al.* 2018; Psomiadis *et al.* 2021].

The integration of remote sensing and hydrological modeling has been identified as a practical and quick approach to predict flash flood hazards in arid regions where data are scarce [Mashaly and Ghoneim 2018]. Arid regions often face challenges related to sparse and irregularly distributed ground-based data, making traditional methods less effective. Remote sensing technologies, such as satellite imagery and aerial sensors, provide a timely and comprehensive source of critical information on land cover, topography, and precipitation patterns. Moreover, the use of remote sensing and GIS has been instrumental in monitoring flash flood impacts, mapping destroyed vegetation cover, and evaluating the impact of flash flood hazards on specific regions, aiding decision-makers in planning protective measures to avoid potential flooding [Sadek *et al.* 2020].

In conclusion, the integration of remote sensing and GIS has proven to be a valuable and effective approach in flood susceptibility modeling. The combination of these technologies has facilitated flood susceptibility assessment, mapping, and monitoring, aiding in decision-making processes and contributing to the overall understanding of flood occurrences and impacts.

2.4.3 Machine Learning Approaches

The use of machine learning methods in flood susceptibility mapping has been widely recognized due to their ability to effectively analyze complex spatial data and provide accurate predictions [Phong 2023]. These methods have been applied in various regions, such as the Tafresh watershed in Iran [Janizadeh *et al.* 2019], Seoul metropolitan city in Korea [Lee *et al.* 2017], and Que Son District in Vietnam [Phong 2023]. The success of machine learning models in flood susceptibility mapping has been attributed to their ability to consider multiple factors such as topography, geology, soil, land use, and hydrological data [Lee *et al.* 2017].

The application of machine learning in flood susceptibility modeling extends to the integration of remote sensing datasets, where machine learning methods have been developed to enhance the accuracy of flood susceptibility predictions [Samanta *et al.* 2018; Liu *et al.* 2021]. Additionally, the use of state-of-the-art machine learning models has become essential for detecting flood-prone zones, with studies employing multiple machine learning models such as random forest, support vector machine, multilayer perceptron, and artificial neural network for flash flood susceptibility modeling [Band *et al.* 2020; Chen *et al.* 2023]. These state-of-the-art machine learning models have become invaluable for flood prediction due to their ability to discern complex patterns within large and diverse spatial datasets [Chen *et al.* 2023], such as digital elevations models, hydrological data, soil properties, satellite imagery, rainfall data, and land use/land cover data.

The potential of machine learning for hydrologic sciences has been recognized, with its successful application in various hydrologic applications, either in stand-alone mode or integrated with process-based modeling [Xu and Liang 2021]. Physics- informed machine learning approaches are also being explored for their application to hydrologic problems, offering a promising avenue for further research and development in flood susceptibility modeling [Maxwell and Condon 2021]. The scalability of machine learning models facilitates their application in various geographic regions and the incorporation of real-time data, ensuring adaptability to changing environmental conditions [Nevo *et al.* 2022].

2.4.4 Hybrid Models and Ensemble Approaches

Flood susceptibility modeling is a critical aspect of disaster risk management, and the use of hybrid models and ensemble approaches has gained significant attention in recent years [Islam *et al.* 2021; Bui *et al.* 2019; Band *et al.* 2020; Nguyen 2022]. These approaches involve integrating various techniques, such as machine learning algorithms, geographic information systems, and remote sensing data, to enhance the accuracy and reliability of flood susceptibility mapping.

Wang *et al.* [2018b] investigated the use of a hybrid technique integrating multi-criteria decision analysis and geographic information systems for flood susceptibility mapping in Shangyou, China. The study demonstrated the potential of hybrid models in enhancing the accuracy of flood susceptibility assessments by achieving an area under the curve (AUC) of 0.988, indicating that that these hybrid models have higher discriminative power and precision in distinguishing between flood and non-flood classes. Additionally, Islam *et al.* [2021] presented two hybrid ensemble machine learning techniques, namely dagging and random subspace, and compared them to baseline models for flood prediction, such as support vector machine (SVM) and artificial neural network (ANN). However, dagging has shown to be superior to the baseline models when evaluated under the receiver operator characteristics (ROC) curve. As shown in Table 1, dagging and random subspace have achieved AUC score of 0.87 and 0.85, respectively when evaluated using a ROC curve performance metric.

Furthermore, Bui *et al.* [2019] proposed an ensemble machine learning model for flood susceptibility modeling, namely, Bagging, Logiboost, and AdaBoost. These models were combined with the fuzzy rule induction algorithm (FURIA) and genetic algorithms (GA) and evaluated using three statistical criteria for model evaluation: sensitivity, specificity, and accuracy. FURIA-GA bagging produced superior results, achieving an accuracy of 0.93, specificity of 0.90, and sensitivity of 0.97 for flood prediction, indicating the effectiveness of novel machine learning ensemble methods in mapping flash flood susceptibility, and suggesting the potential for improved accuracy and reliability in flood susceptibility assessments.

Moreover, Liu *et al.* [2021] emphasized the higher AUC values of hybrid models in flash flood susceptibility assessment, indicating the superior performance of ensemble modeling in this context. Similarly, Nguyen [2022] established hybrid models based on artificial neural networks, random forest, and logistic regression for flood susceptibility mapping, achieving a maximum AUC value of 0.93. These findings emphasize the potential of hybrid models in enhancing the accuracy of flood susceptibility assessments. Additionally, Pandey *et al.* [2021] applied machine learning ensemble models for flood susceptibility zonation mapping, demonstrating the effectiveness of ensemble approaches in capturing the complex dynamics of flood susceptibility in subtropical humid low-relief alluvial plain environments.

In conclusion, the literature demonstrates the growing significance of hybrid models and ensemble approaches in flood susceptibility modeling. These approaches offer enhanced accuracy, cost-effectiveness, and the ability to capture complex relationships among flood predictors. The integration of diverse modeling techniques, including machine learning algorithms, remote sensing data, and GIS, has shown promising results in improving the accuracy, reliability, and precision of flood susceptibility assessments.

2.4.5 Deep Learning Applications

The integration of deep learning algorithms, such as deep belief networks (DBN), recurrent neural networks (RNN), deep neural networks (DNN), and convolutional neural networks (CNN), has demonstrated potential in flood susceptibility modeling, offering high learning flexibility and the ability to detect complex features hidden in the data [Mia *et al.* 2023; Liu *et al.* 2021; Bui *et al.* 2020ba; Kabir *et al.* 2020; Wang *et al.* 2020b]. CNNs excel in spatial feature extraction, making them effective in analyzing satellite imagery, topographic maps, and other geospatial data to identify vulnerable areas [Wang *et al.* 2020a]. On the other hand, RNNs are well-suited for capturing temporal dependencies in hydrological and climate data [Cai and Yu 2022]. Additionally, DNNs have proven to be a transformative approach, leveraging their capacity to learn intricate relationships within diverse datasets [Mia *et al.* 2023]. Moreover, DBNs, with their ability to model hierarchical dependencies, are also valuable in uncovering hidden patterns within intricate environmental variables [Shahabi *et al.* 2020].

Table 1: Table Showing different studies in flood susceptibility modelling using machine learning, hybrid, and deep learning approaches. AUC represents area under Receiver operator characteristic curve score.

Author	Data/Features Indicators	Models/Methods	Results
Tehrany *et al.* [2013]	Topography, geology, morphology and hydrology.	Decision tree (DT), Frequency ratio (FR) and Linear regression (LR).	AUC: FR-LR = 0.906, DT =0.87.
Mojaddadi *et al.* [2017]	Topography, geology, morphology and hydrology.	FR and SVM.	FR-SVM (Accuracy=0.85)
Chapi *et al.* [2017]	Topography, geology, morphology and hydrology.	Logistic model tree (LMT), Bagging and LR.	Bagging-LMT (accuracy = 0.955, AUC= 0.98), LMT (accuracy = 0.909, AUC = 0.974)
Bui *et al.* [2019]	Topography, geology, morphology and hydrology.	Fuzzy rule induced algorithm (FURIA), Genetic Algorithm (GA), Logit-Boost, Bagging and AdaBoost.	Sensitivity = Bagging (0.9672), Specificity = FURIA-GA Bagging (0.8857), Accuracy = FURIA-GA Bagging (0.9387).
Bui *et al.* [2020a]	Topography, geology, morphology and hydrology.	Deep Learning Neural Network (DLNN).	AUC=0.96, F1-Score=0.922, Sensitivity=0.915, specificity=0.933.
Chowdhuri *et al.* [2020]	Topography, geology, morphology and hydrology.	Evidence belief function	AUC: EBF = 0.852
Islam *et al.* [2021]	Topography, geology, morphology and hydrology.	Support vector Machine (SVM), Artificial neural network (ANN), Random Sub-space (RS), Random Forest (RF), and Dragging.	AUC: Dagging model = 0.87, RF = 0.86, RS = 0.85, SVM = 0.84, and ANN = 0.83.
Fang *et al.* [2021]	Topography, geology, morphology and hydrology.	Long short-term memory (LSTM) neural network.	AUC = 0.958, Accuracy = 0.924, Sensitivity = 0.976, specificity = 0.882).
Mia *et al.* [2023]	Topography, geology, morphology and hydrology.	Deep Learning Neural Network (DLNN).	AUC = 0.917, F1-Score = 0.87, Sensitivity = 0.87, specificity = 0.88).

In flood susceptibility modeling, the use of deep learning algorithms has been compared with other machine learning algorithms, such as support vector machines (SVM), logistic regression (LR), and random forest (RF) [Chen *et al.* 2023]. The comparison revealed the effectiveness of deep learning models, particularly in capturing and predicting flooding processes, thus highlighting their superiority in flood susceptibility analysis. Additionally, the integration of deep learning with other methods, such as the analytic hierarchy process (AHP), has been proposed to develop holistic flood risk assessment maps, indicating the potential for combining deep learning with traditional analytical methods for comprehensive flood risk analysis [Bui *et al.* 2022].

The use of deep learning methods has been instrumental in enhancing the robustness and reliability of flood risk assessment models. Studies have highlighted the superior performance of deep learning algorithms, such as alternating decision trees (ADT) and advanced iterative classifier optimizers (ICOs), in flash flood susceptibility mapping, emphasizing their capability to generate more accurate predictions compared to conventional machine learning approaches [Chen *et al.* 2023; Thanh Ngo *et al.* 2023]. Furthermore, the integration of remote sensing data and geographic information systems (GIS) with deep learning techniques has enabled the development of hybrid models, showcasing the potential for comprehensive flash flood susceptibility assessment and mapping [Costache *et al.* 2021].

2.5 Summary and Synthesis of Literature Review

The literature on flood susceptibility modeling reveals a comprehensive exploration of various methodologies, including hydrological and hydraulic models, remote sensing and GIS integration, machine learning approaches, hybrid models, and deep learning applications. These studies emphasize the importance of integrating diverse data sources such as meteorological, geological, hydrological, and topographical variables to enhance the accuracy and reliability of flood prediction models. Traditional hydrological and hydraulic models, while essential, face limitations due to the lack of spatial data and the complexity of natural hydrological processes.

The integration of remote sensing and GIS technologies provides detailed and up-to-date information, significantly enhancing the accuracy of flood susceptibility assessments. Machine learning models have proven effective in analyzing complex spatial data, offering accurate flood susceptibility predictions, while hybrid models and ensemble approaches improve the accuracy and reliability of flood susceptibility mapping. Deep learning algorithms, such as convolutional neural networks (CNNs) and recurrent neural networks (RNNs), show superior performance in capturing and predicting flooding processes.

The shift toward machine-learning techniques is motivated by their ability to capture the nonlinearity and linearity of basins without requiring an in-depth understanding of their physical functions. These models offer advantages in terms of implementation ease, lower computational costs, faster processing, and reduced complexity compared to traditional physical models [Mosavi *et al.* 2018b].

Despite these advancements, several gaps remain in the current flood susceptibility modeling approaches. Data scarcity, particularly in many regions, hinders the accuracy of traditional hydrological and hydraulic models. Accurately representing the heterogeneity of natural hydrological processes remains challenging, and there is a need for more effective integration of diverse data sources to improve model accuracy. Ensuring models are scalable and adaptable to different geographic regions and changing environmental conditions is crucial, as is incorporating real-time data into flood prediction models for timely and effective flood management. These gaps justify the adoption of advanced machine learning and deep learning techniques in this study.

By integrating meteorological, geological, hydrological, and topographical data, the study aims to develop a robust and reliable flood prediction model. The use of CNNs aligns with the broader trend of leveraging deep learning techniques to enhance predictive accuracy and robustness, addressing the limitations of traditional models and improving flood risk management strategies.

Chapter 3

Research Methodology

The research framework is depicted in Figure 2, illustrating the key components and workflow of the study. The process begins with the collection and processing of spatial data, followed by a training-test split. The training set undergoes a k-fold cross-validation process, enhancing the model's robustness. Concurrently, the Bayesian optimization algorithm is employed to fine-tune the model parameters, ensuring optimal performance. Once the model is trained and optimized, it undergoes rigorous evaluation to assess its accuracy, precision, and recall. This evaluation is essential for gauging the model's reliability and generalizability. Finally, the well-trained model is applied to produce flood susceptibility maps.

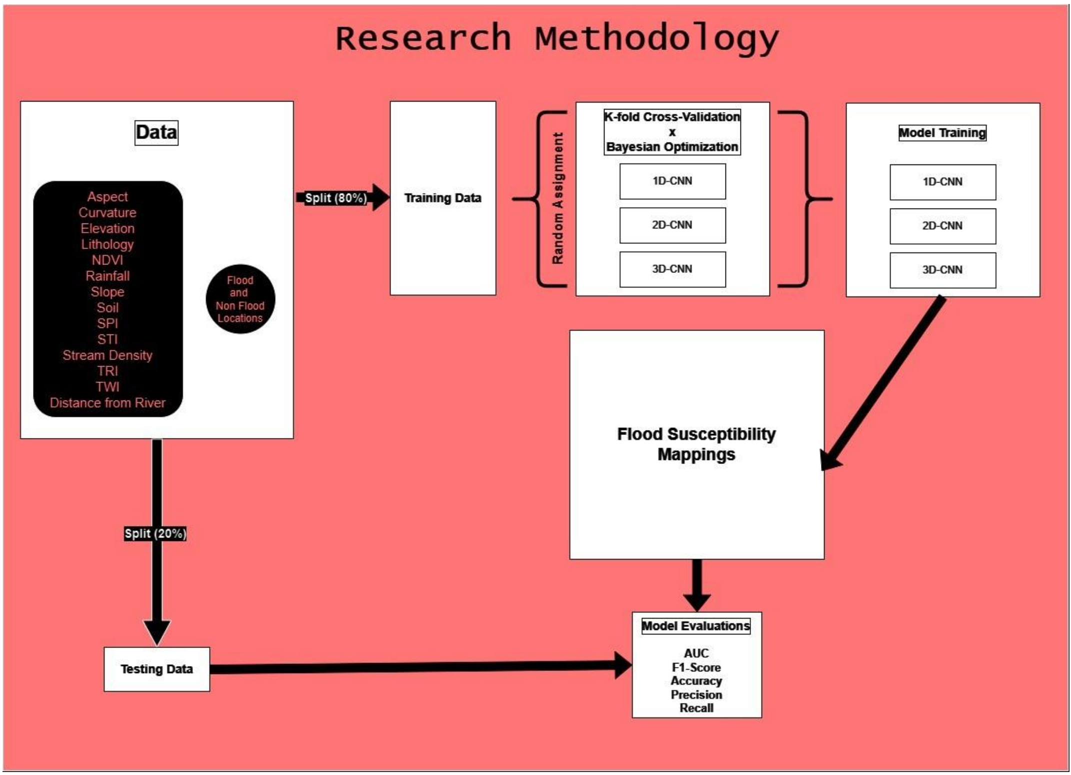

Figure 2: Methodological workflow scheme used in this study. The dataset features are described in detail in Table 2.

3.1 Study Area

The quaternary catchment considered in this study is in the Umgeni Drainage Area in KwaZulu-Natal Province, South Africa namely the uMhlatuzana River catch- ment as shown in Figure 3. According to the Department of Water and Sanitation data, the uMhlatuzana River catchment covers the entire Durban Central City, spanning over three towns. The uMhlatuzana Catchment Area covers an area of 272 km^2 and consists of two major rivers, namely, the uMhlatuzana and Umbilo rivers, with lengths of 51.5 km and 33.42 km, respectively. These rivers run throughout elevations varying from 653 m to 3 m asl, and they confluence at the uMhlatuzana River canal, draining into the Indian Ocean.

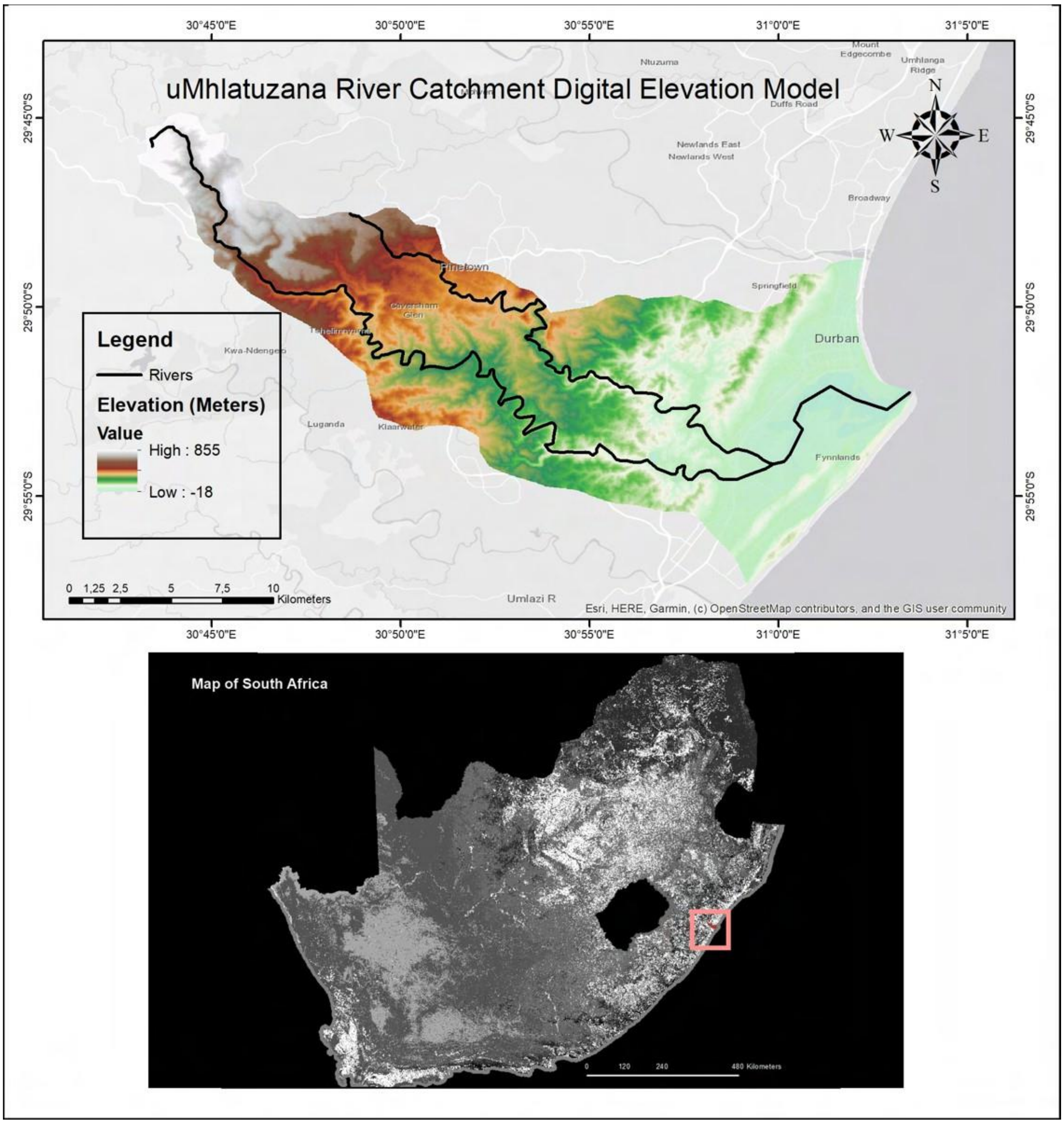

Figure 3: Location Map of study area [USGS 2014].

The average annual rainfall in the catchment area varies between 1500 mm and 800 mm [Cole *et al.* 2018]. The study area has four soil types, with leptosols covering most of the area, and geologically it consists of two lithological groups, namely sand- stone and gneiss. The study area's hydro-geomorphological characteristics, such as basin area and length, were obtained from the Department of Water and Sanitation's

(DWS) website. The river basin slope is calculated using GIS Spatial Analyst tools. Floods are most common in this catchment area, and during the rainy season and heavy storms, the situation is the worst in terms of flooding. World Weather Attribution, as outlined in their report [WWA 2022], states that due to climate change, severe and extreme weather conditions are becoming more frequent and severe in the study area.

3.1.1 Study Area Significance and Motivation

The uMhlatuzana River catchment is a crucial point of interest for flood susceptibility modeling because of its heightened vulnerability to multiple flood triggers, including storm surges, high tides, and heavy precipitation [Busayo *et al.* 2022]. Proximity to the coast introduces unique challenges, such as tidal influences, elevation changes, and storm-driven surges, necessitating a focused modeling approach [Adeyeri *et al.* 2017]. Understanding and accurately predicting flood susceptibility in this catchment area is essential for effective disaster management, infrastructure planning, and resilience building, particularly in the context of increasing climate- related risks and extreme weather events.

3.1.2 History of Flooding in the Study Area

One of the most destructive recent floods in the study area occurred during a subtropical depression that occurred from April 11th to April 12th, 2022. This event caused flash flooding across the study area and surrounding catchments, resulting in the tragic loss of 435 lives, as well as the destruction of livelihoods, leaving thousands homeless. The flood also incurred more than 10 billion Rands in infrastructure damage, as reported by Sivakumar and Fazel-Rastgar [2023].

3.2 Data Preparation and Sources

In this section, a high-level overview of the data used to model flood susceptibility in the uMhlatuzana River catchment is presented. The data extraction and collection methods, as well as the selection of 15 flood conditioning factors, are detailed in Table 2. The choice of these factors is informed by their recognized significance in the context of previous flood susceptibility modeling studies [Tehrany *et al.* 2013; Chapi *et al.* 2017; Mojaddadi *et al.* 2017; Chowdhuri *et al.* 2020; Ali *et al.* 2020]. To effectively analyze flood vulnerability, the preparation of a spatial database is important, considering the unique characteristics of the region of interest.

3.2.1 Digital Elevation Model (DEM) derived Factors

The Digital Elevation Model (DEM) used in this study representing the terrain surface for the uMhlatuzana River catchment is obtained from the EarthExplorer website [Bolstad and Stowe 1994]. The DEM is constructed using shuttle radar topography mission (SRTM) data, offering a cell of 30 m × 30 m spatial resolution and $1^{\circ} \times 1^{\circ}$ tiles. Various factors, such as stream intensity, slope, sediment transport index (STI), topographic ruggedness index (TRI), curvature, stream power index (SPI), elevation, topographic wetness index (TWI), and aspect slope, can be calculated and derived using this DEM through their respective equations on the ArcGIS tool.

Stream intensity is important in flood predictions, indicating the flow magnitude of rivers, proximity to rivers and distribution of watercourses. Higher stream intensity

Table 2: Table showing data sources for this study.

Feature	**Scale/Resolution**	**Data Sources**	**Date of Dataset**
Elevation	30 m	Shuttle Radar Topographic Mission DEM https://www.usgs.gov/	23 Sep, 2014
Curvature	30 m	SRTM DEM derived	23 Sep, 2014
Slope	30 m	SRTM DEM derived	23 Sep, 2014
Aspect Slope	30 m	SRTM DEM derived	23 Sep, 2014
Stream Intensity	30 m	SRTM DEM derived	23 Sep, 2014
Stream Power Index	30 m	SRTM DEM derived	23 Sep, 2014
Sediment Transport Index	30 m	SRTM DEM derived	23 Sep, 2014
Terrain Ruggedness Index	30 m	SRTM DEM derived	23 Sep, 2014
Topographic Wetness Index	30 m	SRTM DEM derived	23 Sep, 2014
Normalized Difference Vegetation Index	30 m	Landsat 8 data https://www.usgs.gov/	2014
Land Use/Land Cover	20 m	SA National Land-Cover Datasets https://egis.environment.gov.za/sa_national_land_cover_datasets	Jan - Dec 2014
Soil Type	1:1 million	South African Soil and Terrain Database https://data.isric.org/	1 Oct, 2008
Lithology	1:1 million	South African Soil and Terrain Database https://data.isric.org/	1 Oct, 2008
Distance from the river	30 m	SRTM DEM Derived plus River Data available on https://www.dws.gov.za/iwqs/gis_data/	23 Sep, 2014
Rainfall	30 m	Center for Hydrological and Remote Sensing (CHRS) https://chrsdata.eng.uci.edu/	2000-present

suggests a more interconnected network influencing flood patterns. This factor helps identify water pathways, confluence points, and contributes to the severity of flooding events. Integrating stream intensity into models improves accuracy, providing a comprehensive understanding of how river networks influence flood susceptibility. For this study, stream intensity is derived using DEM and river data obtained from the Department of Water and Sanitation website (https://www.dws.gov.za/iwqs/wms/data/000key2data.asp, by dividing the flow accumulation by the length of rivers in the study area, providing a measure of stream concentration using ArcGIS tool).

Slope is a crucial factor in flood prediction studies [Chapi *et al.* 2017] and has significant implications on an area's hydrology, influencing runoff speed. A steeper slope reduces water infiltration, leading to increased runoff and potential flooding in low- lying areas. Elevation is another critical consideration, as water typically flows from higher to lower elevations, making high-lying areas less prone to flooding [Botzen *et al.* 2013]. Aspect slope is influential due to its effects on water flow direction, impacting hydrological patterns in the area [Kadavi *et al.* 2018]. Additionally, curvature, categorized as concave, convex, or flat, serves as a flood conditioning factor by influencing infiltration capacity and surface runoff [Bui *et al.* 2019; Chapi *et al.* 2017].

The topographic wetness index (TWI) and stream power index (SPI) are two important hydrology-related factors that evaluate the geographical diversity of flood-prone regions. They are derived using the following equations [Moore and Wilson 1992; Duman *et al.* 2005]:

$$TWI = \ln \frac{A_s}{\tan \beta}, \tag{1}$$

and

$$SPI = A_s \tan \beta, \tag{2}$$

where, β represents the local slope gradient, and A_s is the specific catchment area in m^2/m^{-1}. The SPI represents the erosive strength of water discharge, while the TWI estimates where water will accumulate in areas with elevation differences [Mojad- dadi *et al.* 2017]. TWI significantly influences runoff generation and water discharge accumulations in the study area [Beven *et al.* 1984].

Another critical factor, the terrain roughness index (TRI), is widely used in flood susceptibility modeling due to its ability to capture terrain diversity, identify flow paths, and enhance model accuracy. High TRI values indicate uneven landscapes, influencing water flow and accumulation patterns during floods. Including TRI improves the model's ability to simulate complex interactions, providing a more realistic assessment of flood susceptibility in diverse terrains. It is derived using the following formula:

$$TRI = \frac{mean - min}{max - min}, \tag{3}$$

where this expression illustrates the difference in elevation between neighboring cells. The sediment transport index (STI) represents the erosion and deposition processes occurring in the river catchment and can be derived using the following equation [De Roo 1998]:

$$STI = (m + 1) \frac{A_s}{22.13}^{m} \sin \frac{\beta}{0.0896}^{n}, \tag{4}$$

where A_s is the specific catchment area.

3.2.2 NDVI

The normalized difference vegetation index (NDVI) is a crucial factor in flood prediction [Ali *et al.* 2020; Chowdhuri *et al.* 2020]. It aids in assessing vegetation cover and density in a given area. Areas with limited vegetation are more susceptible to flooding due to lacking the capabilities of reducing water flow velocity and erosivity [Ali *et al.* 2020]. NDVI is computed using the following equation:

$$NDVI = \frac{NIR - RED}{NIR + RED}, \tag{5}$$

where NIR represents the near-infrared band, and RED represents the red band. The near-infrared (NIR) and red bands are used for NDVI computation because NIR is sensitive to chlorophyll content, and healthy vegetation reflects more NIR while absorbing red. This distinction helps assess vegetation health and distinguish it from non-vegetated surfaces. The NIR and Red bands are less affected by atmospheric conditions, ensuring the reliability of NDVI calculations across different sensors and platforms. Their combined use provides a concise and consistent measure of vegetation health for various applications, including flood susceptibility predictions. For this study, the NDVI is calculated using the annual near-infrared and red bands for the year 2014 obtained from Landsat 8 satellite images assembled by the United States geological survey (USGS) EROS Data Center.

3.2.3 LULC

Land use and land cover (LULC) is a crucial factor in flood susceptibility modeling studies and has a significant impact on flood occurrences [Chowdhuri *et al.* 2020]. LULC involves classifying human activities and natural landscape elements over time. Flooding is directly influenced by LULC because it affects surface runoff and sediment movement, which, in turn, can lead to flooding [Islam *et al.* 2021]. LULC regulates the balance between runoff and infiltration, making areas that hinder water infiltration, such as urban areas, more susceptible to flooding.

For this study, the LULC data of the study area for the year 2014 is obtained from the publicly available SA National land-Cover datasets on the Department of Forestry, Fishery, and Environment website (https://egis.environment.gov.za/sa_national_ land_cover_datasets). The LULC classes, extracted using the ArcGIS tool based on study area polygon shapefiles from the SA National Land-Cover datasets, include indigenous forest, dense bush, natural woodland, planted forest, grassland, water bodies, wetlands, barren land, cultivated land, mines, residential, industrial, commercial, and smallholdings.

3.2.4 Lithology and Soil type

Lithology and soil type profoundly influence flooding dynamics. The infiltration capacity, permeability, and porosity of the terrain, determined by these factors, dictate how water interacts with the landscape [Islam *et al.* 2021]. Impermeable lithological features, such as dense rock formations can inhibit water infiltration, leading to increased surface runoff during heavy rainfall. In contrast, permeable lithologies like fractured rocks, facilitate greater infiltration, reducing runoff and potentially lowering flood risks. Sandy soils, for instance, promote rapid infiltration, thereby reducing surface runoff, while impermeable surfaces can amplify runoff, increasing the risk of flooding. Additionally, lithological and soil characteristics impact erosion potential and play an important role in land use planning. Incorporating this information into flood predictions enhances the accuracy of vulnerability assessments, providing valuable insights into the varied behaviors of water across diverse terrains. For the current study, lithology and soil data are obtained from the publicly available South African soil and terrain database, accessible on the ISRIC datahub website (https://data.isric.org).

3.2.5 Distance from the river

Distance from the river signifies the proximity of streams within the drainage system of a region [Mojaddadi *et al.* 2017]. This proximity is significant as the river network serves as the primary pathway for flood discharge and expansion. Flood-affected areas are typically found near the river due to this natural drainage pattern. Therefore, determining the distance to the river is important for identifying flood-vulnerable areas, especially as streams can alter slope stability through erosion.

For this study, the distance from the river map is derived from the DEM and 4th order river layers obtained from the Department of Water and Sanitation website (https://www.dws.gov.za/iwqs/wms/data/000key2data.asp) using the ArcGIS software. The buffer around the river in the study area is created using the Buffer tool, then the elevations values within the buffer are extracted by the mask. As a result, the Near tool is used to calculate the distance from each point in the buffer to the nearest point on the river.

3.2.6 Rainfall

Rainfall is important in flood susceptibility modeling as it directly influences flooding initiation and severity [Bracken *et al.* 2008]. This study focuses on annual rainfall data, with the idea that floods are frequently associated with substantial rainfall. In the context of flood prediction modeling, the choice of annual rainfall is important for a comprehensive assessment of flood susceptibility. Annual rainfall captures the cumulative impact of precipitation, encompassing prolonged periods of heightened rainfall crucial for flooding events. This approach recognizes variable rainfall patterns, ensuring a significant understanding of long-term trends and hydrological responses [Arnaud *et al.* 2002; Tsegaw *et al.* 2020].

The annual rainfall data is sourced from the PERSIANN-Cloud Classification System (https://chrsdata.eng.uci.edu), a system developed by the Center for Hydrometeorology and Remote Sensing (CHRS) to estimate rainfall rates based on remote sensing data. For this study the annual rainfall data of the study area for the year 2014 is considered. The rainfall data is processed using the ArcGIS software and is employed in simulating flooding by integrating it with other flood condition factors during the model training and validation process.

3.2.7 Flood Inundation

Flood inundation, the process by which water overflows its usual boundaries and submerges land, is a complex and dynamic phenomenon with significant implica tions for both natural environments and human settlements [Saksena and Merwade 2015]. A fundamental component of the research methodology is the creation of a comprehensive database compiling historical flood events. This inventory serves as a critical resource for model training and validation [Mojaddadi *et al.* 2017]. One hundred and forty probable flood locations are selected through inundation modeling. Concurrently, an equivalent number of non-flooding locations are chosen with care.

The selection of non-flooding locations is pivotal as it contributes to the creation of dependent binary data for classification. In this binary classification, '1' denotes the presence of flooding, while '0' signifies its absence. This binary dataset forms the foundational basis for the training and testing phases of flood prediction models.

3.3 Jenks Natural Breaks Classification

The Jenks Natural Breaks Classification method, developed by Jenks [1967], is a statistical technique widely employed in thematic mapping and geographic information systems. It optimally classifies data into meaningful groups by minimizing variance within classes and maximizing variance between them. The method iteratively tests class breaks to identify natural groupings, enhancing the interpretability of spatial data. In the context of this study, the Jenks method is used in the ArcGIS tool to classify the spatial data for flood condition factors with continuous values into distinct meaningful classes to ensure that the data is suitable for model training, validation, and testing.

3.4 Convolutional Neural Network (CNN)

The Convolutional Neural Network (CNN) is a sophisticated neural network model specifically designed for processing structured data arrays like images. In this research, CNN is proposed as a method for predicting flood vulnerability in the uMhlatuzana catchment area. The CNN architecture comprises three interconnected layers: input, output, and multiple hidden layers. Among these, the hidden layers consist of convolutional and pooling layers. Convolutional layers play a crucial role in identifying and extracting features from images by iteratively applying convolutional kernels or filters across the entire image [Wang *et al.* 2020a].

Meanwhile, pooling layers serve to reduce the size or dimensionality of the input data. Like convolutional layers, the pooling layer make use of sliding windows to apply a fixed operation to each $(n \times n)$ region of a feature map, but without any weights. Instead, these operations apply an aggregation function to the values within their receptive fields [Chen *et al.* 2016]. The pooling layer typically involves maximum pooling, where the highest pixel value within the receptive field is chosen for the output array, and average pooling, which computes the average value within the receptive field for the output array [Yu *et al.* 2014]. In this study, three distinct CNN architectures are developed to predict the likelihood of flooding and generate susceptibility maps.

3.4.1 1D-CNN, 2D-CNN and 3D-CNN Architecture Structure

The structure of the one-dimensional CNN (1D-CNN) includes an input layer, one convolutional layer, one maximum pooling layer, one fully connected layer, and an output layer. Training of the model is conducted using one-dimensional data, as depicted in Figure 4. For the current scope of this study, the input data is of dimensions

$(f \times 1)$, where f signifies the number of flood factors. Convolutional kernels of size $(c \times 1)$ are employed to filter the input data, resulting in a layer with (m) feature maps. Subsequently, the maximum pooling layer of size $(d \times 1)$ is used to halve the size or dimensionality of the data in the resulting fully connected layer. Fully connected layers serve to rearrange the extracted information. Finally, the output layer comprises (n) neural units, representing the result of the overall network.

The structure of the two-dimensional CNN (2D-CNN) includes an input layer, two convolutional layers, two maximum pooling layers, one fully connected layer, and an output layer. Training of the model is performed using two-dimensional data, as depicted in Figure 4. In the current scope of this study, the input data possesses dimensions of $(f \times f)$, where f denotes the number of flood factors. Convolutional kernels of size $(c \times c)$ are applied to filter the input data, resulting in a layer with M feature maps. Subsequently, the maximum pooling layer of size $(d \times d)$ is employed to reduce the size or dimensionality of the data in the resulting convolutional layer by half. Furthermore, the resulting (m) features are forwarded to the second convolutional layer, which also comprises (m) convolutional kernels of size $(c \times c)$. These resulting (m) features from the second convolutional layer are then processed by a $(d \times 1)$ maximum pooling layer. Fully connected layers are employed to reorganize the extracted information. Finally, the output layer contains (n) neural units, representing the result of the overall network.

The structure of the three-dimensional CNN (3D-CNN) includes input layer, one convolutional layer, one maximum pooling layer, one fully connected layer, and an output layer. In the context of this study, the input data forms a matrix of size $(f \times w \times w)$, where f denotes the number of flood factors and w represents the window size of the image patches. Convolutional kernels of size $(c \times c \times c)$ are employed to filter the input data, resulting in a layer with (m) feature maps. Subsequently, the maximum pooling layer of size $(d \times d \times d)$ is used to reduce the size or dimensionality of the data in the resulting convolutional layer by half. The two fully connected layers serve to reorganize the extracted information. Finally, the output layer comprises (n) neural units, representing the result of the overall network.

3.4.2 Modelling Process of CNN

The pixels of 15 flood factors for all selected flood and non-flood locations in the study area were extracted to produce 1-dimensional vector of size (15×1) as input data for 1D-CNN. The 1-dimensional vector is the represented as binary matrix of (15×15) suitable as the input data for 2D-CNN as shown in Figure 4. Finally, for 3D-CNN the 15 flood factors are stacked to produce a three-dimensional image of size $(15 \times 752 \times 1229)$ with 30 m spatial resolution as shown in Figure 5. The centre pixels and their neighbouring pixels are extracted to produce a three-dimensional image patch using a moving window size of (w). Each image patch sample has a size of $(15 \times w \times w)$ containing all the attributes and spatial data of flood condition elements.

The input data is processed through a series of operations that begin with a high-level feature map and progress through convolutional and pooling operations. A fully connected layer reorganizes and combines the data after each process. Finally, using a nonlinear activation function, the classification results are converted to classification results.

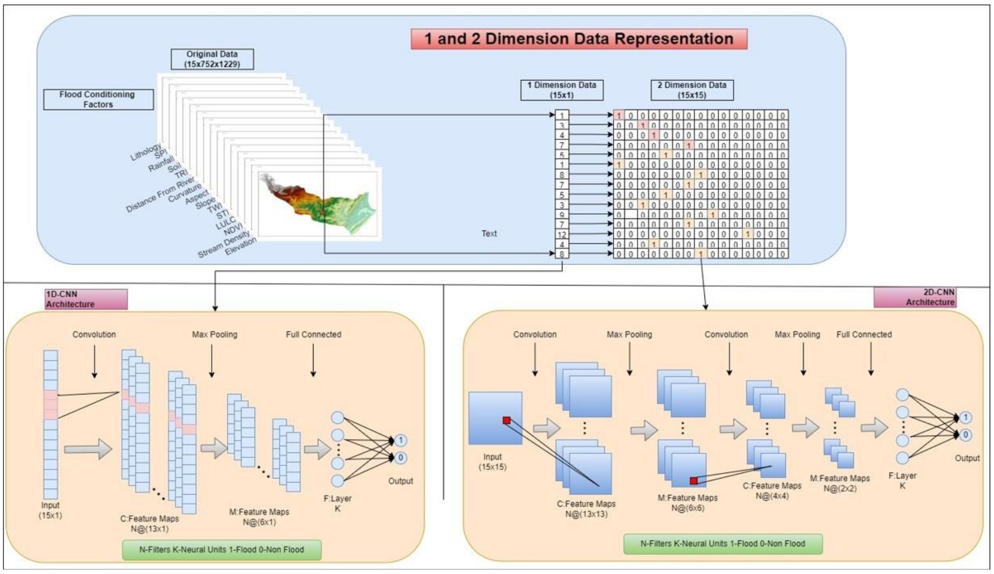

Figure 4: Data Representation and Modelling process of 1D and 2D CNNs

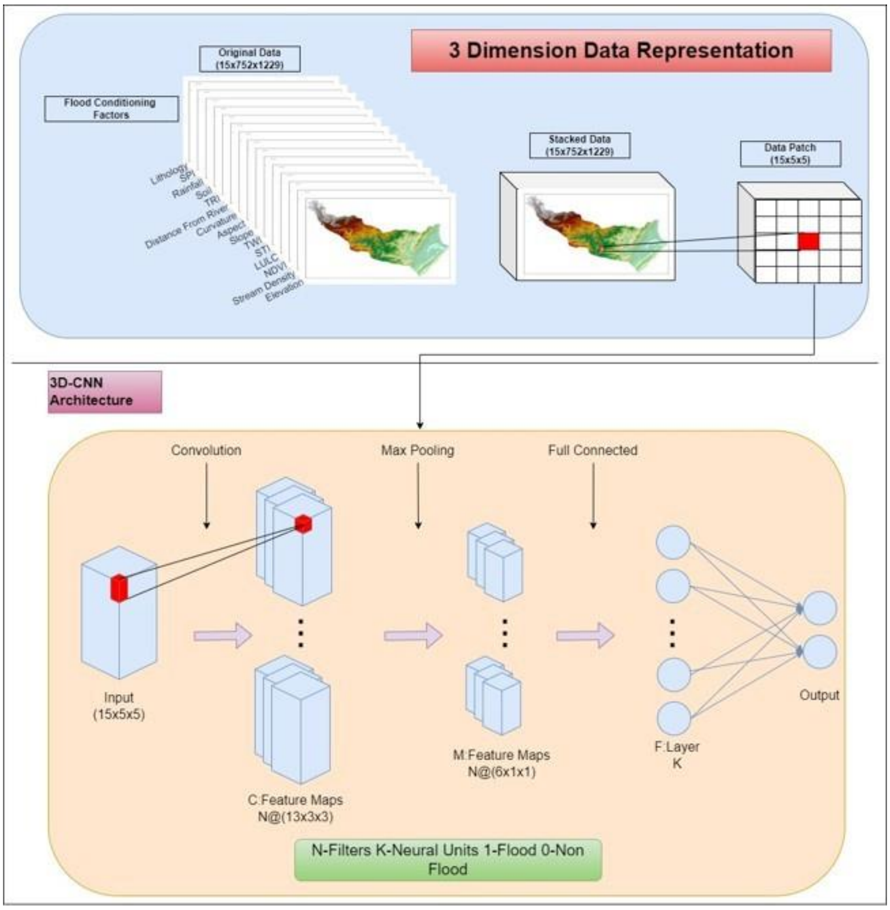

Figure 5: Data Representation and Modelling process of 3D CNN.

3.5 Frequency Ratio and Information Gain Ratio

This section briefly explains frequency ratio (FR) and information gain ration (IGR) methods, which can be used to statistically analyze the relationship between flood events and flood conditioning factors. FR is a statistical method that can be used to determine the impact of flood conditioning factors on historical flood events in the area of interest [Mojaddadi *et al.* 2017]. FR is derived using the following equation:

$$FR = \frac{\left(\frac{N_{pix}(SX_i)}{\sum_{i=1}^{m}(SX_i)}\right)}{\left(\frac{N_{pix}(X_j)}{\sum_{i=1}^{n}N_{pix}(X_j)}\right)}, \tag{6}$$

where the number of flooded pixels in class i of factor X is represented by $N_{pix}(SX_i)$,and the total number of pixels within factor X_j is denoted as $N_{pix}(X_j)$. Here, m represents the number of classes in factor X_i, and n is the total number of flood factors in the study area [Shafapour Tehrany *et al.* 2019]. The FR value < 1 depicts a weak connection, indicating a less discriminatory influence on predicting flooding. [Li *et al.* 2017].

Information Gain Ratio (IGR) has recently gained popularity in flood susceptibility modeling [Khosravi *et al.* 2019; Islam *et al.* 2021; Fang *et al.* 2021], and it is widely used for feature selection. IGR quantifies the significance of the flood conditioning factors and their categories with flooding. Higher IGR ratios are always associated with factors that are of greater importance for prediction models. The expected in- formation is derived using the following equation:

$$H(S) = -\sum_{i=1}^{n} P_i \log_2(P_i), \tag{7}$$

where S is the training set containing n classes, and P_i denotes the likelihood that the sample belongs to class i. The average entropy is calculated using the following equation:

$$E(A) = -\sum_{i=1}^{m} P_i H(S), \tag{8}$$

where A is a factor with m number of splits. The split information value is the possible information that can be attained by separating S into m parts, corresponding to m outcomes on the attribute A and is derived using the following equation:

$$SplitInf_A(S) = -\sum_{i=1}^{m} \frac{S_i}{S} \log_2 \frac{S_i}{S}, \tag{9}$$

where S_i represents the i-th class of the training set. Lastly, the feature importance (FI) value is denoted using the following equation:

$$FI = \frac{H(S) - E(A)}{SplitInf_A(S)}. \tag{10}$$

The FI ranges from 0 to 1, and factors with values closer to 1 are considered to be key predictors of flood susceptibility.

3.6 Bayesian optimization for Hyperparameter Tuning

Bayesian optimization is a powerful technique for hyperparameter tuning in machine learning and optimization tasks. It is particularly useful when the search space for hyperparameters is complex, high-dimensional, or expensive to evaluate. Bayesian optimization uses probabilistic models to predict the performance of different hyperparameter configurations, allowing for efficient exploration of the parameter space and finding optimal configurations with fewer evaluations [Snoek *et al.* 2012].

The optimization procedure is based on the Bayes' theorem [Koch and Koch 1990], which can be denoted using the following equation:

$$P(X|Y) = \frac{P(Y|X)P(X)}{P(Y)}, \tag{11}$$

where X is the input data of the convolutional layer, and its input dimension varies depending on the CNN architecture structure. Y denotes the output of the fully connected layer of the respective CNNs. The Bayes' theorem represents the fundamental concept of Bayesian optimization. The core principle of Bayesian optimization is to combine the prior distribution of the objective function $f(\text{conv}(w_k, X) + b_k)$ with sample information (evidence) to derive the posterior distribution of the function. This posterior information is then used to identify where the objective function $f(\text{conv}(w_k, X) + b_k)$ is maximized, according to a predefined optimization criterion. The term w_k in the objective function represents the convolution kernel weight vector, a 2D-matrix, or a 3D-matrix depending on the dimensions of the CNN in question. The terms b_k and $\text{conv}(w_k, X)$ represent the bias and convolution operator respectively [Li *et al.* 2023].

For this study the bayesian optimization is used to optimize the hyperparameters of all three architectures of the CNNs model ensuring that the models perform at their optimal best. The overview of how Bayesian optimization for hyperparameter tuning for CNNs applications is as follows:

1. Specify the hyperparameters for tuning and their respective ranges.
2. Define the objective function that takes a set of these hyperparameters as input and returns the scalar performance metric. In this study, the objective function is based on CNN models, and the scalar performance metric is the F1 Score.
3. Choose the surrogate model to estimate the objective function's behavior. In this study, the Gaussian Process (GP) is selected as the surrogate model.
4. Randomly choose an initial set of hyperparameter configurations and evaluate their performance using the objective function. These data points are used to initialize the surrogate model.
5. Define the acquisition function, which guides the search by balancing exploration and exploitation. In this study, the acquisition function considered is the Expected Improvement (EI), which has shown superiority over other acquisition functions [Snoek *et al.* 2012].
6. Use the optimization algorithm to maximize the acquisition function and identify the next set of hyperparameters to evaluate in the objective function.

7. Train and evaluate the CNNs model with the selected hyperparameter configuration.
8. Incorporate the new data point (hyperparameter configuration and performance) into the surrogate model to update the model's belief about the objective function.
9. Iteratively repeat steps 5 to 8 for a fixed number of iterations or until a stopping criterion is met.
10. Finally, select the hyperparameter configuration that yields the best performance on the objective function (CNNs model).

3.6.1 Gaussian Process (GP)

A Gaussian process is a fundamental component of Bayesian optimization, serving as the surrogate model that captures the probabilistic relationship between hyperparameters and the objective function. Unlike other models that yield point estimates, a GP characterizes the entire distribution of the function, providing predictions and uncertainty estimates [Ki and Rasmussen 2006]. It represents the function as a collection of correlated Gaussian variables, making it well-suited for modeling complex, non-linear functions.

In Bayesian optimization, the GP is continually updated as new data points, corresponding to different hyperparameter configurations and their associated objective function values, are observed. This sequential learning allows the GP to adapt and refine its estimates, focusing on regions of the search space with the potential for high performance while exploring areas of uncertainty. The GP's predictive mean and variance are employed in calculating acquisition functions, which guide the search for the optimal hyperparameter configuration by balancing exploration and exploitation. By leveraging the rich probabilistic information provided by the GP, Bayesian optimization efficiently navigates high-dimensional search spaces, minimizes the number of objective function evaluations, and ultimately finds optimal hyperparameter configurations for machine learning models and other applications [Snelson and Ghahramani 2006; Rasmussen and Nickisch 2010].

3.6.2 Acquisition Function: Expected Improvement (EI)

The expected improvement (EI) is an important component of Bayesian optimization, expertly navigating the exploration-exploitation trade-off. This acquisition function quantifies the anticipated gain in performance that can be achieved by assessing the objective function at specific points within the search space [Mockus 1998]. EI strikes a balance between exploring regions where the performance of the objective function is uncertain and exploiting areas where high performance is likely. It achieves this by first calculating the improvement over the best-known objective function value and then assessing the probability that the objective function value at a candidate point exceeds the current best [Scott *et al.* 2011].

EI serves as an exploration metric in regions of high uncertainty, where it encourages the algorithm to explore and discover uncharted territory, and as an exploitation metric in areas where performance is expected to be high, albeit with a smaller but positive value. The point with the highest Expected Improvement is selected for evaluation, and this process iteratively refines the surrogate model, leading to more informed decisions and ultimately the discovery of the optimal solution or hyperparameter configuration [Jones *et al.* 1998; Hennig and Schuler 2012]. In summary, EI is a vital tool in Bayesian optimization, facilitating efficient search in complex, high-dimensional spaces, and making it particularly valuable for hyperparameter tuning and optimization tasks with expensive objective function evaluations.

3.7 Data Augmentation

Data augmentation is a commonly employed technique in deep learning, especially in the context of CNNs [Wang *et al.* 2020a]. It enhances model generalization by artificially diversifying the training dataset. By applying transformations like rotations and flips to the original spatial data, data augmentation helps the CNN learn invariant features, reducing overfitting and improving the model's robustness to variations in real-world data. By exposing the model to a wider range of augmented data during training, it can better adapt to different scenarios. In this study, the spatial data for flood condition factors have been transformed through rotation and horizontal and vertical flipping to increase the number of data samples as shown in Figure 6.

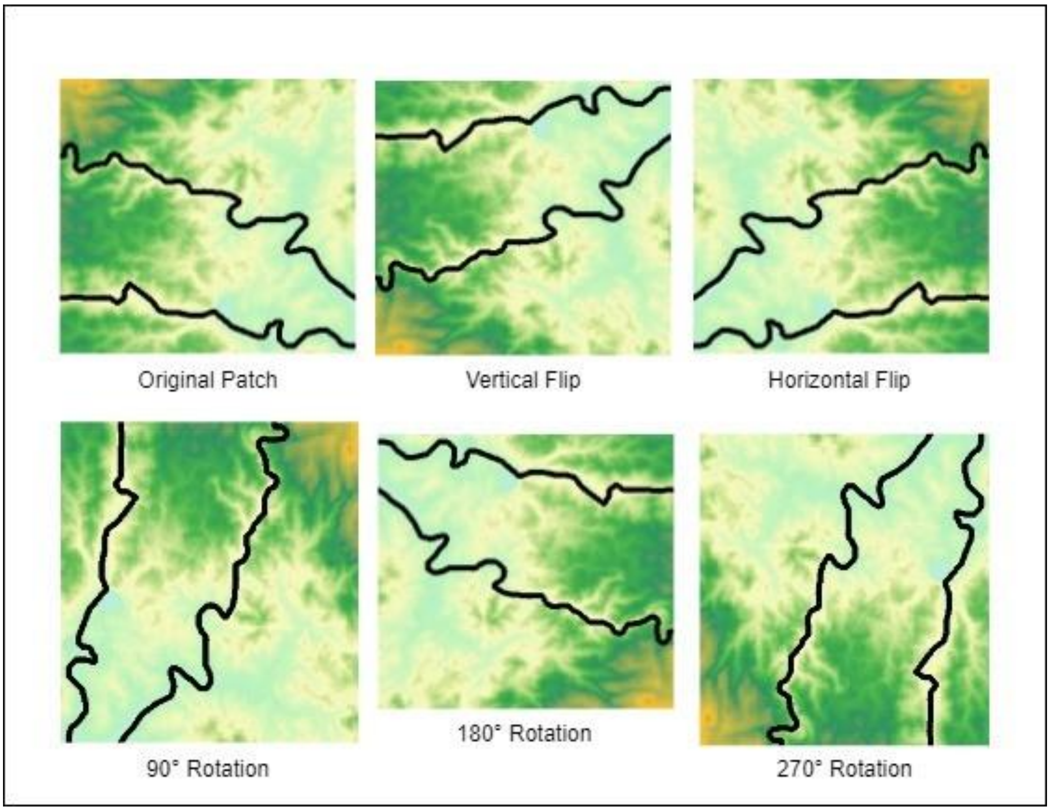

Figure 6: Data Augmentation for 2D-CNN and 3D-CNN data representations.

3.8 Model Evaluation

This section presents various techniques and methods used for evaluating the performance of the proposed CNN models in this study.

3.8.1 K-Fold Cross Validation

K-fold cross-validation is a widely employed technique for evaluating the performance of predictive models [Fushiki 2011; Yadav and Shukla 2016]. In the context of this study, the training set is divided into 10 subsets. Subsequently, all three different architectures of CNN models are trained and validated 10 times, with each iteration using a different fold for validation and the remaining folds for training. This iterative process contributes to ensuring the robustness and generalizability of the models by systematically assessing their performance across diverse segments of the data. The comprehensive evaluation obtained through K-fold cross-validation enhances the reliability and applicability of the CNN models to different dimensions and types of data. This technique is particularly valuable for assessing how well the models generalize to new, unseen data, providing insights into their effectiveness and potential areas for improvement [Anguita *et al.* 2012].

3.8.2 Area under Curve and Statistical Criteria

For this study, the area under curve (AUC) score and statistical criterion for model evaluation, namely accuracy, precision, recall and F1-score, are used to test the model's performance. The evaluation metrics aforementioned are derived as follows:

$$Accuracy = \frac{TP + TN}{TP + TN + FP + FN}, \tag{12}$$

$$Precision = \frac{TP}{TP + FP}, \tag{13}$$

$$Recall = \frac{TP}{TP + FN}, \tag{14}$$

and

$$F1 - Score = \frac{2 \cdot Precision \cdot Recall}{Precision + Recall}, \tag{15}$$

where True Positives (TP) are instances where the model correctly predicted the flood class. True Negatives (TN) are instances where the model correctly predicted the non-flood class. False Positives (FP) are instances where the model incorrectly predicted the flood class, and False Negatives (FN) are instances where the model incorrectly predicted the non-flood class [Mojaddadi *et al.* 2017; Wang *et al.* 2020a; Fang *et al.* 2021]. The precision is a measure of how many of the samples predicted as 'flood' by the model were related to a flood event. Recall measures the model's ability to correctly identify instances related to flood events among all actual flood instances. Finally, the F1-Score is the harmonic mean of precision and recall, providing a balance between making accurate 'flood' predictions and capturing actual 'flood' instances.

3.8.3 Training Test Split

In the research methodology, the choice of an 80:20 training-test split is pivotal for robust model evaluation. Allocating 80% of the dataset to training ensures that the CNNs have an ample amount of data to learn and extract meaningful features. The remaining 20% is reserved for testing, allowing for a rigorous assessment of the model's generalization performance on unseen data. This splits strikes a balance between providing the model with sufficient training instances for effective learning and maintaining a substantial portion for unbiased evaluation.

Moreover, subjecting the 80% training subset to a 10-fold cross-validation further strengthens the evaluation process. This approach systematically evaluates the model performance across various subsets, helping to identify potential overfitting and ensuring that the model generalizes well to diverse data scenarios. The 80:20 split, complemented by 10-fold cross-validation, is integral to establishing a robust flood prediction model that demonstrates high accuracy and reliability when applied to new and unseen data

3.9 Conclusions

The methodology chapter outlines a comprehensive framework for flood susceptibility modeling in the uMhlatuzana River catchment. The process begins with the collection and processing of spatial data, followed by a training-test split and k-fold cross-validation to enhance model robustness. Bayesian optimization is employed to fine-tune model parameters, ensuring optimal performance. The chapter details the use of convolutional neural networks (CNN) in three architectures (1D, 2D, and 3D) to predict flood vulnerability, leveraging diverse data sources such as digital elevation models, land use, lithology, soil type, and rainfall. Data augmentation techniques and rigorous model evaluation methods, including accuracy, precision, recall, and F1-score, are also discussed to ensure the reliability and generalizability of the models.

This chapter significantly contributes to the dissertation by providing a detailed and systematic approach to flood susceptibility modeling, addressing the identified gaps in data integration and model accuracy. The use of advanced machine learning techniques, particularly CNNs, and the incorporation of Bayesian optimization for hyperparameter tuning, represent a novel approach in the field. This methodological framework not only enhances the predictive accuracy of flood models but also offers a scalable and adaptable solution for flood risk management in diverse geographic regions.

Chapter 4

Results

To accomplish the research objectives, a series of experiments were conducted for this study. These objectives comprised i) determining the critical predictors of flood vulnerability using the Frequency Ratio (FR) method, a well-established technique in the domain of geospatial analysis, and ii) developing and applying deep learning models to produce flood susceptibility maps specific to the uMhlatuzana River catchment. This required the utilization of advanced neural network architectures and machine learning algorithms to process and analyze complex geospatial data.

4.1 Frequency Ratio Results

This section presents the analysis of the frequency ratio (FR) of different classes of flood conditioning factors. The FR method is used to gauge the probability of flooding occurring within the region associated with each category of a conditioning factor, providing insights into the relative importance and impact of these factors on flood events.

The frequency ratio (FR) of different classes of flood condition factors is shown in Figure 7 and flood factors are visualized in Figure 8. The frequency ratio (FR) method can gauge the probability of flooding occurring within the region associated with each category of a conditioning factor. The FR score is computed by comparing the flood occurrence percentage to the overall percentage within a given class of each flood conditioning factor [Mojaddadi *et al.* 2017; Tehrany *et al.* 2013]. The soil comprises of four classes, namely Leptosols (LPd), Regosols (RGe), Acrisols (ACh), and Fluvisols (FLe) as shown in Figure 8j. Acrisols and Fluvisols have FR values of
0.59 and 3.83, respectively, while LPd and RGe have FR values of 0, indicating lower chances of flood occurrence for these soil types.

The lithology comprises of two classes: SC2 (sandstone, greywacke, and arkose) and MA2 (gneiss) as shown in Figure 8e. They are associated with FR values of 1.95 and 0, respectively. This indicates that flood events in the study area associated with terrains comprising lithology types classified under SC2. Aspect, representing the direction a slope faces, is categorized into nine classes: Flat, North, Northeast, East, Southeast, South, Southwest, West, and Northwest as shown in Figure 8a. In the study area, Southeast is the most common aspect direction covering 17% of area as shown in Table 3. Additionally, flat terrain stands out with an FR value of 3.83, while other aspect classes exhibit significantly lower FR values in comparison. This indicates that, in the study flood events are mostly associated with flat terrains.

Curvature of the study area comprises of concave, flat, and convex slope as shown in Figure 8b. Concave and Convex shapes are the most dominant slope forms covering 44% and 43% of the study area, respectively as shown in Table 3. The concave and flat slopes have FR values of 1.60 and 1.52, respectively, while the convex slope exhibits a significantly lower FR value. This indicates that the concave and flat forms are more likely to be vulnerable to floods, while the convex is less likely to be vulnerable to floods.

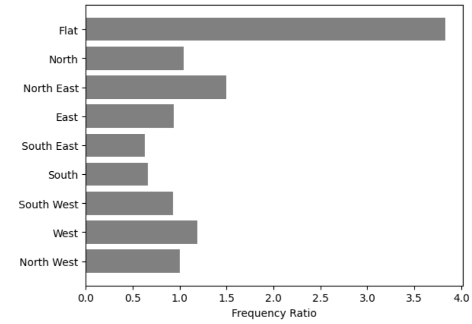

(a) Aspect

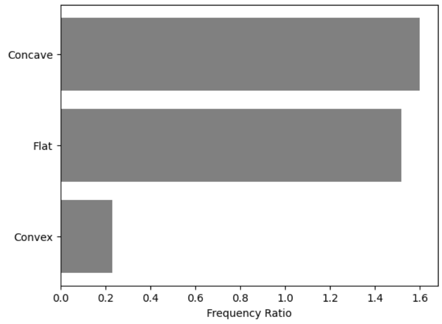

(b) Curvature

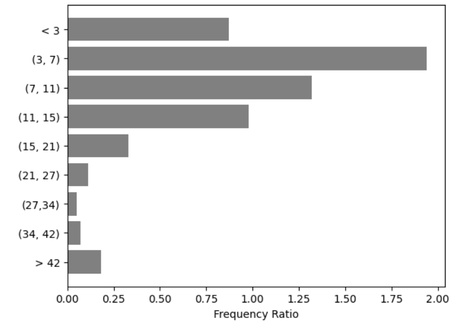

(c) Distance From River

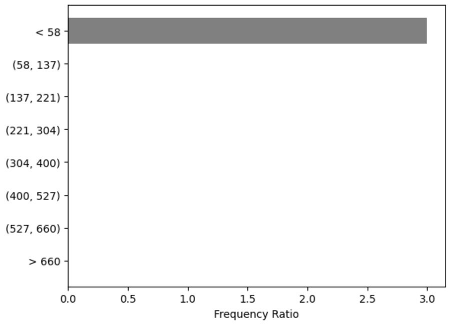

(d) Elevation

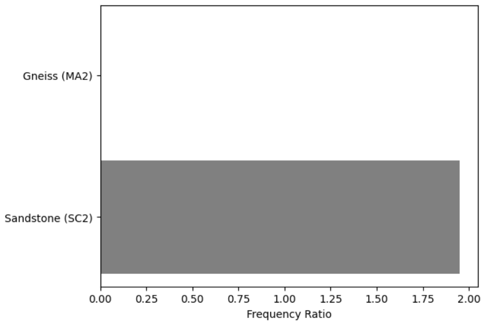

(e) Lithology

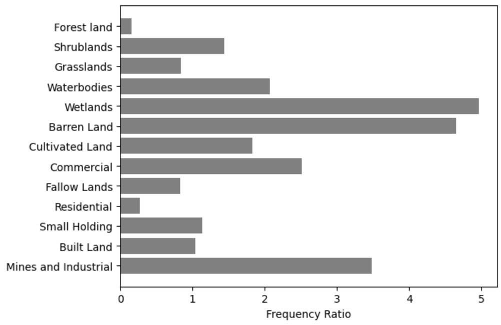

(f) LULC

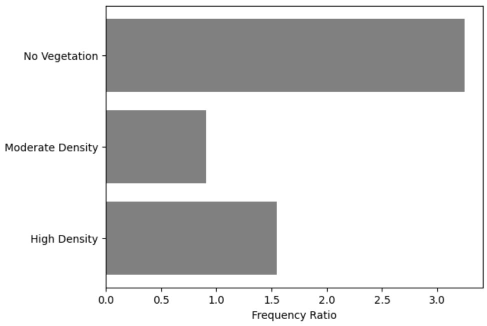

(g) NDVI

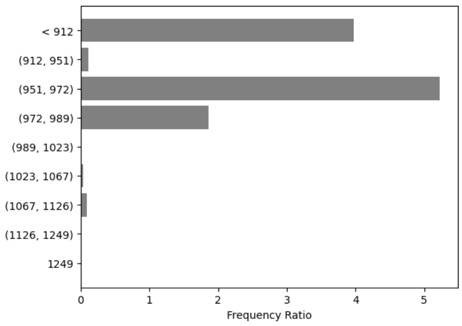

(h) Rainfall

Figure 7: The frequency ratio (FR) is applied to assess the spatial relation between conditioning factors and the likelihood of floods. A greater FR score suggests that the particular category indicates a heightened risk of flooding.

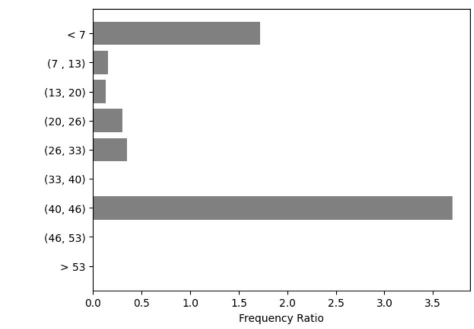

(i) Slope

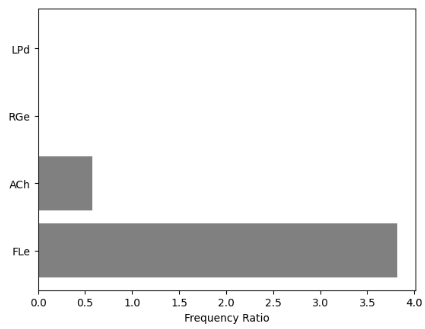

(j) Soil

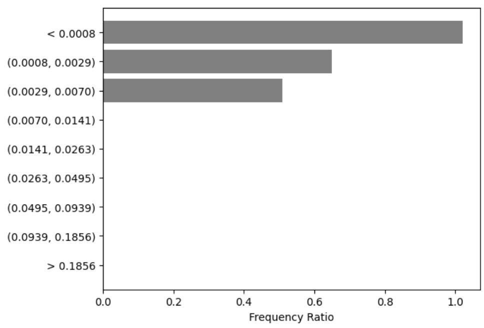

(k) SPI

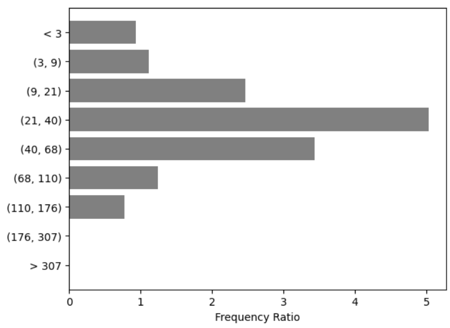

(l) STI

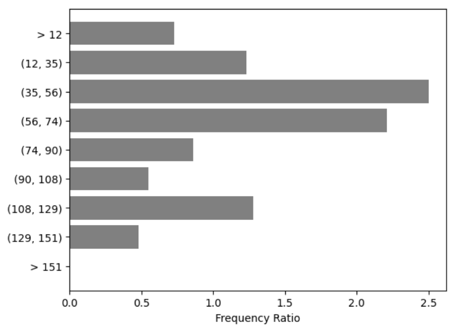

(m) Stream Intensity

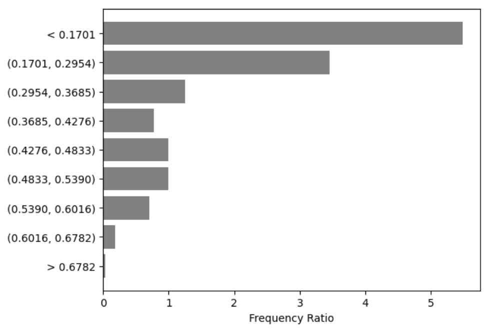

(n) TR

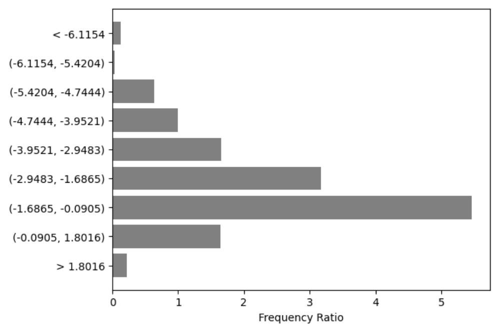

(o) TWI

Figure 7: continued.

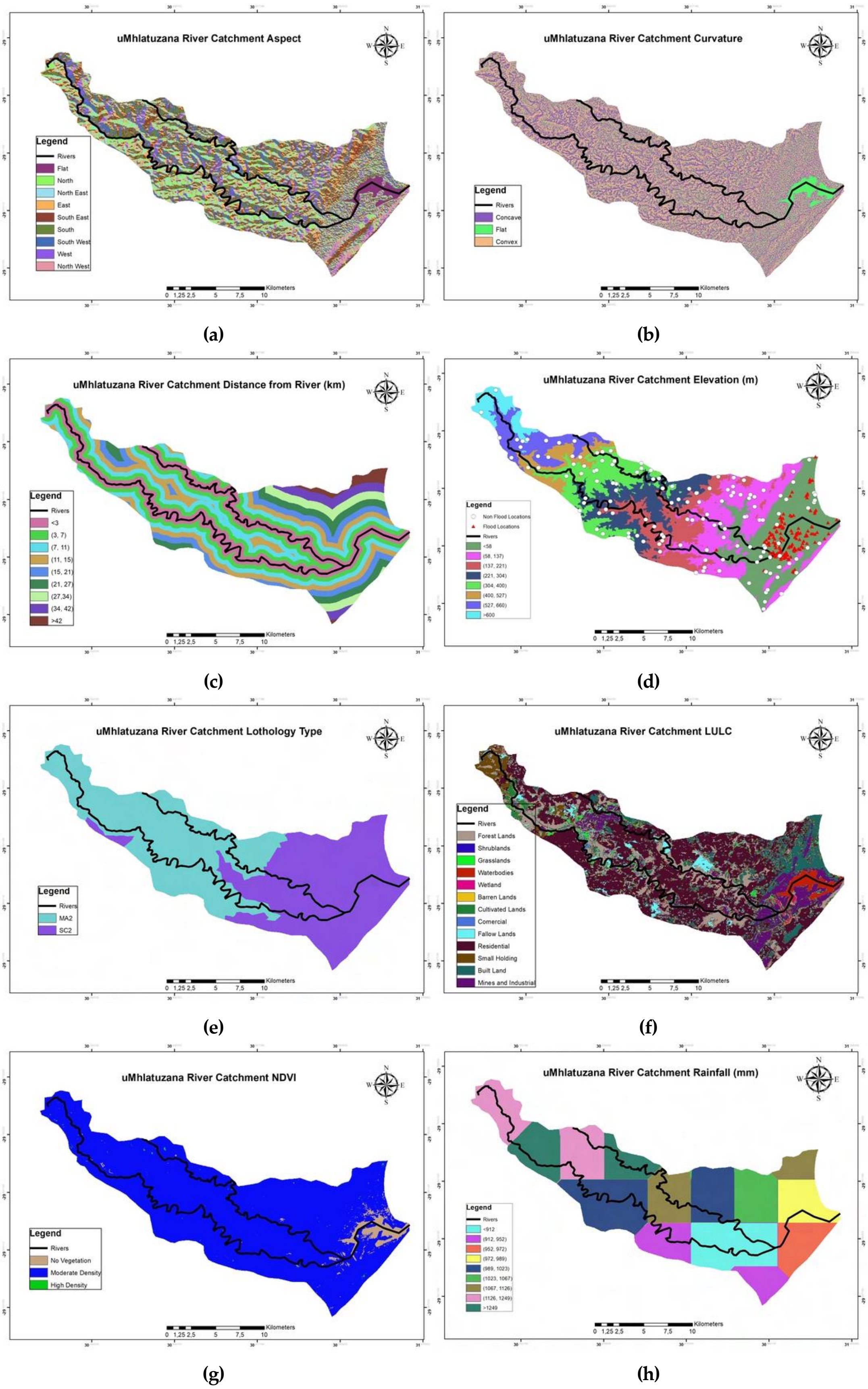

(a) (b)

(c) (d)

(e) (f)

(g) (h)

Figure 8: Thematic maps of flood conditioning factors of the study area.

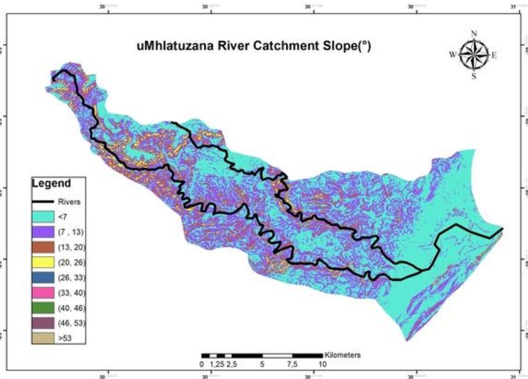

(i)

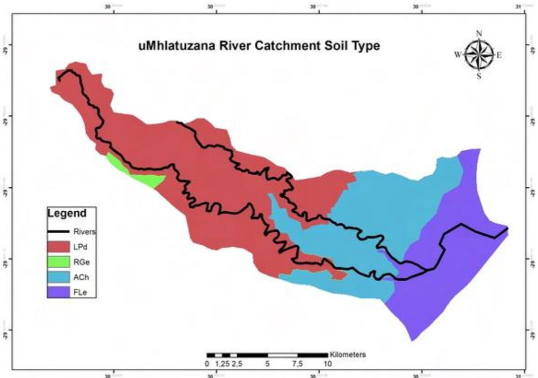

(j)

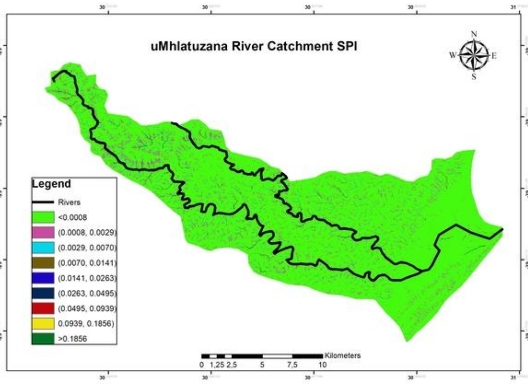

(k)

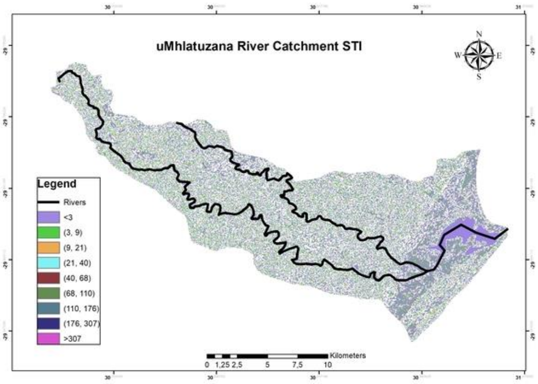

(l)

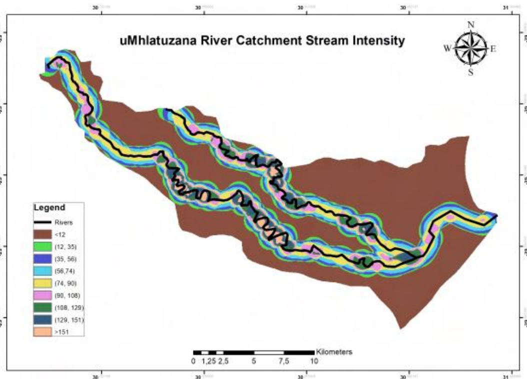

(m)

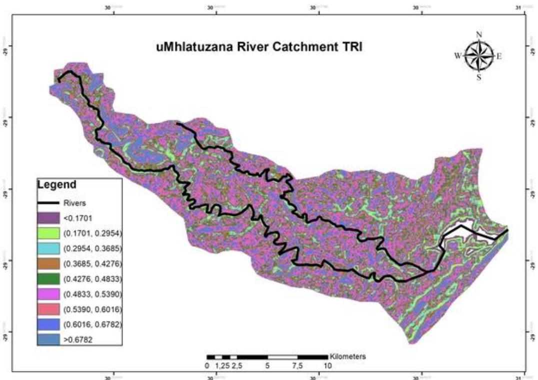

(n)

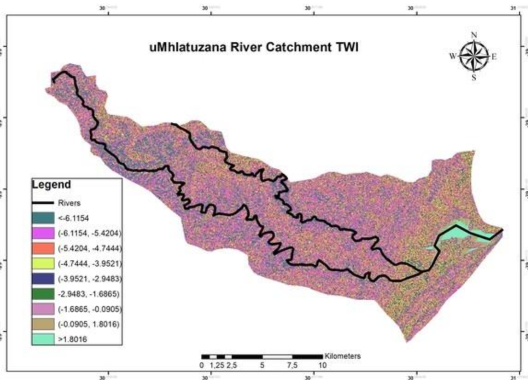

(o)

Figure 8: continued.

The land use/land cover (LULC) in the study area comprises of 13 distinct classes, namely: forest lands, water bodies, wetlands, barren lands, cultivated lands, grasslands, commercial areas, fallow lands, residential zones, small holdings, mines and industrial, and built lands as shown in Figure 8f. The proportions of these LULC classes are shown in Table 3. Among these classes, wetlands and barren lands exhibit significantly higher FR values of 4.97 and 4.65, respectively, in contrast to other LULC classes. This indicates that wetlands and barren lands are more likely to be vulnerable to flooding.

Elevations within the study area span a range from 0 m to 855 m and have been classified into eight distinct classes: < 58 m, 58-137 m, 137-221 m, 221-304 m, 304-400 m, 400-527 m, 527-660 m, and greater than 660 m as shown in Figure 8d. The most prevalent elevation class identified is '< 58 m' characterized by a FR value of 3.88 which is significantly higher than our other classes, indicating that this class is mostly associated with flood events.

The distance from the river within the study area spans a range from 0 km to 57 km and has been classified into nine distinct classes: < 3 km, 3-7 km, 7-11 km, 11-15 km, 15-21 km, 21-27 km, 27-34 km, 34-42 km, and > 43 km as shown in Figure 8c. It is important to note that more than 90% of historical flood locations are associated with areas in close proximity to the river or water bodies as shown in Table 3, and those areas exhibit higher FR values than those located further away from the river.

The slope in the study area is classified into nine distinct classes: 0-7 degrees, 7-13 degrees, 13-20 degrees, 20-26 degrees, 26-33 degrees, 33-40 degrees, 40-46 degrees, 46-53 degrees, and >53 degrees as shown in Figure 8i. The class '0-7 degrees' is the predominant class in the study area covering 53% of area as shown in Table 3 and exhibits a higher FR value of 1.72, with other slope classes significantly lower except for class '40-46 degrees' which has FR value of 3.70. This indicates that flat slopes are more vulnerable to floods.

The annual rainfall in the study area spans a range of 1447 mm to 882 mm with an average of 1007 mm and has been classified into nine distinct classes: 882-912 mm, 912-951 mm, 951-972 mm, 972-989 mm, 989-1023 mm, 1023-1067 mm, 1067-1126 mm, 1126-1249 mm, and > 1249 mm as shown in Figure 8h. The classes '951-972 mm' and '882-912 mm' exhibit higher FR values of 5.23 and 3.98, while other exhibit significantly lower FR values.

Terrain roughness index (TRI) is classified into nine distinct classes: <0.1701, (0.1701, 0.2954], (0.2954, 0.3685], (0.3685, 0.4276], (0.4276, 0.4833], (0.4833, 0.5390], (0.5390, 0.6016], (0.6016, 0.6782], and >0.6782 as shown in Figure 8n. The class '<0.1701' has higher FR value of 5.48 which is significantly higher than the ones of other TRI classes indicating higher chances of being vulnerable to flooding. Stream Power Index (SPI) is also classified into nine distinct classes: <0.0008, (0.0008, 0.0029], (0.0029, 0.0070], (0.0070, 0.0141], (0.0141, 0.0263], (0.0263, 0.0495], (0.0495, 0.0939], (0.0939, 0.1856], and >0.1856 as show in Figure 8k. The class '<0.0008' has a higher FR value of 1.02 indicating that this class is mostly associated with floods in the study area.

Topographic wetness index (TWI) is classified into nine distinct classes: <-6.1154, (-6.1154, -5.4204], (-5.4204, -4.7444], (-4.7444, -3.9521], (-3.9521, -2.9483], (-2.9483, -1.6865], (-1.6865, -0.0905], (-0.0905, 1.8016], and >1.8016 as shown in Figure 8o. The class '(-1.6865, -0.0905]' has a higher FR value of 5.47 indicating increased flooding risk. Sediment Transport Index is also classified into nine distinct classes: <3, 3-9, 9-21, 21-40, 40-68, 68-110, 110-176, 176-307, >307 as shown in Figure 8l. The class '21-40' has a higher FR value of 5.03 indicating increased flooding risk.

Stream intensity in the study area is classified into nine distinct classes: 0-12, 12-35, 35-56, 56-74, 74-90, 90-108, 108-129, 129-151, and >151. The class '35-56' has a FR value of 2.50. Lower stream intensity typically indicates fewer or absence pathways for water to flow through a watershed, diminishing drainage capacity and increasing the risk of flooding during heavy rainfall.

Table 3: Table showing the results of Frequency Ratio Method.

Flood Factors	Classes	Total Pixels	% Total Pixels	Flood Pixels	% Flood Pixels	FR
Soil Type	LPd	160131	48.65	0	48.65	0
	Rge	3714	1.13	0	1.13	0
	Ach	93644	28.45	144	28.45	0.59
	Fle	71712	21.79	721	21.79	3.83
Lithology	MA2	160461	48.75	0	48.75	0
	SC2	168699	51.25	865	51.25	1.95
Aspect	Flat	8159	2.5	82	2.5	3.83
	North	39375	12.07	108	12.07	1.04
	Northeast	36716	11.26	145	11.26	1.5
	East	43581	13.36	108	13.36	0.94
	Southeast	56983	17.47	94	17.47	0.63
	South	50612	15.52	82	15.52	0.62
	Southwest	33477	10.26	82	10.26	0.93
	West	26158	8.02	82	8.02	1.19
	Northwest	31112	9.54	82	9.54	1
Curvature	Concave	143304	43.52	604	43.52	1.6
	Flat	43505	13.21	174	13.21	1.52
	Concvex	142441	43.26	87	43.26	0.23
LULC	Forest land	44994	13.66	19	13.66	0.16
	Shrublands	7660	2.33	29	2.33	1.44
	Grasslands	8594	2.61	19	2.61	0.84
	Waterbodies	16946	5.14	92	5.14	2.07
	Wetland	3603	1.09	47	1.09	4.97
	Barren Land	7531	2.29	92	2.29	4.65
	Cultivated Land	9589	2.91	46	2.91	1.83
	Comercial	4089	1.24	27	1.24	2.51
	Fallow Lands	16110	4.89	35	4.89	0.83
	Residential	140337	42.6	98	42.6	0.27
	Small Holding	14008	4.25	42	4.25	1.14
	Built Land	30170	9.16	83	9.16	1.05
	Mines and Industrial	25814	7.84	236	7.84	3.48
NDVI	No Vegetation	11947	3.63	102	3.63	3.25
	Moderate Density	316812	96.22	761	96.22	0.91
	High Density	490	0.15	2	0.15	1.55
TWI	<-6.1154	42856	13.14	15	13.14	0.13
	(-6.1154, -5.4204)	76058	23.32	59	23.32	0.3

Table 3: continued.

	(-5.4204, -4.7444)	74854	22.95	125	22.95	0.64
	(-4.7444, -3.9521)	54817	16.81	144	16.81	1
	(-3.9521, -2.9483)	33023	10.12	144	10.12	1.66
	(-2.9483, -1.6865)	18584	5.7	155	5.7	3.17
	(-1.6865, -0.0905)	12944	3.97	186	3.97	5.47
	(-0.0905, 1.8016)	7877	2.41	34	2.41	1.64
	>1.8016	5160	1.58	3	1.58	0.22
TRI	<0.1701	4098	1.2	59	1.2	5.48
	(0.1701, 0.2954)	12529	3.65	114	3.65	3.46
	(0.2954, 0.3685)	33037	9.64	109	9.64	1.26
	(0.3685, 0.4276)	53755	15.68	110	15.68	0.78
	(0.4276, 0.4833)	67408	19.66	176	19.66	0.99
	(0.4833, 0.5390)	67951	19.82	178	19.82	1
	(0.5390, 0.6016)	55836	16.29	102	16.29	0.7
	(0.6016, 0.6782)	34795	10.15	16	10.15	0.18
	>0.6782	13439	3.92	1	3.92	0.03
Stream intensity	<12	180293	54.8	347	54.8	0.73
	(12, 35)	18866	5.73	61	5.73	1.23
	(35, 56)	21900	6.66	144	6.66	2.5
	(56, 74)	24812	7.54	144	7.54	2.21
	(74, 90)	36238	11.01	82	11.01	0.86
	(90, 108)	19244	5.85	28	5.85	0.55
	(108, 129)	14012	4.26	47	4.26	1.28
	(129, 151)	9522	2.89	12	2.89	0.48
	>151	4102	1.25	0	1.25	0
STI	<3	105246	58.99	257	58.99	0.93
	(3, 9)	47852	26.82	140	26.82	1.11
	(9, 21)	15432	8.65	100	8.65	2.47
	(21, 40)	5527	3.1	73	3.1	5.03
	(40, 68)	2432	1.36	22	1.36	3.44
	(68, 110)	1221	0.68	4	0.68	1.25
	(110, 176)	494	0.28	1	0.28	0.77
	(176, 307)	186	0.1	0	0.1	0
	>307	33	0.02	0	0.02	0
SPI	<0.0008	301696	92.5	815	92.5	1.03
	(0.0008, 0.0029)	17434	5.35	30	5.35	0.65
	(0.0029, 0.0070)	4441	1.36	6	1.36	0.51
	(0.0070, 0.0141)	1630	0.5	0	0.5	0
	(0.0141, 0.0263)	652	0.2	0	0.2	0
	(0.0263, 0.0495)	234	0.07	0	0.07	0
	(0.0495, 0.0939)	45	0.01	0	0.01	0
	(0.0939, 0.1856)	28	0.01	0	0.01	0
	>0.1856	13	0	0	0	0
Slope (∘)	<7	172509	52.89	784	52.89	1.73
	(7, 13)	110072	33.75	46	33.75	0.16
	(13, 20)	33123	10.16	12	10.16	0.14
	(20, 26)	7623	2.34	6	2.34	0.3
	(26, 33)	2155	0.66	2	0.66	0.35

Table 3: continued.

	(33, 40)	551	0.17	0	0.17	0
	(40, 46)	103	0.03	1	0.03	3.7
	(46, 53)	33	0.01	0	0.01	0
	>53	4	0	0	0	0
Rainfall (mm)	<912	42036	12.77	440	12.77	3.98
	(912, 951)	32874	9.98	10	9.98	0.12
	(951, 972)	21397	6.5	294	6.5	5.23
	(972, 989)	22666	6.88	111	6.88	1.86
	(989, 1023)	66365	20.16	0	20.16	0
	(1023, 1067)	24736	7.51	2	7.51	0.03
	(1067, 1126)	33788	10.26	8	10.26	0.09
	(1126, 1249)	46227	14.04	0	14.04	0
	> 1249	39161	11.89	0	11.89	0
Elevation (m)	< 58	84670	25.72	864	25.72	3.88
	(58, 137)	63995	19.44	0	19.44	0
	(137, 221)	42553	12.92	0	12.92	0
	(221, 304)	42271	12.84	0	12.84	0
	(304, 400)	40391	12.27	0	12.27	0
	(400, 527)	16240	4.93	0	4.93	0
	(527, 660)	25862	7.85	0	7.85	0
	> 660	13268	4.03	0	4.03	0
Distance From River (km)	< 3	77102	23.42	176	23.42	0.87
	(3, 7)	66474	20.19	338	20.19	1.94
	(7, 11)	58149	17.66	201	17.66	1.32
	(11, 15)	42818	13	110	13	0.98
	(15, 21)	28762	8.74	25	8.74	0.33
	(21, 27)	22477	6.83	7	6.83	0.12
	(27,34)	14769	4.49	2	4.49	0.05
	(34, 42)	12299	3.74	2	3.74	0.06
	> 42	6400	1.94	3	1.94	0.18

4.2 Information Gain Ratio for Feature Importance

This section delves into the significance of various flood conditioning factors by calculating their information gain ratio (IGR) values. The analysis highlights the relative importance of each factor in predicting flood events, providing insights into their contributions to flood susceptibility modeling.

To further explore the importance of flood conditioning factors on flood events, the information gain ratio (IGR) values for the 15 flood conditioning factors are calculated. All factors are deemed potentially important, and they have a positive impact on flood event occurrence. Notably, TWI and rainfall exhibit significantly higher IGR values of 0.3755 and 0.2835, respectively than other 13 flood conditioning fac- tors as shown in Table 4, indicating their greater significance in flood susceptibility modeling and ability to accurately predict flood.

Table 4: Table showing the significance of flood conditioning factors using the IGR method: Factors with higher Information Gain ratio (IGR) values play a more crucial role in prediction models, while those with an IGR value of zero make no contribution to flood events.

Flood Factors	**Information Gain Ration**
Topographic Wetness Index (TWI)	**0.3755**
Rainfall	0.2835
Stream Intensity	0.2286
Sediment Transport Index (STI)	0.2155
Lithology	0.1091
Soil	0.0973
Distance from the River	0.0489
Terrain Ruggedness Index (TRI)	0.0329
Slope	0.0313
Stream Power Index (SPI)	0.0225
Land Use/Land Cover (LULC)	0.0188
Normalized Difference Vegetation Index (NDVI)	0.0151
Elevation	0.0054
Aspect	0.0035
Curvature	0.0025

4.3 CNN Model Construction

In this study, three CNN architectures are constructed for flood prediction. Additionally, three different sets of training and test data in various dimensions are pre- pared, as shown in subsection 3.4.2. The training sets suitable for each of the three CNN dimensions are fed into the respective CNN models, each subjected to 10-fold cross-validation for hyperparameter optimization. The aim is to maximize the performance of each respective CNN model through Bayesian optimization.

Moreover, the hyperparameter combinations that maximized the performance of each CNN model are subsequently used to train the final CNN model for that specific dimension. This model is then used to generate susceptibility maps. It is significant to note that, in 3D CNNs, the window size serves as a critical parameter. This hyperparameter significantly affects the neural network's ability to process and extract features from 3D data. A larger window size can capture more global features and patterns, while a smaller window size can focus on local details [Israel *et al.* 2021].

4.4 Bayesian Optimization: CNNs Hyperparameter Tuning

This section presents the findings from the experiments conducted using Bayesian optimization on three architectures of convolutional neural networks (CNN): 1D- CNN, 2D-CNN, and 3D-CNN. The results highlight the impact of hyperparameter tuning on model performance and the comparative effectiveness of each CNN architecture.

In this study, Bayesian optimization has been experimented on three architectures of convolutional neural networks (CNN), namely: 1D CNN, 2D CNN, and 3D CNN. The hyperparameters considered for these three CNN architectures are shown in Table 5 and the class mapping of CNNs optimizers and activation used are shown in Table 6. For all three CNN architecture, the Bayesian optimization experiments for hyperparameter tuning is utilized in combination with 10-fold cross-validation. Consequently, this leads to the discovery of hyperparameters that result in a more robust and reliable model, as the performance is assessed across multiple subsets of the data, reducing the risk of overfitting or underestimating the true performance.

Table 5: Table showing the parameters of the CNN in question for hyperparameterization and their respective classes or ranges for finding the best parameters that maximize the performance of all three CNN architectures (please refer to Table 6 for detailed information with regards to the class mapping for the Activation and Optimizer).

Parameters	Classes/Range	1D CNN	2D CNN	3D CNN
Filters	10-200	Yes	Yes	Yes
Neural Units	10-200	Yes	Yes	Yes
Activation	0-9	Yes	Yes	Yes
Optimizer	0-7	Yes	Yes	Yes
Epochs	10-100	Yes	Yes	Yes
batch Size	200-1000	Yes	Yes	Yes
Learning Rate	0.01-1	Yes	Yes	Yes
Dropout Rate	0-1	No	Yes	Yes
Normalization	0-1	No	No	Yes

Table 6: Table showing class mapping of CNN Optimizer and Activation parameters.

Class	Activation	Optimizer
0	ReLu	SGD
1	Sigmoid	Adam
2	Softplus	RMSprop
3	Softsign	Adadelta
4	Tanh	Adagrad
5	SeLu	Adamax
6	Elu	Nadam
7	Exponential	Ftrl
8	LeakyReLU	

A 1-dimensional CNN has been developed to address flood prediction challenges, achieving an F1 score of 0.879, as depicted in Figure 9. This performance is attributed to the incorporation of bayesian optimization alongside a robust 10-fold cross-validation strategy. This approach ensured thorough testing of the model's effectiveness, instilling a high level of confidence in its generalization capabilities and mitigating the risk of overfitting. The use of Bayesian optimization ensures a systematic exploration across a broad range of hyperparameter configurations, ultimately leading to the identification of a set of hyperparameters that optimizes the 1D-CNN model's performance as shown in Table 7.

A 2-dimensional CNN yielded improvements in flood prediction by achieving an F1 score of 0.914 compared to 0.879 achieved by 1- dimensional CNN as shown in Figure 9. This performance can be attributed to the inherent ability of 2-dimensional CNNs to capture spatial patterns and dependencies within data, which are particularly valuable in tasks like flood prediction where geographical information plays a significant role.

The 3-dimensional CNN has been run with three different window sizes (5, 7, and 9) due to computational constraints, demonstrating its capabilities by achieving F1 scores of 0.891 for the window size 5, 0.903 for the window size 7, and 0.934 for the window size 9. The performance is attributed to the 3D CNN's ability to capture the spatial patterns and temporal dependencies within the data. This is particularly vital in flood prediction, where understanding the evolution of flood-related events over time is critical. This achievement emphasizes the potential of 3-dimensional CNNs in tackling complex geospatial and temporal machine learning tasks with a degree of precision and reliability.

It is significant to note that while the performance of 3-dimensional CNN gradually increases with larger window sizes, larger windows may pose the risk of overfitting. As the network becomes more capable of memorizing intricate details within these larger windows, there is a potential hindrance to its ability to generalize well to unseen data [Irvine and Israel 2022].

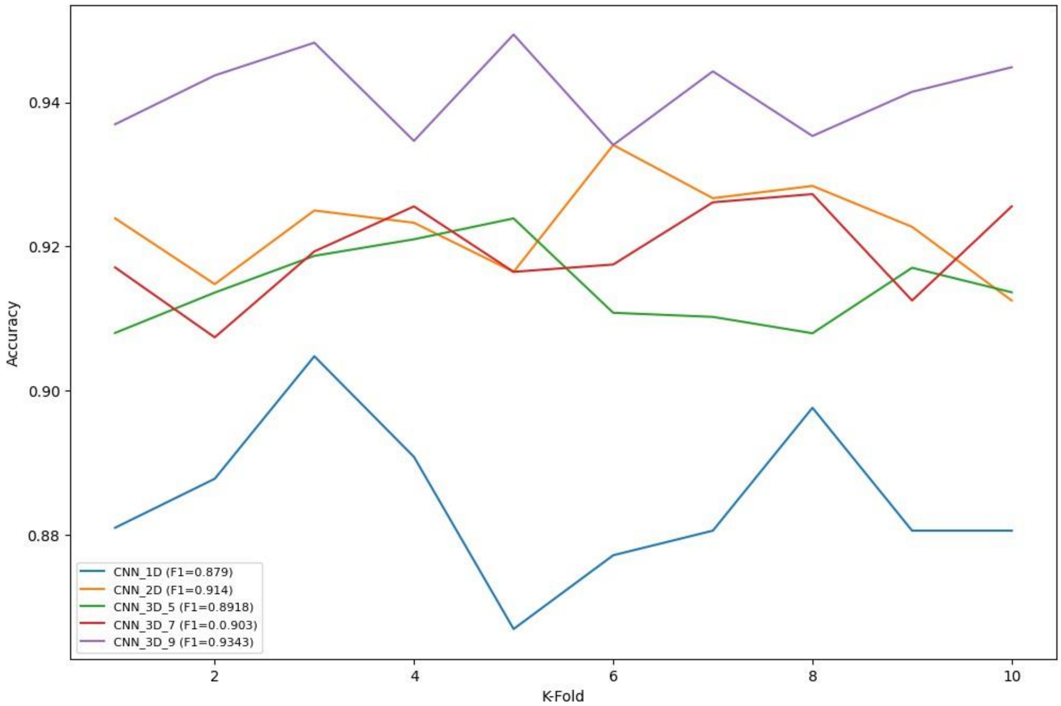

Figure 9: Bayesian optimization, in combination with 10-fold cross-validation, is employed to determine the hyperparameters that maximize the performance of all three CNN architectures.

Table 7: Table showing the best hyperparameters that maximize the performance of all three CNN architectures, where BS is Batch Size, DR is Dropout Rate, LR is Learning Rate, and NU is Neural Units. This hyperparameters are used to fit the final models.

Parameters	1D-CNN	2D-CNN	3D-CNN
Activation	Elu	Elu	Softplus
Batch Size	307	307	808
Dropout rate		0.53	0.12
Epochs	58	44	70
Filters	81	143	143
Learning rate	0.70	0.82	0.66
Neural Units	166	98	188
Optimizer	Adadelta	Adadelta	Adadelta
Normalization			0.78

4.5 CNN Model Experiments and Evaluations

4.5.1 1D-CNN Model

This subsection presents the findings from the experiments conducted using the 1D-CNN model. The results highlight the model's performance across multiple runs, emphasizing the impact of feature selection and augmentation on its predictive accuracy and robustness.

In this study, the 1D-CNN model has been run 6 times as shown in Figure 10. The initial phase involved the selection of the top ten features, carefully chosen based on information gain ratio for feature importance. Subsequently, a systematic augmentation of the feature set is implemented to evaluate the individual contributions of features to the performance of the 1D-CNN model. As seen in Figure 10, both ac- curacy and F1 score demonstrated a nearly identical and gradual increase with the expansion of features. This consistent trend emphasizes the model's robustness and the collective relevance of the selected features.

The 1D-CNN Model when run using all 15 flood factors, achieved a higher F1 score and accuracy of 0.89 and 0.88 respectively. The F1 score value signifies a well-balanced model performance with a good trade-off between making accurate positive predictions (precision) and capturing most actual flood cases (recall). Addi- tionally, the 1D-CNN achieved a precision of 0.84 for flood class indicating that approximately 84% of the instances the model predicted as floods were indeed floods. The recall is 0.93, highlighting the model's ability to correctly identify actual flood cases. This is a good results in the context of flood predictions since the model can capture about 93% of floods present in the study area. Finally, the 1D-CNN model achieved an AUC score of 0.935, indicating its high discriminative power and its effectiveness in distinguishing between positive and negative classes. The confusion matrices used to describe the performance of all 1D-CNN 6 experiments are shown in Figure 11 and the results of all six experiment are shown in Table 8.

4.5.2 2D-CNN Model

This subsection presents the findings from the experiments conducted using the 2D-CNN model. The results highlight the model's enhanced performance and its ability to capture spatial relationships more effectively than the 1D-CNN.

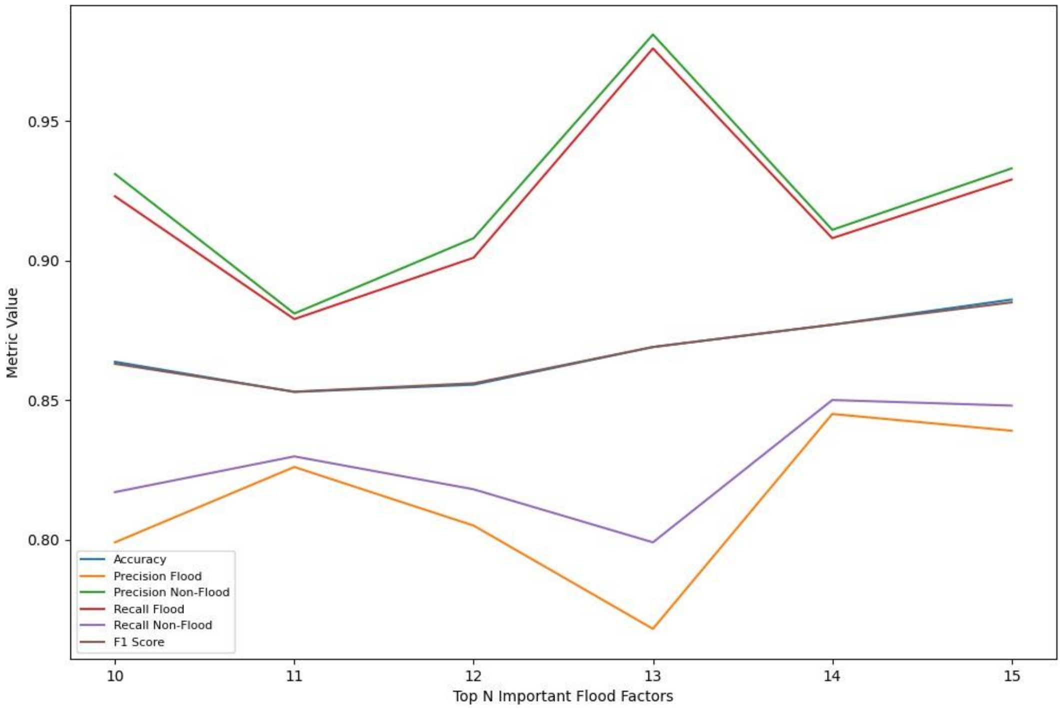

Figure 10: 1D-CNN Model experiments in conjunction with information gain ratio for feature importance.

Table 8: Table showing a breakdown of performance metrics values for all 6 experiments of the 1D-CNN model. PF is the precision of flood classes, PFN is the precision of non- flood, RF is the recall of flood class, and RFN is the recall of non-flood class.

Top N Features	Accuracy	PF	PNF	RF	RNF	F1 Score
10	0.8637	0.799	0.931	0.923	0.817	0.863
11	0.8529	0.826	0.881	0.879	0.829	0.853
12	0.8555	0.805	0.908	0.901	0.818	0.856
13	0.869	0.768	0.981	0.976	0.799	0.869
14	0.877	0.845	0.911	0.908	0.85	0.877
15	0.886	0.839	0.933	0.929	0.848	0.885

The 2D-CNN represents an improvement over the 1D-CNN. The 2D-CNN has achieved an F1 score and accuracy of 0.912 and 0.913 respectively. The F1 score value indicates the trade-off between precise positive predictions and effective flood case prediction. Additionally, the 2D-CNN has achieved a precision of 0.85 indicating that 85% of the model's positive flood predictions were accurate. Moreover, the 2D-CNN has achieved a recall of 0.972 and an AUC score of 0.97 indicating a substantial enhancement in the model's discriminative power and its ability to effectively distinguish between positive and negative classes. This higher AUC score demonstrates the 2D-CNN's superiority in capturing the intricacies of flood prediction. The confusion matrix used to describe the performance of 2D-CNN is shown in Figure 12.

4.5.3 3D-CNN Model

This subsection presents the findings from the experiments conducted using the 3D-CNN model. The results highlight the model's performance across multiple feature

Testing Set			
TARGET / OUTPUT	Flood	Non Flood	SUM
Flood	299 40.74%	75 10.22%	374 79.95% 20.05%
Non Flood	25 3.41%	335 45.64%	360 93.06% 6.94%
SUM	324 92.28% 7.72%	410 81.71% 18.29%	634 / 734 86.38% 13.62%

(a) 1D-CNN model experiment with top 10 features on a set of test data.

Testing Set			
TARGET / OUTPUT	Flood	Non Flood	SUM
Flood	309 42.10%	65 8.86%	374 82.62% 17.38%
Non Flood	43 5.86%	317 43.19%	360 88.06% 11.94%
SUM	352 87.78% 12.22%	382 82.98% 17.02%	626 / 734 85.29% 14.71%

(b) 1D-CNN model experiment with top 11 features on a set of test data.

Testing Set			
TARGET / OUTPUT	Flood	Non Flood	SUM
Flood	301 41.01%	73 9.95%	374 80.48% 19.52%
Non Flood	33 4.50%	327 44.55%	360 90.83% 9.17%
SUM	334 90.12% 9.88%	400 81.75% 18.25%	628 / 734 85.56% 14.44%

(c) 1D-CNN model experiment with top 12 features on a set of test data.

Testing Set			
TARGET / OUTPUT	Flood	Non Flood	SUM
Flood	285 38.83%	89 12.13%	374 76.20% 23.80%
Non Flood	7 0.95%	353 48.09%	360 98.06% 1.94%
SUM	292 97.60% 2.40%	442 79.86% 20.14%	638 / 734 86.92% 13.08%

(d) 1D-CNN model experiment with top 13 features on a set of test data.

Testing Set			
TARGET / OUTPUT	Flood	Non Flood	SUM
Flood	316 43.05%	58 7.90%	374 84.49% 15.51%
Non Flood	32 4.36%	328 44.69%	360 91.11% 8.89%
SUM	348 90.80% 9.20%	386 84.97% 15.03%	644 / 734 87.74% 12.26%

(e) 1D-CNN model experiment with top 14 features on a set of test data.

Testing Set			
TARGET / OUTPUT	Flood	Non Flood	SUM
Flood	314 42.78%	60 8.17%	374 83.96% 16.04%
Non Flood	24 3.27%	336 45.78%	360 93.33% 6.67%
SUM	338 92.90% 7.10%	396 84.85% 15.15%	650 / 734 88.56% 11.44%

(f) 1D-CNN model experiment with top 15 features on a set of test data.

Figure 11: Confusion matrices assessing the performance of 1D-CNN experiments. The green and red shaded blocks for the flood class represent the True Positive and True Negative cases, respectively. The green and red shaded blocks for the non-flood class represent the False Negative and False Positive cases, respectively.

Testing Set			
TARGET / OUTPUT	Flood	Non Flood	SUM
Flood	1821 41.38%	328 7.45%	2149 84.74% 15.26%
Non Flood	54 1.23%	2198 49.94%	2252 97.60% 2.40%
SUM	1875 97.12% 2.88%	2526 87.02% 12.98%	4019 / 4401 91.32% 8.68%

Figure 12: Confusion matrices assessing the performance of 2D-CNN experiments. The green and red shaded blocks for the flood class represent the True Positive and True Negative cases, respectively. The green and red shaded blocks for the non-flood class represent the False Negative and False Positive cases, respectively.

augmentations and its ability to capture complex spatial and temporal relationships in flood prediction.

The 3D-CNN model is run with six different feature augmentations using information gain ratio for feature importance. Like the 1D-CNN experiments, the first set consisted of the top 10 ranked important features to evaluate the individual contributions of features to the performance of the 3D-CNN model. As seen in Figure 13, both accuracy and F1 score demonstrate a nearly identical and gradual increase with the expansion of features. Similar trends were observed in the 1D-CNN experiments, emphasizing the model's robustness and the collective relevance of the selected features.

The 3D-CNN model, experimented with all 15 factors ordered by their importance, achieved an F1 score and accuracy of 0.933. This balanced performance is reflected in the F1 score. Additionally, the 3D-CNN achieved a precision of 0.903, indicating an unparalleled level of capability in ensuring that approximately 90% of the model's positive flood predictions were indeed floods. Moreover, the 3D-CNN achieved a recall of 0.96 and an AUC score of 0.98, indicating that the model has a higher discriminative power and precision in distinguishing between flood and non-flood classes. The confusion matrices used to describe the performance of the 3D-CNN experiments are shown in Figure 14 and the results of all six experiment are shown in Table 9.

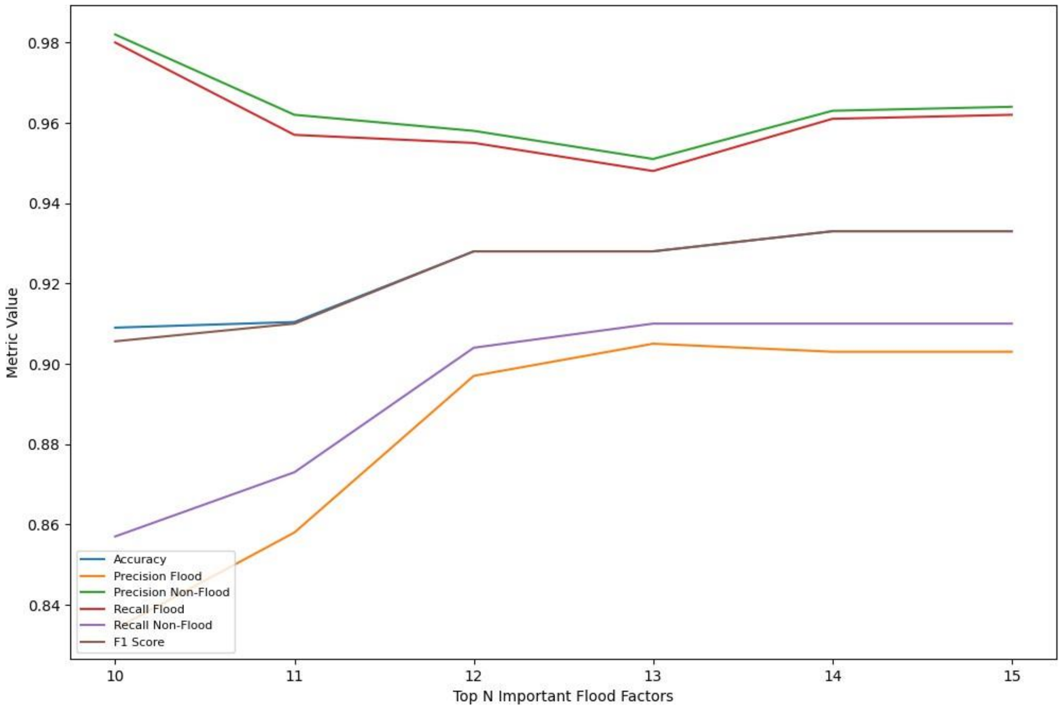

Figure 13: 3D-CNN Model experiments in conjunction with information gain ratio for feature importance.

Table 9: Table showing a breakdown of performance metrics values for all 6 experiments of the 3D-CNN model. PF is the precision of flood classes, PFN is the precision of non- flood, RF is the recall of flood class, and RFN is the recall of non-flood class.

Top N Features	Accuracy	PF	PNF	RF	RNF	F1 SCore
10	0.909	0.834	0.982	0.98	0.857	0.9056
11	0.9104	0.858	0.962	0.957	0.873	0.91
12	0.928	0.897	0.958	0.955	0.904	0.928
13	0.928	0.905	0.951	0.948	0.91	0.928
14	0.933	0.903	0.963	0.961	0.91	0.933
15	0.933	0.903	0.964	0.962	0.91	0.933

4.6 Conclusions

The results of this study demonstrate the effectiveness of using convolutional neural networks (CNN) models for flood susceptibility modeling in the uMhlatuzana River catchment. The experiments conducted with 1D, 2D, and 3D CNN architectures reveal that each model has its strengths, with the 3D-CNN showing the highest performance due to its ability to capture both spatial and temporal patterns. The use of Bayesian optimization for hyperparameter tuning significantly enhanced the models' performance, ensuring robust and reliable predictions. The frequency ratio (FR) and information gain ratio (IGR) analyses further highlighted the critical flood conditioning factors, such as topographic wetness index (TWI) and rainfall, which play a significant role in flood prediction.

Overall, this study emphasizes the importance of integrating advanced machine learning techniques with geospatial data to improve flood risk management. The findings

Testing Set

TARGET / OUTPUT	Flood	Non Flood	SUM
Flood	1929 43.83%	261 5.93%	2190 88.08% 11.92%
Non Flood	154 3.50%	2057 46.74%	2211 93.03% 6.97%
SUM	2083 92.61% 7.39%	2318 88.74% 11.26%	3986 / 4401 90.57% 9.43%

(a) 3D-CNN model experiment with top 10 features on a set of test data.

Testing Set

TARGET / OUTPUT	Flood	Non Flood	SUM
Flood	1812 41.17%	378 8.59%	2190 82.74% 17.26%
Non Flood	14 0.32%	2197 49.92%	2211 99.37% 0.63%
SUM	1826 99.23% 0.77%	2575 85.32% 14.68%	4009 / 4401 91.09% 8.91%

(b) 3D-CNN model experiment with top 11 features on a set of test data.

Testing Set

TARGET / OUTPUT	Flood	Non Flood	SUM
Flood	1964 44.63%	226 5.14%	2190 89.68% 10.32%
Non Flood	92 2.09%	2119 48.15%	2211 95.84% 4.16%
SUM	2056 95.53% 4.47%	2345 90.36% 9.64%	4083 / 4401 92.77% 7.23%

(c) 3D-CNN model experiment with top 12 features on a set of test data.

Testing Set

TARGET / OUTPUT	Flood	Non Flood	SUM
Flood	1982 45.04%	208 4.73%	2190 90.50% 9.50%
Non Flood	108 2.45%	2103 47.78%	2211 95.12% 4.88%
SUM	2090 94.83% 5.17%	2311 91.00% 9.00%	4085 / 4401 92.82% 7.18%

(d) 3D-CNN model experiment with top 13 features on a set of test data.

Testing Set

TARGET / OUTPUT	Flood	Non Flood	SUM
Flood	1977 44.92%	213 4.84%	2190 90.27% 9.73%
Non Flood	81 1.84%	2130 48.40%	2211 96.34% 3.66%
SUM	2058 96.06% 3.94%	2343 90.91% 9.09%	4107 / 4401 93.32% 6.68%

(e) 3D-CNN model experiment with top 14 features on a set of test data.

Testing Set

TARGET / OUTPUT	Flood	Non Flood	SUM
Flood	1978 44.94%	212 4.82%	2190 90.32% 9.68%
Non Flood	79 1.80%	2132 48.44%	2211 96.43% 3.57%
SUM	2057 96.16% 3.84%	2344 90.96% 9.04%	4110 / 4401 93.39% 6.61%

(f) 3D-CNN model experiment with top 15 features on a set of test data.

Figure 14: Confusion matrices assessing the performance of 3D-CNN experiments. The green and red shaded blocks for the flood class represent the True Positive and True Negative cases, respectively. The green and red shaded blocks for the non-flood class represent the False Negative and False Positive cases, respectively.

provide valuable insights into the relative importance of various flood conditioning factors and demonstrate the potential of CNNs in producing accurate flood susceptibility maps. These results can inform future research and practical applications in flood prediction and disaster management, contributing to more effective planning and mitigation strategies in flood-prone areas.

Chapter 5

Discussion

5.1 Analysis of Flood Factors and Flood Occurrence

The study employs frequency ratios to investigate the interrelationship between flood factors and their occurrences. This analysis delves into the quantitative distribution of these factors, offering insights into their interconnections. In this section, the implications of these frequency ratios are explored, providing a concise understanding of the important relations between identified flood factors within the research scope.

The higher FR value of Acrisols and Fluvisols indicates higher chances of flood occurrence for these soil types. Acrisols and Fluvisols have low permeability, indicating a less likelihood of water infiltration and, consequently, an increased chance of flood occurrences [Yu *et al.* 2015; Figueiredo *et al.* 2009]. Moreover, the FR values of Lithology indicates that flood occurrences are more likely on terrains comprising lithology types classified under SC2 such as sandstone, greywacke, and arkose. These lithology types in the study area are found on areas near the coast and they are also known for their low permeability, suggesting a reduced capacity for water infiltration and an increased likelihood of flooding [Dong *et al.* 2010].

The higher FR value on the flat aspect aligns with the general understanding that floods tend to occur more frequently on low-lying or flat surfaces when the rate of rainfall exceeds the ground's capacity to absorb or channel runoff effectively [Wolman and Leopold 1957]. This phenomenon is rooted in the principle that water naturally flows from higher to lower elevations, making low-lying or flat areas more susceptible to flood occurrences.

The concave and flat slopes have FR values of 1.60 and 1.52, respectively, indicating an increased susceptibility to flooding. The higher FR values align with research conducted by Sensoy and Kara [2014] on the impact of slope shape on runoff, suggesting that concave and flat slopes result in higher runoff rates compared to convex slopes. Consequently, this heightened runoff contributes to downstream flooding events. Concave slopes are particularly significant as they tend to accumulate water and are more susceptible to flooding due to their inward channeling of water, forming low-lying areas at the base of the slope [Izzard and Hicks 1946]. It is essential to note that prolonged or intense rainfall can impose substantial stress on natural drainage systems. This environmental challenge can lead to flooding on flat surfaces. When precipitation rates exceed the ground's absorption and conveyance capacities, water accumulates on the surface, ultimately resulting in flood events [Bevc 1997].

The FR values of wetlands and barren lands under LULC indicates these classes are more prone to flooding. Wetlands are predominantly low-lying areas characterized by waterlogged soils and a high water table, making them naturally susceptible to flooding [Acreman and Holden 2013]. During periods of heavy rainfall, wetlands function as natural flood control systems, effectively absorbing excess water. However, they can be overwhelmed when floodwaters surpass their storage and drainage capacity, thus increasing their vulnerability to flooding [Acreman and Holden 2013].

Barren lands, on the other hand, are often marked by poor vegetation cover, which reduces their ability to absorb and retain water compared to more vegetated areas [Kabanda and Palamuleni 2013]. The lack of vegetation on barren lands makes them highly susceptible to surface runoff [Radwan *et al.* 2019]. Consequently, rainwater flows more easily across these areas, leading to flooding, particularly during sudden and heavy rainfall events. It is important to note that within the study area, barren lands are primarily located in regions characterized by the Acrisols soil group as it can be seen in Figure 8f and Figure 8j, respectively. Acrisols are associated with low permeability, indicating a reduced likelihood of water infiltration and, consequently, an increased risk of flooding.

The class '$<$ 58 m' for elevation is characterized by a higher FR value of 3.88. This class primarily covers regions near the coast and towards the river mouth within the study catchment area. It is worth noting that areas along the coast are susceptible to severe weather events, including tropical cyclones. As a consequence, there is a heightened risk of rising sea levels leading to coastal flooding in the adjacent areas [Grab and Nash 2023; Bopape *et al.* 2021].

The FR value observed within areas that are in close proximity to rivers in the study area is consistent with the phenomenon that areas in close proximity to rivers are more prone to flooding. The risk of flooding increases as one approaches the river, particularly during heavy rainfall or when the river overflows its banks. Moreover, regions near a river are commonly situated within what is known as a floodplain. Floodplains are low-lying areas adjacent to the river that naturally exhibit susceptibility to periodic flooding.

The FR values for slope classes indicate an increased flood risk on less steep slopes. Steeper slopes, known for accelerating water flow during heavy rainfall [Hou *et al.* 2018], contribute to higher volumes and velocities of water in rivers and streams on sloped terrain. This heightened flow elevates the risk of downstream or low-lying area flooding [Ogato *et al.* 2020], particularly in regions with steep slopes where natural water channels have sharper inclines. The swift downhill flow increases the risk of severe flooding downstream. Additionally, steeper slopes, often characterized by rocky or impermeable terrain [Radwan *et al.* 2019], lack water retention capacity. This limitation results in intense surface runoff during heavy rainfall, significantly amplifying flood risk in low-lying regions.

The FR values for stream intensity classes indicate an increased flood risk in regions with lower stream intensity. Lower stream intensity implies fewer pathways for water to navigate through a watershed, diminishing drainage capacity and heightening the risk of flooding during heavy rainfall. Stream intensity is closely linked to the topography of a region. In high-elevation areas, a higher intensity density is common due to natural drainage patterns [Tehrany *et al.* 2013 2015; Wang *et al.* 2020a]. Conversely, in flatter landscapes, stream intensity may be lower, rendering them more susceptible to flooding. Stream intensity also influences the frequency and magnitude of flooding events. Areas with low stream intensity may experience infrequent but severe floods during significant rainfall, whereas regions with high stream intensity may encounter more frequent but less severe flooding events.

5.2 Flood Conditioning Factors Importance and Contribution

The evaluation of flood conditioning factors importance is important for understanding the factors driving flood susceptibility within the uMhlatuzana river catchment. The information gain ratio (IGR), a measure quantifying the contribution of each predictor variable, offers valuable insights into their respective impacts on flood susceptibility. The IGR values of all 15 flood conditioning factors are shown in Table 4. The topographic wetness index (TWI) emerges as a substantial determinant of flood susceptibility, with the highest IGR of 0.3755. Higher TWI values may correlate with increased water accumulation, influencing susceptibility patterns.

Rainfall, with an IGR of 0.2835, proves to be a key factor in flood susceptibility. This variable highlights the direct influence of precipitation patterns on the likelihood of flooding events. Additionally, stream intensity, with an IGR of 0.2286, emphasizes the relevance of stream intensity in flood susceptibility. Areas with lower stream intensity may exhibit increased vulnerability to flooding. Furthermore, Sediment Transport Index (STI), with an IGR of 0.2155, also emphasizes its relevance in flood susceptibility. This variable captures the interaction between soil properties and topography, contributing to the overall vulnerability assessment.

Lithology and Soil Type with IGRs of 0.1091 and 0.0973, respectively, contribute moderately to flood susceptibility, emphasizing the importance of subsurface characteristics in influencing susceptibility patterns. Distance from the river, with an IGR of 0.0489, exhibits a moderate impact, indicating that proximity to rivers is a factor, albeit less influential than other variables. Topographic Ruggedness Index (TRI) and slope contribute to flood susceptibility, albeit to a lesser extent, with IGRs of 0.0329 and 0.0313, respectively. These variables capture terrain complexity and slope steepness, influencing susceptibility patterns.

Stream Power Index (SPI), Land Use and Land Cover (LULC), and NDVI demonstrate relatively lower IGRs (0.0225, 0.0188, and 0.0151, respectively), but they remain relevant contributors, emphasizing the multifaceted nature of flood susceptibility. SPI helps in understanding the erosive potential and flood dynamics within the catchment, LULC and NDVI highlight the complex interplay between land cover, land use, and vegetation in flood vulnerability. Elevation, aspect, and curvature exhibit the least influence on flood susceptibility with IGRs of 0.0054, 0.0035, and 0.0025, respectively. While these factors play a role, their impact is comparatively lower.

In conclusion, understanding the significance of these variables by comprehending the variable importance derived from IGR is crucial for developing accurate and reliable flood susceptibility models. These findings provide valuable insights for prioritizing mitigation efforts and emphasizes the multifaceted nature of flood vulnerability within the uMhlatuzana River Catchment.

5.3 Hyperparameter Tuning for CNN Models

The Bayesian optimization and rigorous 10-fold cross-validation played important roles in fine-tuning the hyperparameters, ensuring that the models were operating at peak efficiency. This exploration highlights the value of selecting the most suitable CNN dimensionality for specific tasks and emphasizes the importance of hyperparameter optimization in achieving best predictive performance. The hyperparameters that achieved exceptional performance across all instances of CNN architecture, have been utilized to fit the final models, respectively, for producing flood susceptibility maps of the study area. Furthermore, by leveraging the optimized hyperparameters, the CNN models are poised to deliver more accurate and reliable predictions, which are critical for disaster management and response planning.

5.4 Model Performance Assessment

5.4.1 1D-CNN Model

The 1D-CNN model displays strong overall performance in flood susceptibility modeling, evident in key metrics such as accuracy, precision, recall, AUC score, and F1-score as shown in Table 8. With an accuracy of 0.886, the model demonstrates a high level of proficiency in correctly classifying instances, showcasing its potential effectiveness in distinguishing flood-prone areas from those at lower risk.

Precision is a crucial metric, and the model excels in both flood and non-flood classes. A precision of 0.839 for flood classes indicates an 83.9% accuracy in predicting flooding, while a precision of 0.933 for non-flood classes highlights a 93.3% accuracy in identifying areas not susceptible to flooding. This balanced precision emphasizes the model's reliability in minimizing false positives and negatives. Additionally, recall, essential for capturing flood-prone areas, is robust at 0.929 for flood classes, capturing 92.9% of actual flood-prone areas. The recall for non-flood classes is 0.848, indicating a solid performance in identifying 84.8% of non-flood instances. These recall values emphasize the model's efficacy in early warning systems and comprehensive disaster management.

The AUC score, a measure of the model's ability to discriminate between flood and non-flood instances, is high at 0.935. This signifies the model's ability in distinguishing between the two classes, adding to its credibility in flood susceptibility modeling. Additionally, the F1-score, balancing precision and recall, yields a value of 0.885. This score reflects a blend of precision and recall, reinforcing the model's effectiveness in handling imbalanced datasets common in flood susceptibility modeling.

It is essential to highlight that despite the notable achievements of 1D-CNN when assessed using diverse metrics, exhibit limitations in its capacity to generalize effectively or accurately identify areas prone to flooding within the study area. As evident from the flood susceptibility mapping depicted in Figure 16a, the model demonstrates limitations in generalizing flood vulnerability to areas beyond those directly affected by inundation. This challenge in generalization can be attributed to the inherent constraints of the 1D-CNN employed in this study.

The limitations of a 1D-CNN stem from both its design and application. In a 1D-CNN, the convolutional operation considers only a local region of the input space along a single dimension. This means that each output value is determined by a small window of input values, and the network does not inherently capture relationships between neighbouring pixels in the data. For applications like flood susceptibility mapping, where spatial dependencies can extend over larger areas, this limitation hinders the model's ability to grasp the broader context

Additionally, flood susceptibility mapping inherently involves understanding the spatial context and relationships between different geographic locations. In a 1D- CNN, the spatial context is constrained to a single dimension, which may not be sufficient for capturing the complex interactions between neighboring pixels in a 2-dimensional or 3-dimensional space.

5.4.2 2D-CNN Model

The utilization of 2D-CNN for flood susceptibility assessment has shown success, as evidenced by the achieved accuracy of 0.913, precision of 0.85, recall of 0.972, AUC score of 0.97, and an F1-score of 0.912. The obtained accuracy of 0.913 reflects the overall effectiveness of the 2D-CNN in distinguishing between flood-prone and non-flood-prone areas. The model's precision of 0.85 emphasizes its ability to minimize false positives, indicating a high degree of confidence in the predicted flood-affected regions. Moreover, the recall value of 0.972 signifies the model's proficiency in capturing a significant portion of actual flood occurrences, minimizing false negatives.

The AUC score of 0.97 provides valuable insights into the model's ability to discriminate between positive and negative instances. The AUC score nearing 1.0 signifies an excellent discriminative capability, highlighting the robustness of the 2D-CNN in differentiating between areas susceptible and non-susceptible to floods. This metric is crucial in assessing the model's performance across varying threshold values and is indicative of its reliability in real-world applications.

The F1-score, a harmonic mean of precision and recall, offers a balanced evaluation of the model's performance. With an F1-score of 0.912, the 2D-CNN demonstrates a blend of precision and recall, indicating a robust compromise between minimizing false positives and false negatives. This balance is particularly important in flood susceptibility mapping, where both commission (false positives) and omission (false negatives) errors can have significant consequences.

The flood susceptibility mapping produced by the 2D-CNN in Figure 16b suggests that 2D-CNNs are better equipped to generalize flood vulnerability in the study area than 1D-CNNs. This improvement can be attributed to the concept of transforming the 1-dimensional extension of the flood feature vector into a 2-dimensional space, as previously illustrated in the CNN data representation in Figure 4. As a result, the 2D-CNN can capture the spatial patterns of the fifteen flood factors across the study area. The transition from a 1-dimensional representation to a 2-dimensional ensured that the 2D-CNN model can effectively analyze and generalize flood susceptibility beyond areas directly impacted by inundation.

In conclusion, the application of 2D-CNN in flood susceptibility mapping has demonstrated excellent accuracy, precision, recall, AUC score, and F1-score. The robustness of the model emphasizes the potential of deep learning approaches in addressing complex geospatial challenges.

5.4.3 3D-CNN Model

The flood susceptibility modeling using 3D-CNN has demonstrated promising results, achieving an overall accuracy of 0.933. This high accuracy indicates the efficacy of the proposed model in accurately classifying areas prone to flooding. The precision values further substantiate the model's ability to correctly identify flood and non-flood classes, with a precision of 0.903 for flood classes and 0.964 for non- flood classes. These precision scores highlight the model's proficiency in minimizing false positives, a critical aspect when dealing with flood susceptibility mapping as misclassifying non-flood areas as susceptible could lead to unnecessary resource allocation and heightened concerns for residents.

The recall values for flood and non-flood classes, standing at 0.962 and 0.91, respectively, emphasizes the model's capacity to effectively capture instances of flooding. The high recall for flood classes indicates that the 3D-CNN model excels in identifying areas that are truly susceptible to flooding, minimizing the risk of false negatives. Conversely, the recall for non-flood classes at 0.91 indicates a satisfactory performance in correctly identifying areas that are not susceptible to flooding, mitigating the potential for neglecting regions that may require attention.

The AUC score of 0.935 is indicative of the model's ability to discriminate between flood and non-flood classes across different threshold settings. This metric is crucial in evaluating the model's overall discriminative power and its capability to handle imbalanced datasets, which is common in flood susceptibility mapping. Additionally, the F1-score, a harmonic mean of precision and recall, is a comprehensive metric that considers both false positives and false negatives. The F1-score of 0.98 achieved by the 3D-CNN model signifies a robust balance between precision and recall, showcasing its ability to minimize both types of classification errors simultaneously. This is particularly crucial in flood susceptibility modeling, where a balanced approach is essential to ensure the model's reliability in identifying vulnerable areas.

The high performance across all these metrics collectively suggests that the 3D-CNN model is a potent tool for flood susceptibility mapping than the proposed 1D-CNN and 2D-CNN models. The integration of three-dimensional convolutional operations allows the model to capture spatial relationships in the input data, considering the volumetric nature of environmental data. This capability enables the model to discern complex patterns and dependencies within the input data, contributing to its superior performance

The flood susceptibility mapping generated by the 3-dimensional CNN, as shown in Figure 16c, prominently showcases the advanced capabilities of 3D CNNs in generalizing flood vulnerability across the study area. This performance is attributed to the unique strengths of 3D CNNs, which enable them to capture the spatial patterns of flood-related features and the intricate spatial relationships and dependencies between neighboring pixels. By considering these spatial relationships and dependencies, the 3D CNN can provide a more comprehensive assessment of flood vulnerability, expanding its scope to areas that may not have directly experienced inundation.

Furthermore, the results presented here demonstrate the model's generalization ability and robustness across different scenarios. The high accuracy, precision, recall, AUC, and F1-score collectively validate the 3D-CNN model's effectiveness in flood susceptibility mapping and highlight its potential for practical applications in disaster management and mitigation efforts.

5.4.4 Conclusions

In conclusion, the development of these models opens a new frontier in geospatial analysis, enabling a deeper understanding into the complex spatial dynamics that contribute to flood susceptibility. The comprehensive approach of these CNN models aligns with the growing demand for advanced techniques in flood risk assessment, offering a valuable tool for understanding and mitigating the impacts of floods in various regions [Mosavi *et al.* 2018a]. These advanced models can significantly aid in addressing flood-related challenges by providing more accurate pre- dictions and by identifying vulnerable areas that might be overlooked by traditional methods [Kumar *et al.* 2023; Guo *et al.* 2021].

5.5 Model Sensitivity Analysis

Sensitivity analysis serves as a valuable tool in evaluating the robustness and reliability of flood susceptibility models by systematically examining the influence of changes in input variables on the model's output. This study analyzes two random manipulations for the modeling processes of both 1D-CNN and 3D-CNN, and one random manipulation for the 2D-CNN modeling process to measure the sensitivity of these models and effectively prove that their results are robust, not accidental.

The first random manipulation is achieved through 10 k-fold cross-validation, where 10 random training and testing sets are selected. Consequently, 10 CNN models were constructed for 1D-CNN, 2D-CNN, and 3D-CNN architectures for evaluation. The results of these models for 10 different settings are shown in Figure 9. The evaluation criteria demonstrate reasonable and stable fluctuations for 2D-CNN and 3D-CNN models, while for the 1D-CNN model, the evaluation criteria demonstrate unstable fluctuations.

The mean and standard deviation of accuracy for 1D-CNN model are 0.88 and 0.01, respectively. The lower value of standard deviation indicates that the accuracy score across 10 settings is clustered around the mean. Additionally, the results also indicate that the 1D-CNN model is not sensitive to the randomness of the training and test split processes resulting from 10 k-fold cross-validation and that it is robust and reliable for flood susceptibility modeling, despite demonstrating unstable fluctuations when evaluated across 10 settings.

Moreover, the 2D-CNN model achieved a mean accuracy of 0.92 and a standard deviation of 0.006, which is significantly lower than that of the 1D-CNN model. The results also indicate that the accuracies across the 10 settings are significantly clustered around the mean. As a result, the 2D-CNN model is not sensitive to the random- ness of the training and test split processes resulting from 10 k-fold cross-validation, demonstrating its robustness and reliability for flood susceptibility modeling.

Furthermore, the 3D-CNN model achieved a mean accuracy of 0.94 and a standard deviation of 0.005, which are significantly lower than the values achieved by both the 1D-CNN and 2D-CNN models. As a result, the 3D-CNN model is also not sensitive to the randomness of the training and test split processes resulting from 10 k-fold cross-validation, underscoring its robustness and reliability for flood susceptibility modeling.

The second random manipulation is achieved through information gain ratio for feature importance. Initially, the 1D-CNN and 3D-CNN models are trained and tested using the top 10 features. These features are gradually increased according to their importance to construct 6 CNN models for both architectures. The results of the 1D-CNN model and 3D-CNN model for 6 different settings are shown in Table 8 and Table 9, respectively. As can be seen, all evaluation criteria demonstrate reasonable and stable fluctuations.

The mean and standard deviation of accuracy for the 1D-CNN model are 0.86 and 0.01, respectively. The lower value of standard deviation indicates that the accuracies across the 6 settings are clustered around the mean. Additionally, the results suggest that the 1D-CNN model exhibits resilience and stability, showing insensitivity to variations in the number of input variables. This finding emphasizes the model's robustness and reliability for flood susceptibility modeling, suggesting its suitability for consistent and accurate predictions across different scenarios.

Moreover, the 3D-CNN model achieved a mean accuracy of 0.92 with a standard deviation of 0.01. Like the 1D-CNN model, the 3D-CNN model demonstrates insensitivity to changes in the number of input variables. This characteristic not only highlights the model's robustness but also reinforces its reliability for flood susceptibility modeling. The results collectively indicate that both the 1D-CNN and 3D-CNN models exhibit stable performance, making them promising candidates for accurate flood risk assessments, even in scenarios with varying input configurations.

5.6 Model Uncertainty Analysis and Quantification

To analyze the uncertainty of applying CNNs in flood susceptibility modeling, susceptibility estimates from 10 different settings for 1D-CNN, 2D-CNN, and 3D-CNN, with different training and testing sets resulting from 10 k-fold cross-validation, are considered. The mean of the 10 susceptibility estimates, each consisting of 329 250 grid cells representing the study area for each of the CNN architectures, is calculated. The values of susceptibility estimates represent the likelihood of flood susceptibility for specific grid cells. A comparison of a single susceptibility estimates for three CNN architectures, as illustrated in Figure 16, and the mean susceptibility estimate is shown in Figure 15.

As shown in Figure 15, all three dimensions of CNN have achieved significantly higher correlations of 0.93, 0.97, and 0.99 for 1D-CNN, 2D-CNN, and 3D-CNN models respectively, when comparing a single susceptibility estimate with the average susceptibility estimate, indicating that the susceptibility maps generated by these models are robust. It is significant to note that while the 1D-CNN model exhibits a higher correlation, it still lacks in its ability to produce stable predictions, as shown in Figure 15a.

Additionally, it can be observed from Figure 15c and Figure 15e that 2D-CNN and 3D-CNN models have a higher ability to produce stable predictions. The points are scattered closely to the line of best fit, indicating that a stronger relationship exists across all 10 susceptibility estimates produced by both 2D-CNN and 3D-CNN architectures.

To quantify the uncertainty of CNN flood prediction models, a measure proposed by Guzzetti *et al.* [2006] which involves comparison of mean susceptibility estimate and 2 standard deviation of the susceptibility estimate is used. As shown in Figure 15b, Figure 15d, and Figure 15f, the mean susceptibility estimate on the x-axis is compared with 2 standard deviations of the susceptibility estimates of all 3 CNN

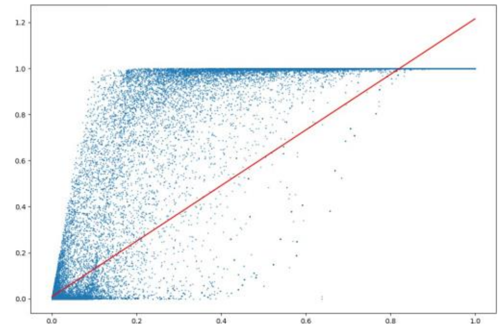

(a) Comparing a single susceptibility estimate (y-axis) with the average susceptibility estimate (x-axis) for 1D-CNN model. The linear regression is defined by $y = 0.01 + 1.21x$ and the correlation coefficient $r^2 = 0.93$.

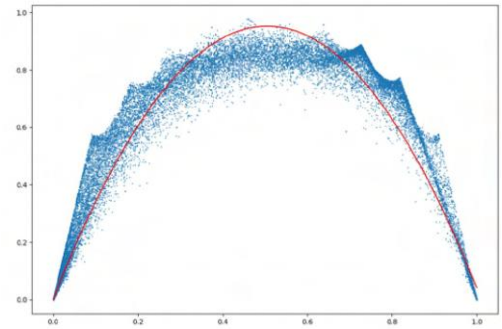

(b) The average susceptibility estimate (x-axis) against double the standard deviation of the susceptibility estimate (y-axis) for 1D-CNN. The quadratic regression line is defined by $y = -3.72x^2 + 3.76x$.

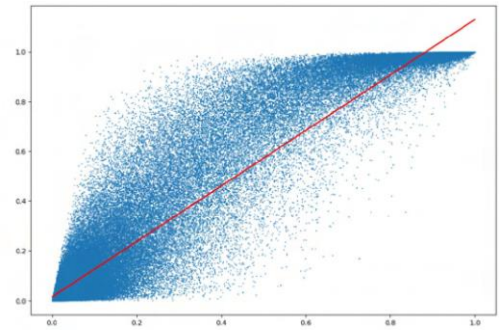

(c) Comparing a single susceptibility estimate (y-axis) with the average susceptibility estimate (x-axis) for 2D-CNN model. The linear regression is defined by $y = 0.01 + 1.11x$ and the correlation coefficient $r^2 = 0.97$.

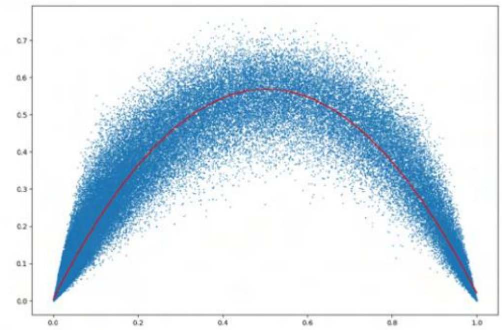

(d) The average susceptibility estimate (x-axis) against double the standard deviation of the susceptibility estimate (y-axis) for the 2D-CNN model. The quadratic regression line is defined by $y = -2.23x^2 + 2.24x$.

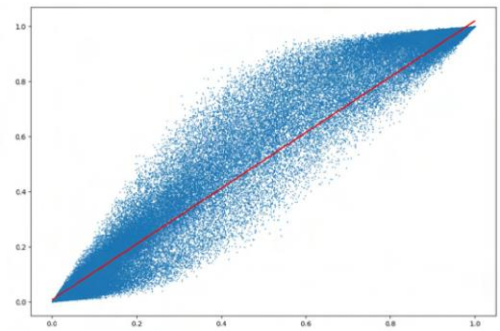

(e) Comparing a single susceptibility estimate (y-axis) with the average susceptibility estimate (x-axis) for 3D-CNN model. The linear regression is defined by $y = 0.01 + 1.01x$ and the correlation coefficient $r^2 = 0.99$.

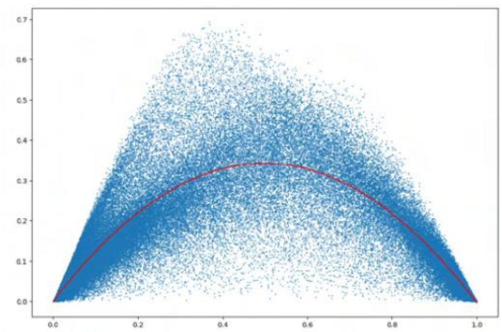

(f) The average susceptibility estimate (x-axis) against double the standard deviation of the susceptibility estimate (y-axis) for 3D-CNN. The quadratic regression line is defined by $y = -1.38x^2 + 1.37x$.

Figure 15: Uncertainty analysis of CNN models.

architectures shown in Figure 16. It can be observed across all CNN models that the standard deviation increases from low susceptibility zones to moderate and then decreases from moderate to high susceptibility zones. This indicates that all 3 CNN models have a higher ability to achieve stable predictions in low and high flood susceptibility zones. Additionally, the scatter point distribution is sparse across all instances of CNN models for moderate susceptibility zones, indicating that these models are not able to stably predict if a grid cell with moderate susceptibility in the study area can be flooded or not.

5.7 Comparison with Other Models

To prove the effectiveness of the CNN models proposed for flood susceptibility modeling, various benchmark deep learning techniques are considered for comparison: layer stacking sequential-long short-term memory (LSS-LSTM) neural network, regular deep learning neural network (DLNN), and deep learning neural network with iterative classifier optimizer (DLNN-ICO) [Bui *et al.* 2020a; Fang *et al.* 2021; Mia *et al.* 2023]. The evaluation metrics, including accuracy, F1 score, and AUC score, provide a complete view of the models' capabilities. In this study, three CNN architectures (1D-CNN, 2D-CNN, and 3D-CNN) are compared with benchmark models (LSS-LSTM, DLNN, and DLNN-ICO). The results of these benchmark models are shown in Table 10.

Firstly, the 1D-CNN model demonstrated strong performance with an AUC score of 0.935, accuracy of 0.886, and F1 score of 0.885 as shown in Table 10. These results suggest that the model effectively captures patterns in the input data, showcasing its potential for flood susceptibility modeling. While benchmark models exhibited slightly higher accuracy and F1 scores, the differences were marginal. In comparison with benchmark models, the accuracy of 1D-CNN is lower than the achieved by DLNN and LSS-LSTM which are 0.921 and 0.920 respectively. The F1 score varies with DLNN achieving higher value of 0.922 and 1D-CNN achieving least value of 0.885. The AUC scores reflected a competitive performance, with DLNN leading at 0.96, closely followed by LSS-LSTM at 0.958, 1D-CNN at 0.935, and DLNN-ICO at 0.917.

Moreover, the 2D-CNN model surpassed the 1D-CNN, achieving an AUC score of 0.935, accuracy of 0.913, and F1 score of 0.912, as shown in Table 10. The utilization of spatial information in 2D-CNN appears to enhance the model's discriminative power, leading to improved predictive performance. In comparison with bench- mark models, the 2D-CNN's accuracy of 0.913 falls slightly below DLNN's 0.9215 but outperforms LSS-LSTM's 0.9195. The F1 score of 0.912 is in close proximity to DLNN's 0.922, underscoring its effectiveness in balancing precision and recall. The AUC score of 0.97 2D-CNN outperforms the achieved by the benchmark models, emphasizing its consistent discriminatory power in distinguishing flood susceptibility classes.

Finally, it is evident that the 3D-CNN model consistently outperforms LSS-LSTM, DLNN, and DLNN-ICO when evaluated using various performance matrices as shown in Table 10. The benchmark models, while achieving competitive results, fall short of the performance achieved by the 3D-CNN. LSS-LSTM achieved an AUC score of 0.958 and accuracy of 0.9195, showcasing competitive performance in capturing flood susceptibility. DLNN demonstrated an AUC score of 0.96, accuracy of 0.921, and F1 score of 0.922, indicating its effectiveness in predictive modeling.

Table 10: Table showing the results of the proposed CNN and the Benchmark model.

Models	Accuracy	F1 Score	AUC Score
1D-CNN	0.886	0.885	0.935
2D-CNN	0.913	0.912	0.97
3D-CNN	**0.933**	**0.933**	**0.980**
DLNN	0.921	0.922	0.960
DLNN-ICO		0.870	0.917
LSS-LSTM	0.920		0.958

DLNN-ICO, while achieving an F1 score of 0.87, lagged in terms of AUC score with a value of 0.917. This suggests that while DLNN-ICO may perform well in certain aspects, its overall discriminatory power may not match that of the 3D-CNN.

5.8 Spatial Distribution of Susceptibility

Flood susceptibility maps play a crucial role in unraveling and forecasting areas prone to flooding, offering valuable insights into the intricate relationship between the landscape and the occurrence of floods. The connection between flood susceptibility maps and actual flood events relies on the integration of diverse spatial information, facilitating a more informed assessment of flood risk. These maps are essentially predictive tools utilizing spatial data, such as topography, land use, and hydrological features, to estimate the likelihood of flooding in different regions. As shown in Figure 16, the maps pinpoint areas with higher vulnerability based on historical flood occurrences and identified flood conditioning factors. By comprehending the spatial patterns and relationships within the landscape, these maps become proactive instruments for risk mitigation and disaster management.

The flood susceptibility index on these maps in Figure 16 is classified into five classes: 'very low,' 'low,' 'moderate,' 'high,' and 'very high'. Where 'very low' represents areas with minimal susceptibility to flooding, 'low' implies a slightly higher risk, 'moderate' indicates a moderate risk, 'high' suggests a significant risk, and 'very high' represents the highest susceptibility level. This classification is achieved using the natural breaks (Jenks) method [Jenks 1967], a technique grouping data values into meaningful categories based on their distribution characteristics. Additionally, the risk proportion of the predicted flood susceptibility zones in the study area are shown in Table 11.

Examining the spatial patterns of flood susceptibility across the study area, as indicated by the CNN model results, reveals distinctive risk zones. In the 1D-CNN model, most of the study area exhibits very low flood susceptibility (96.4%), with localized areas of higher susceptibility, particularly in the very high-risk category (2.53%). The 2D-CNN model demonstrates a more diverse risk distribution, with a substantial portion having very low susceptibility (74.19%) and significant areas of higher risk, notably in the very high-risk category (10.93%). The 3D-CNN model emphasizes a spatial pattern where a large portion has very low susceptibility (84.10%), but with a concentration of high and very high-risk areas, comprising 12.34% of the total area.

In terms of geographical characteristics, it is noteworthy that high susceptibility zones are often associated with low-elevation areas proximate to water bodies and

Table 11: Table showing the risk proportion of predicted flood susceptibility zones in the catchment area and likelihood range for each susceptibility zones.

Flood Susceptibility Zone	1D-CNN	2D-CNN	3D-CNN
Very Low	(0-0.10)-96.4%	(0-0.09)-74.19%	(0-0.11)-84.10%
Low	(0.10-0.35)-0.42%	(0.09-0.31)-6.52%	(0.11 -0.36)-1.33%
Moderate	(0.35-0.59)-0.30%	(0.31-0.56)-3.92%	(0.36-0.64)-0.97%
High	(0.59-0.80)-0.34 %	(0.56-0.80)-4.45%	(0.64-0.89)-1.26%
Very High	(0.80-1)-2.53%	(0.80-1)-10.93%	(0.89-1)-12.34%

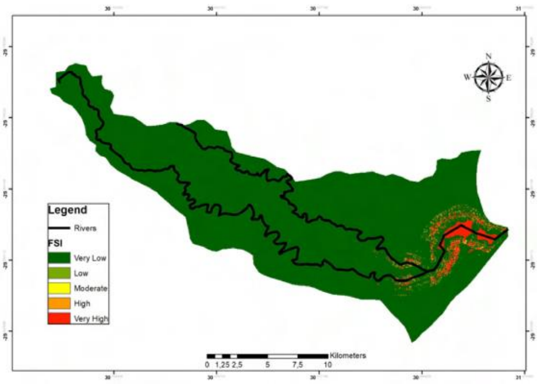

(a) 1D-CNN

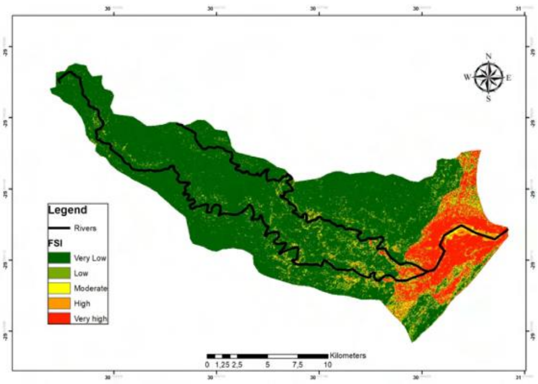

(b) 2D-CNN

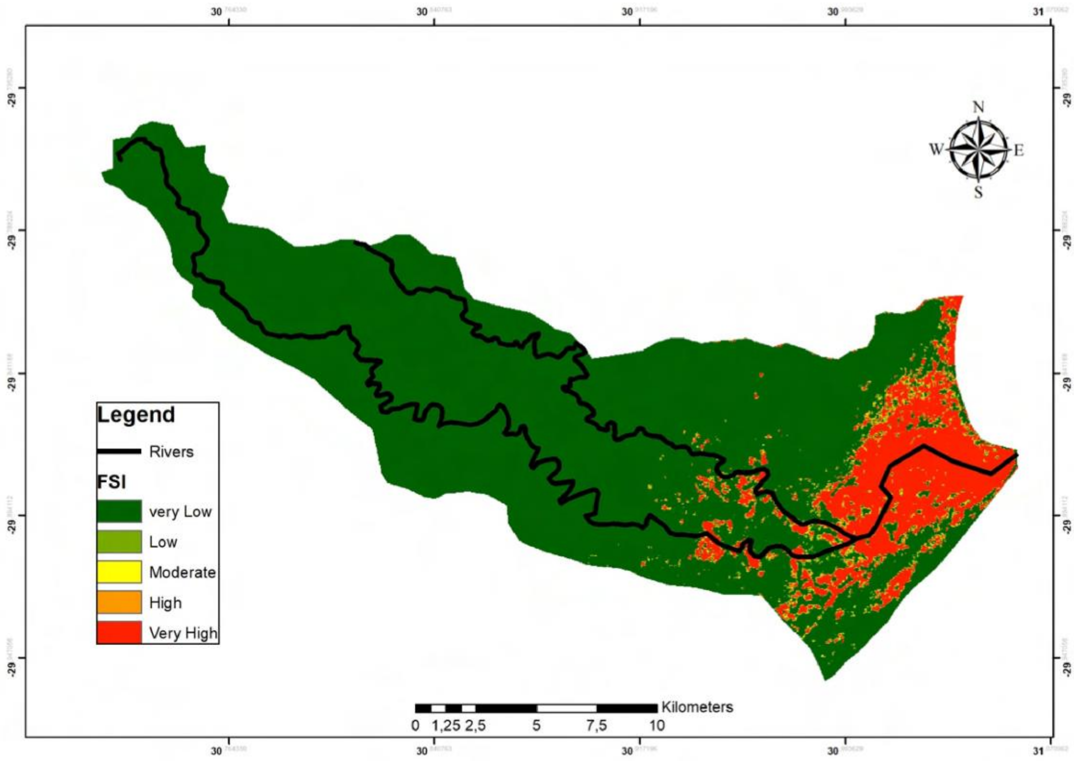

(c) 3D-CNN.

Figure 16: uMhlatuzana River catchment flood susceptibility maps of different CNN models.

coastal regions. Similar conclusions have been reached by various studies [Mojaddadi *et al.* 2017; Wang *et al.* 2020a; Fang *et al.* 2021]. These areas, identified as high and very high-risk zones by all three CNN models, demand focused attention in flood risk management planning. Despite variations among the models, there is a consistent identification of areas with higher susceptibility. Investigating model discrepancies, potentially related to assumptions or input data, is crucial to enhance the accuracy of risk assessments.

An integrated approach, considering insights from all three models, can provide a more comprehensive understanding of flood susceptibility, allowing for a nuanced interpretation of risk patterns. Areas identified as high and very high-risk zones should be targeted for localized interventions, such as improved drainage systems, early warning systems, and community awareness programs.

Importantly, high susceptibility zones, particularly those in low-elevation areas near water bodies and coastal regions, require specific attention due to their heightened vulnerability [Woodruff *et al.* 2013]. These areas often serve as critical focal points for flood risk mitigation efforts. Continuous monitoring and adaptation of strategies based on observed outcomes will contribute to building more resilient communities in the face of potential flooding events.

5.9 Practical Implications

The findings from the CNN models hold profound practical implications for effective flood risk management. They offer valuable insights that can guide decision-making in diverse areas such as land-use planning, disaster preparedness, and infrastructure development.

The outcomes of the CNN models in flood susceptibility modeling carry significant real-world implications for managing flood risks, providing valuable insights that can shape various aspects of land-use planning, disaster preparedness, and infrastructure development. Here are some key practical implications:

The high accuracy, F1 score, and AUC score achieved by the 3D-CNN model emphasizes its effectiveness in identifying areas at a higher risk of flooding. This precision informs land-use planning by identifying zones where development should be limited, or specific measures should be implemented to mitigate flood risks. Decision- makers can utilize these findings to designate land for infrastructure projects that are less vulnerable to flooding, thus minimizing potential damages.

Accurate floods predictions play an important role in disaster preparedness. The CNN models, especially the 3D-CNN, provide a reliable foundation for anticipating flood-prone areas. Emergency response teams can leverage this information to develop more effective evacuation plans, strategically allocate resources, and establish early warning systems tailored to specific regions. Timely and precise information enhances overall preparedness and response to flood events, potentially minimizing the impact on communities.

Understanding the flood susceptibility of different regions is crucial for guiding infrastructure development. The findings from the 3D-CNN model indicate that it surpasses the performance of benchmark models, showcasing its potential for accurately assessing flood risk in various contexts. This information guides decisions on where to invest in resilient infrastructure and where additional protective measures are required. Avoiding construction in high-risk zones and enhancing infrastructure in vulnerable areas can contribute to more resilient communities.

The CNN models can help municipalities and institutions anticipate the impact of climate change on flood patterns. This information is crucial for long-term planning, enabling municipalities to develop strategies for climate change adaptation and resilience. Additionally, municipalities and institutions can use CNN-based flood susceptibility models to allocate resources effectively during both the response and recovery phases. This includes deploying personnel, equipment, and financial resources based on the predicted severity of flooding in different areas.

In conclusion, the practical implications of the CNN models results for flood risk management are extensive. These models serve as a powerful tool for decision-makers, urban planners, and emergency response teams to make informed choices in land-use planning, disaster preparedness, and infrastructure development. The precision and accuracy of the CNN models contribute to more effective and targeted strategies, ultimately enhancing the resilience of communities in the face of potential flood events.

5.10 Conclusions

The findings from this study emphasize the intricate interplay between various flood conditioning factors and their impact on flood susceptibility within the uMhlatuzana River Catchment. The analysis revealed that soil types such as Acrisols and Fluvisols, lithology, slope shape, and land use significantly influence flood occurrences due to their low permeability and runoff characteristics. The study also highlighted the importance of topographic features, with flat and concave slopes, low elevation areas, and regions near rivers being more prone to flooding. The application of CNN models, particularly the 3D-CNN, demonstrated great performance in accurately predicting flood-prone areas, emphasizing the model's ability to capture complex spatial patterns and dependencies. This advanced modeling approach pro- vides a robust tool for flood risk assessment, offering valuable insights for disaster management and mitigation strategies.

In conclusion, the integration of CNN models in flood susceptibility mapping represents a significant advancement in geospatial analysis, enabling more precise and reliable predictions of flood risk. The study's findings have practical implications for land-use planning, infrastructure development, and disaster preparedness, guiding decision-makers in implementing effective flood mitigation measures. The high accuracy and reliability of the 3D-CNN model highlight its potential for enhancing flood risk management practices.

Chapter 6

Conclusions

This dissertation aimed to address two primary research questions: identifying the critical predictors of flood vulnerability within the uMhlatuzana River catchment and evaluating the accuracy, robustness, and reliability of the proposed CNN modeling process in predicting flood vulnerability. Through a comprehensive analysis using frequency ratio (FR) and information gain ratio (IGR), the study identified key predictors such as topographic wetness index (TWI) and rainfall, which significantly influence flood susceptibility. The CNN models, particularly the 3D-CNN, demonstrated high accuracy and reliability in predicting flood-prone areas, underscoring the effectiveness of deep learning techniques in flood susceptibility modeling.

The objectives of generating flood vulnerability maps and developing methodologies to quantify uncertainties were successfully achieved. The CNN models provided detailed and accurate flood susceptibility maps, which can be integrated into real-time monitoring systems for timely alerts and practical insights. The study also contributed to the existing knowledge on machine learning applications in flood susceptibility modeling, particularly in the South African context, and highlighted the importance of deep learning techniques in enhancing flood prediction and risk management. These findings support the global need to build resilience against climate-related issues, offering valuable tools for disaster preparedness and infrastructure planning.

6.1 Summary of Results

The 1D-CNN, 2D-CNN, and 3D-CNN models were developed and evaluated for flood susceptibility modeling, each exhibiting varying degrees of performance. The 1D-CNN demonstrated a commendable AUC score of 0.935, accuracy of 0.886, and F1 score of 0.885. While competitive with the benchmark LSS-LSTM in terms of accuracy and F1 score, the 1D-CNN fell slightly behind in AUC score. This model's strength lies in its ability to effectively capture spatial patterns in flood-prone areas.

The 2D-CNN model showcased notable improvements, achieving an AUC score of 0.935, accuracy of 0.913, and F1 score of 0.912. This model outperformed both the 1D-CNN and the benchmark LSS-LSTM, particularly excelling in precision and recall. The 2D-CNN's capability to analyze spatial relationships in two dimensions enhances its suitability for flood susceptibility modeling, making it a promising tool for applications requiring detailed spatial analysis.

The 3D-CNN model emerged as the top performer, attaining an AUC score of 0.98, accuracy of 0.933, and F1 score of 0.933. This model's incorporation of three-dimensional information proved highly effective, surpassing both the 1D-CNN and 2D-CNN models as well as outperforming the benchmark models across all metrics. The 3D- CNN's exceptional accuracy and discriminatory ability make it an asset for applications demanding highly precise flood susceptibility predictions.

In applications such as flood risk assessment, emergency response planning, and land-use management, the CNN models offer significant advantages. Their ability to process and analyze spatial features at different scales, particularly evident in the 2D-CNN and 3D-CNN, enhances their utility in capturing complex patterns associated with flood susceptibility. These models can contribute to more informed decision-making by providing accurate and timely information to authorities and stakeholders. Furthermore, their adaptability to diverse geographical regions and datasets positions CNN models as versatile tools for addressing the evolving challenges of flood management and mitigation strategies. As technology continues to advance, the application of CNN models in flood susceptibility modeling is poised to play a pivotal role in building resilient and sustainable communities.

6.2 Limitations

A significant limitation of CNN models in flood susceptibility modeling is their dependence on the quality and representativeness of training data. Incomplete or biased datasets can lead to suboptimal model performance, as the model may fail to generalize well to diverse environmental conditions. Ensuring the availability of comprehensive and unbiased datasets is crucial for enhancing the reliability and robustness of CNN-based flood susceptibility models.

CNN models may struggle with generalizing patterns to unseen regions or scenarios. Overfitting to the training data and insufficient representation of diverse geographical contexts can impact the model's ability to provide accurate predictions in real-world applications. Rigorous testing on varied datasets is necessary to evaluate and address these generalization challenges.

The implementation of CNN models, particularly those involving three-dimensional convolutional operations, often requires substantial computational resources. This poses a limitation in resource-constrained environments, hindering the practical adoption of CNN models for flood susceptibility modeling. Exploring more efficient computational strategies is essential to make these models more widely applicable.

Flood susceptibility is inherently influenced by temporal dynamics, including seasonal variations and climate changes. CNN models, primarily designed for spatial analysis, may not inherently capture these temporal aspects. This limitation necessitates additional considerations, or hybrid approaches to incorporate temporal dynamics effectively into flood susceptibility modeling.

6.3 Future Research Directions

This research lays the foundation for future endeavors in flood susceptibility modeling. To address the identified limitations, future research could focus on enhancing data quality through advanced remote sensing techniques and the integration of real-time data streams. Additionally, expanding the study to encompass diverse geographical regions would contribute to the development of more universally applicable models.

Future research can be focused on enhancing the ability of convolutional neural network (CNN) models to perform well on data they have not seen during training. This could involve exploration into transfer learning approaches, domain adaptation methods, or hybrid models that integrate CNNs with other machine learning techniques. This exploration aims to elevate adaptability to unforeseen scenarios and diverse regions.

Moreover, efforts in flood susceptibility modelling can be directed towards investigating and implementing more computationally efficient strategies for CNN models, particularly those using three-dimensional convolutional operations. This includes the adoption of model compression techniques, parallel processing, or hardware acceleration to make CNN models more accessible in resource-constrained environments.

In the context of flood susceptibility modeling, an important area for future research can involve the integration of climate change scenarios. Understanding the evolving climate patterns and their impact on flood occurrences is essential for effective risk assessment and management.

Bibliography

[Acreman and Holden 2013] M Acreman and J Holden. How wetlands affect floods. *Wetlands*, 33:773–786, 2013.

[Adeyeri *et al.* 2017] OE Adeyeri, KA Ishola, and EC Okogbue. Climate change and coastal floods: the susceptibility of coastal areas of Nigeria. *Journal of Coastal Zone Management*, 20(2):1000443, 2017.

[Afriyanie *et al.* 2022] D Afriyanie, Miga Magenika Julian, and Henky Nugraha. Urban flood resilience through spatial plan in Bandung city, Indonesia. *IOP Conference Series Earth and Environmental Science*, 986:012052, 2022.

[Al-Sabhan *et al.* 2003] W Al-Sabhan, M Mulligan, and GA Blackburn. A real-time hydrological model for flood prediction using GIS and the www. *Computers, Environment and Urban Systems*, 27(1):9–32, 2003.

[Ali *et al.* 2020] Sk Ajim Ali, Farhana Parvin, Quoc Bao Pham, Matej Vojtek, Jana Vojteková, Romulus Costache, Nguyen Thi Thuy Linh, Hong Quan Nguyen, Ateeque Ahmad, and Mohammad Ali Ghorbani. GIS-based comparative assessment of flood susceptibility mapping using hybrid multi-criteria decision-making approach, naïve Bayes tree, bivariate statistics and logistic regression: a case of Topl'a basin, Slovakia. *Ecological Indicators*, 117:106620, 2020.

[Anguita *et al.* 2012] Davide Anguita, Luca Ghelardoni, Alessandro Ghio, Luca Oneto, Sandro Ridella, et al. The'k'in k-fold cross validation. *ESANN*, 441–446, 2012.

[Arnaud *et al.* 2002] Patrick Arnaud, Christophe Bouvier, Leonardo Cisneros, and Ramon Dominguez. Influence of rainfall spatial variability on flood prediction. *Journal of Hydrology*, 260(1-4):216–230, 2002.

[Band *et al.* 2020] Shahab S. Band, Saeid Janizadeh, Subodh Chandra Pal, Asish Saha, Rabin Chakrabortty, Assefa M. Melesse, and Amir Mosavi. Flash flood susceptibility modeling using new approaches of hybrid and ensemble tree-based machine learning algorithms. *Remote Sensing*, 12(21):3568, 2020.

[Bankoff and Lee 1986] SG Bankoff and SC Lee. A critical review of the flooding literature. *Multiphase Science and Technology*, 3:95–180, 1986.

[Bevc 1997] Dimitri Bevc. Flooding the topography: Wave-equation datuming of land data with rugged acquisition topography. *Geophysics*, 62(5):1558–1569, 1997.

[Beven *et al.* 1984] KJ Beven, MJ Kirkby, N Schofield, and AF Tagg. Testing a physically-based flood forecasting model (topmodel) for three UK catchments. *Journal of Hydrology*, 69(1-4):119–143, 1984.

[Bolstad and Stowe 1994] PV Bolstad and T Stowe. An evaluation of DEM accuracy: elevation, slope, and aspect. *Photogrammetric Engineering & Remote Sensing*, 60(11):1327–1332, 1994.

[Bopape *et al.* 2021] Mary-Jane M Bopape, Ezekiel Sebego, Thando Ndarana, Bathobile Maseko, Masindi Netshilema, Morne Gijben, Stephanie Landman, Elelwani Phaduli, Gift Rambuwani, Louis Van Hemert, et al. Evaluating South African Weather Service information on Idai tropical cyclone and kwaZulu-Natal flood events. *South African Journal of Science*, 117(3-4):1–13, 2021.

[Botzen *et al.* 2013] WJW Botzen, JCJH Aerts, and JCJM Van den Bergh. Individual preferences for reducing flood risk to near zero through elevation. *Mitigation and Adaptation Strategies for Global Change*, 18(2):229–244, 2013.

[Bracken *et al.* 2008] LJ Bracken, NJ Cox, and J Shannon. The relationship between rainfall inputs and flood generation in south–east Spain. *Hydrological Processes: An International Journal*, 22(5):683–696, 2008.

[Brivio *et al.* 2002] PA Brivio, R Colombo, M Maggi, and R Tomasoni. Integration of remote sensing data and GIS for accurate mapping of flooded areas. *International Journal of Remote Sensing*, 23(3):429–441, 2002.

[Brown *et al.* 2017] P Brown, A Daigneault, and D Gawith. Climate change and the economic impacts of flooding on Fiji. *Climate and Development*, 9(6):493–504, 2017.

[Bui *et al.* 2019] DT Bui, P Tsangaratos, P-TT Ngo, TD Pham, and BT Pham. Flash flood susceptibility modeling using an optimized fuzzy rule based feature selection technique and tree based ensemble methods. *Science of the Total Environment*, 668:1038–1054, 2019.

[Bui *et al.* 2020a] Dieu Tien Bui, Nhat-Duc Hoang, Francisco Martínez-Álvarez, Phuong-Thao Thi Ngo, Pham Viet Hoa, Tien Dat Pham, Pijush Samui, and Romulus Costache. A novel deep learning neural network approach for predicting flash flood susceptibility: A case study at a high frequency tropical storm area. *Science of the Total Environment*, 701:134413, 2020.

[Bui *et al.* 2020b] Quang-Thanh Bui, Quoc-Huy Nguyen, Xuan Linh Nguyen, Vu Dong Pham, Huu Duy Nguyen, and Van-Manh Pham. Verification of novel integrations of swarm intelligence algorithms into deep learning neural network for flood susceptibility mapping. *Journal of Hydrology*, 581:124379, 2020.

[Bui *et al.* 2022] QD Bui, C Luu, SH Mai, HT Ha, HT Ta, and BT Pham. Flood risk mapping and analysis using an integrated framework of machine learning models and analytic hierarchy process. *Risk Analysis*, 43:1478–1495, 2022.

[Busayo *et al.* 2022] ET Busayo, AM Kalumba, GA Afuye, AO Olusola, 0 Ololade, and IR Orimoloye. Rediscovering South Africa: Flood disaster risk management through ecosystem-based adaptation. *Environmental and Sustainability Indicators*, 15:100–175, 2022.

[Cai and Yu 2022] Bo Cai and Yaoxiang Yu. Flood forecasting in urban reservoir using hybrid recurrent neural network. *Urban Climate*, 42:101086, 2022.

[Chaerani *et al.* 2020] Diah Chaerani, Muttaqien Rodhiya Robbi, Elis Hertini, Endang Rusyaman, and Erick Paulus. Determining flood protection strategy with uncertain parameter using adjustable robust counterpart methodology. *Jurnal Ilmu Dasar*, 21(1);27-34, 2020.

[Chapi *et al.* 2017] K Chapi, VP Singh, A Shirzadi, H Shahabi, DT Bui, BT Pham, and K Khosravi. A novel hybrid artificial intelligence approach for flood susceptibility assessment. *Environmental Modelling & Software*, 95:229–245, 2017.

[Chen *et al.* 2016] Yushi Chen, Hanlu Jiang, Chunyang Li, Xiuping Jia, and Pedram Ghamisi. Deep feature extraction and classification of hyperspectral images based on convolutional neural networks. *IEEE Transactions on Geoscience and Remote Sensing*, 54(10):6232–6251, 2016.

[Chen *et al.* 2023] Y. Chen, X. Zhang, K. Yang, S. Zeng, and A. Hong. Modeling rules of regional flash flood susceptibility prediction using different machine learning models. *Frontiers in Earth Science*, 11:1117004, 2023.

[Chowdhuri *et al.* 2020] I Chowdhuri, SC Pal, and R Chakrabortty. Flood susceptibility mapping by ensemble evidential belief function and binomial logistic regression model on river basin of eastern India. *Advances in Space Research*, 65(5):1466–1489, 2020.

[Cole *et al.* 2018] Megan J Cole, RM Bailey, JDS Cullis, and MG New. Spatial inequality in water access and water use in South Africa. *Water Policy*, 20(1):37–52, 2018.

[Costache *et al.* 2021] Romulus Costache, Alireza Arabameri, Thomas Blaschke, Quoc Bao Pham, Binh Thai Pham, Manish Pandey, Aman Arora, Nguyn Th Thùy Linh, and Iulia Costache. Flash-flood potential mapping using deep learning, alternating decision trees and data provided by remote sensing sensors. *Sensors*, 21(1):280, 2021.

[Dano *et al.* 2019] Umar Lawal Dano, Abdul-Lateef Balogun, Abdul Nasir Matori, Khmaruzzaman Wan Yusouf, Ismaila Rimi Abubakar, Mohamed Ahmed Said Mohamed, Yusuf A. Aina, and Biswajeet Pradhan. Flood susceptibility mapping using GIS-based analytic network process: A case study of Perlis, Malaysia. *Water*, 11(3):615, 2019.

[De Roo 1998] APJ De Roo. Modelling runoff and sediment transport in catchments using GIS. *Hydrological Processes*, 12(6):905–922, 1998.

[Dong *et al.* 2010] Jia-Jyun Dong, Jui-Yu Hsu, Wen-Jie Wu, Toshi Shimamoto, Jih-Hao Hung, En-Chao Yeh, Yun-Hao Wu, and Hiroki Sone. Stress-dependence of the permeability and porosity of sandstone and shale from TCDP Hole-A. *International Journal of Rock Mechanics and Mining Sciences*, 47(7):1141–1157, 2010.

[Doswell *et al.* 1996] CA Doswell, HE Brooks, and RA Maddox. Flash flood forecasting: An ingredients-based methodology. *Weather and Forecasting*, 11(4):560– 581, 1996.

[Douben 2006] K Douben. Characteristics of river floods and flooding: a global overview, 1985–2003. *Irrigation and Drainage: The Journal of the International Commission on Irrigation and Drainage*, 55(S1):S9–S21, 2006.

[Du *et al.* 2010] W. Du, G. FitzGerald, M. Clark, and X. Hou. Health impacts of floods. *Prehospital and Disaster Medicine*, 25:265–272, 2010.

[Duman *et al.* 2005] TY Duman, T Çan, Ö Emre, M Keçer, A Dog˘an, S¸ Ates¸, and S Durmaz. Landslide inventory of northwestern Anatolia, Turkey. *Engineering Geology*, 77(1-2):99–114, 2005.

[Evans *et al.* 2020] B. Evans, A. S. Chen, S. Djordjevic´, J. L. Webber, A. G. Gómez, and J. R. Stevens. Investigating the effects of pluvial flooding and climate change on traffic flows in Barcelona and Bristol. *Sustainability*, 12:2330, 2020.

[Fang *et al.* 2020] Zhice Fang, Yi Wang, Ling Peng, and Haoyuan Hong. Integration of convolutional neural network and conventional machine learning classifiers for landslide susceptibility mapping. *Computers & Geosciences*, 139:104470, 2020.

[Fang *et al.* 2021] Zhice Fang, Yi Wang, Ling Peng, and Haoyuan Hong. Predicting flood susceptibility using LSTM neural networks. *Journal of Hydrology*, 594:125734, 2021.

[Fanta and Sime 2022] Sewmehon Sisay Fanta and Chala Hailu Sime. Performance assessment of SWAT and HEC-HMS model for runoff simulation of Toba watershed, Ethiopia. *Sustainable Water Resources Management*, 8:1–16, 2022.

[Feng and Beighley 2020] Dongmei Feng and R. Edward Beighley. Identifying uncertainties in hydrologic fluxes and seasonality from hydrologic model components for climate change impact assessments. *Hydrology and Earth System Sciences*, 24(5):2253-2267, 2020.

[Figueiredo *et al.* 2009] Tomás Figueiredo, Felícia Fonseca, Alice Bompastor, and José Andrade. Hydrological properties of soils in scrublands of Montesinho Natural Park, NE Portugal: a map-based approach. In *EcoHCC'09, International Conference on Ecohydrology and Climate Change. Tomar*, 2009.

[Furquim *et al.* 2016] G Furquim, G Pessin, BS Faiçal, EM Mendiondo, and Jó Ueyam. Improving the accuracy of a flood forecasting model by means of machine learning and chaos theory. *Neural Computing and Applications*, 27(5):1129–1141, 2016.

[Fushiki 2011] Tadayoshi Fushiki. Estimation of prediction error by using k-fold cross-validation. *Statistics and Computing*, 21:137–146, 2011.

[Grab and Nash 2024] SW Grab and David J Nash. A new flood chronology for KwaZulu-Natal (1836–2022): The April 2022 Durban floods in historical context. *South African Geographical Journal*, 106(4):476-497, 2024.

[Guo *et al.* 2021] Kaihua Guo, Mingfu Guan, and Dapeng Yu. Urban surface water flood modelling–a comprehensive review of current models and future challenges. *Hydrology and Earth System Sciences*, 25(5):2843–2860, 2021.

[Guzzetti *et al.* 2006] Fausto Guzzetti, Paola Reichenbach, Francesca Ardizzone, Mauro Cardinali, and Mirco Galli. Estimating the quality of landslide susceptibility models. *Geomorphology*, 81(1-2):166–184, 2006.

[Harter *et al.* 2004] Thomas Harter, Jan W Hopmans, RA Feddes, et al. *Role of vadose zone flow processes in regional scale hydrology: Review, opportunities and challenges*. Kluwer, 2004.

[Hennig and Schuler 2012] Philipp Hennig and Christian J Schuler. Entropy search for information-efficient global optimization. *Journal of Machine Learning Research*, 13(6):1809-1837, 2012.

[Hou *et al.* 2018] Jingming Hou, Kaihua Guo, Feifei Liu, Hao Han, Qiuhua Liang, Yu Tong, and Peng Li. Assessing slope forest effect on flood process caused by a short-duration storm in a small catchment. *Water*, 10(9):1256, 2018.

[Huang *et al.* 2019] H. Huang, X. Chen, X. Wang, X. Wang, and L. Liu. A depression-based index to represent topographic control in urban pluvial flooding. *Water*, 11:2115, 2019.

[Irvine and Israel 2022] John M Irvine and Steven A Israel. Configuring CNN architectures for performance. *Geospatial Informatics XII*, 12099:94–100, 2022.

[Islam *et al.* 2021] Abu Reza Md Towfiqul Islam, Swapan Talukdar, Susanta Mahato, Sonali Kundu, Kutub Uddin Eibek, Quoc Bao Pham, Alban Kuriqi, and Nguyen Thi Thuy Linh. Flood susceptibility modelling using advanced ensemble machine learning models. *Geoscience Frontiers*, 12(3):101075, 2021.

[Israel *et al.* 2021] Ieuan M. Israel, Steven A. Israel, and John M. Irvine. Factors influencing CNN performance. *2021 IEEE Applied Imagery Pattern Recognition Workshop (AIPR)*, pages 1–4, 2021.

[Izzard and Hicks 1946] Carl F Izzard and WI Hicks. Hydraulics of runoff from developed surfaces. *Proc. Highway Research Board*, 26:129–150, 1946.

[Janizadeh *et al.* 2019] S. Janizadeh, M. Avand, A. Jaafari, T. V. Phong, M. Bayat, E. Ahmadisharaf, I. Prakash, B. T. Pham, and S. Lee. Prediction success of machine learning methods for flash flood susceptibility mapping in the Tafresh watershed, Iran. *Sustainability*, 11:5426, 2019.

[Jenks 1967] George F Jenks. The data model concept in statistical mapping. *International year book of Cartography*, 7:186–190, 1967.

[Jones *et al.* 1998] Donald R Jones, Matthias Schonlau, and William J Welch. Efficient global optimization of expensive black-box functions. *Journal of Global Optimization*, 13:455–492, 1998.

[Jouma and Dadaser-Celik 2021] Nada Jouma and Filiz Dadaser-Celik. Assessing hydrologic alterations due to reservoirs and intensified irrigation in a semi-arid agricultural river basin using SWAT. *Irrigation and Drainage*, 71(2):452-471, 2021.

[Kabanda and Palamuleni 2013] Tabaro H Kabanda and LG Palamuleni. Land use/cover changes and vulnerability to flooding in the Harts catchment, South Africa. *South African Geographical Journal*, 95(1):105–116, 2013.

[Kabir *et al.* 2020] Syed Kabir, Sandhya Patidar, Xilin Xia, Qiuhua Liang, Jeffrey Neal, and Gareth Pender. A deep convolutional neural network model for rapid prediction of fluvial flood inundation. *Journal of Hydrology*, 590:125481, 2020.

[Kadavi *et al.* 2018] PR Kadavi, C-W Lee, and S Lee. Application of ensemble-based machine learning models to landslide susceptibility mapping. *Remote Sensing*, 10(8):1252, 2018.

[Khosravi *et al.* 2019] Khabat Khosravi, Himan Shahabi, Binh Thai Pham, Jan Adamowski, Ataollah Shirzadi, Biswajeet Pradhan, Jie Dou, Hai-Bang Ly, Gyula Gróf, Huu Loc Ho, et al. A comparative assessment of flood susceptibility modeling using multi-criteria decision-making analysis and machine learning methods. *Journal of Hydrology*, 573:311–323, 2019.

[Ki and Rasmussen 2006] Williams Christopher Ki and Carl Edward Rasmussen. Gaussian processes for machine learning. *International Journal of Neural Systems*, 14, 2006.

[Koch and Koch 1990] Karl-Rudolf Koch and Karl-Rudolf Koch. Bayes' theorem. *Bayesian Inference with Geodetic Applications*, pages 4–8, 1990.

[Kumar *et al.* 2023] Vijendra Kumar, Kul Vaibhav Sharma, Tommaso Caloiero, Darshan J Mehta, and Karan Singh. Comprehensive overview of flood modeling approaches: A review of recent advances. *Hydrology*, 10(7):141, 2023.

[Lee *et al.* 2017] Sunmin Lee, Jeong-Cheol Kim, Hyung-Sup Jung, Moung Jin Lee, and Saro Lee. Spatial prediction of flood susceptibility using random-forest and boosted-tree models in Seoul metropolitan city, Korea. *Geomatics Natural Hazards and Risk*, 8(2):1185-1203, 2017.

[Li *et al.* 2017] Langping Li, Hengxing Lan, Changbao Guo, Yongshuang Zhang, Quanwen Li, and Yuming Wu. A modified frequency ratio method for landslide susceptibility assessment. *Landslides*, 14(2):727–741, 2017.

[Li *et al.* 2023] Xiaofei Li, Hainan Guo, Langxing Xu, and Zezheng Xing. Bayesian- based hyperparameter optimization of 1d-cnn for structural anomaly detection. *Sensors*, 23(11):5058, 2023.

[Liu *et al.* 2021] Jun Liu, Jiyan Wang, Junnan Xiong, Weiming Cheng, Huaizhang Sun, Zhiwei Yong, and Nan Wang. Hybrid models incorporating bivariate statistics and machine learning methods for flash flood susceptibility assessment based on remote sensing datasets. *Remote Sensing*, 13(23):4945, 2021.

[Makhaya 2022] Chris Makhaya. *KZN flood disaster: 'Water was quickly rising and I saw that my house would fall'*, May 2022.

[Mashaly and Ghoneim 2018] Jehan Mashaly and Eman Ghoneim. Flash flood hazard using optical, radar, and stereo-pair derived DEM: Eastern Desert, Egypt. *Remote Sensing*, 10(8):1204, 2018.

[Maxwell and Condon 2021] RM Maxwell and LE Condon. A physics-informed, machine learning emulator of a 2d surface water model: what temporal networks and simulation-based inference can help us learn about hydrologic processes. *Water*, 13:3633, 2021.

[Mia *et al.* 2023] Md. Uzzal Mia, Tahmida Naher Chowdhury, Rabin Chakrabortty, Subodh Chandra Pal, Muhammad Khalid, Romulus Costache, and Abu Reza Md. Islam. Flood susceptibility modeling using an advanced deep learning-based iterative classifier optimizer. *Land*, 12(4):810, 2023.

[Mockus 1998] J. Mockus. *The application of Bayesian methods for seeking the extremum*, 1998.

[Mojaddadi *et al.* 2017] H Mojaddadi, B Pradhan, H Nampak, N Ahmad, and AH Ghazali. Ensemble machine-learning-based geospatial approach for flood risk assessment using multi-sensor remote-sensing data and GIS. *Geomatics, Natural Hazards and Risk*, 8(2):1080–1102, 2017.

[Moore and Wilson 1992] ID Moore and JP Wilson. Length-slope factors for the revised universal soil loss equation: Simplified method of estimation. *Journal of Soil and Water Conservation*, 47(5):423–428, 1992.

[Mosavi *et al.* 2018a] Amir Mosavi, Pinar Ozturk, and Kwok-wing Chau. Flood prediction using machine learning models: Literature review. *Water*, 10(11):1536, 2018.

[Mosavi *et al.* 2018b] Amir Mosavi, Timon Rabczuk, and Annamária R. Varkonyi-Koczy. Reviewing the novel machine learning tools for materials design. In Dumitru Luca, Lucel Sirghi, and Claudiu Costin, editors, *Recent Advances in Technology Research and Education*, pages 50–58, Cham, 2018. Springer International Publishing.

[Munawar *et al.* 2022] Hafiz Suliman Munawar, Ahmed WA Hammad, and S Travis Waller. Remote sensing methods for flood prediction: A review. *Sensors*, 22(3):960, 2022.

[Nederhoff *et al.* 2023] Kees Nederhoff, Tim Leijnse, Kai Parker, Jennifer J. Thomas, Andy O'Neill, Maarten van Ormondt, Robert B. McCall, Li H. Erikson, Patrick L. Barnard, Amy C. Foxgrover, Wouter Klessens, Norberto C. Nadal-Caraballo, and Chris Massey. Tropical or extratropical cyclones: What drives the compound flood hazard, impact, and risk for the United States southeast Atlantic coast? *Natural Hazards*, 102:8779-8825, 2023.

[Nevo *et al.* 2022] Sella Nevo, Efrat Morin, Adi Gerzi Rosenthal, Asher Metzger, Chen Barshai, Dana Weitzner, Dafi Voloshin, Frederik Kratzert, Gal Elidan, Gideon Dror, et al. Flood forecasting with machine learning models in an operational framework. *Hydrology and Earth System Sciences*, 26(15):4013–4032, 2022.

[Nguyen 2022] Huu Duy Nguyen. Flood susceptibility assessment using hybrid machine learning and remote sensing in Guang Tri Province, Vietnam. *Transactions in GIS*, 26(7):2776-2801, 2022.

[Nikoobakht *et al.* 2022] Shahrzad Nikoobakht, Mohammad Azarafza, Haluk Akgün, and Reza Derakhshani. Landslide susceptibility assessment by using convolutional neural network. *Applied Sciences*, 12(12):5992, 2022.

[Nunes Correia *et al.* 1998] Francisco Nunes Correia, Filipe Castro Rego, Maria Da Grac̆a Saraiva, and Isabel Ramos. Coupling GIS with hydrologic and hydraulic flood modelling. *Water Resources Management*, 12:229–249, 1998.

[Ogato *et al.* 2020] Gemechu Shale Ogato, Amare Bantider, Ketema Abebe, and Davide Geneletti. Geographic information system (GIS)-based multicriteria analysis of flooding hazard and risk in Ambo town and its watershed, West Shoa zone, Oromia regional state, Ethiopia. *Journal of Hydrology: Regional Studies*, 27:100659, 2020.

[Olatunji *et al.* 2023] Raufu Ibrahim Olatunji, Ibrahim Mukai'la, Kafayat Olanai'yan, and Zachariah Awodele. Application of remote sensing and geographical information system (GIS) in flood vulnerability mapping: A scenario of Akure South, Nigeria. *International Journal of Environment and Geoinformatics*, 10(1):90-99, 2023.

[Pandey *et al.* 2021] Manish Pandey, Aman Arora, Alireza Arabameri, Romulus Costache, Naveen Kumar, Varun Mishra, Hoang Nguyen, Jagriti Mishra, Masood Ahsan Siddiqui, Yogesh Ray, Sangeeta Soni, and Uma Kant Shukla. Flood susceptibility modeling in a subtropical humid low-relief alluvial plain environment: Application of novel ensemble machine learning approach. *Frontiers in Earth Science*, 9:659296, 2021.

[Pham *et al.* 2020] B. T. Pham, M. Avand, S. Janizadeh, T. V. Phong, N. Al-Ansari, L. S. Ho, S. Das, H. V. Le, A. Amini, S. K. Bozchaloei, F. Jafari, and I. Prakash. GIS based hybrid computational approaches for flash flood susceptibility assessment. *Water*, 12:683, 2020.

[Phong 2023] Tran Van Phong. Modeling and mapping of flood susceptibility at Que Son district, Quang Nam province, Vietnam using CatBoost. *IOP Conference Series: Materials Science and Engineering*, 1289:012019, 2023.

[Pourali *et al.* 2016] SH Pourali, Colin Arrowsmith, Nicholas Chrisman, AA Matkan, and David Mitchell. Topography wetness index application in flood-risk-based land use planning. *Applied Spatial Analysis and Policy*, 9:39–54, 2016.

[Psomiadis *et al.* 2021] Emmanouil Psomiadis, Lefteris Tomanis, Antonis Kavvadias, Konstantinos X. Soulis, Nikos Charizopoulos, and Spyros Michas. Potential dam breach analysis and flood wave risk assessment using HEC-RAS and remote sensing data: A multicriteria approach. *Water*, 13(3):364, 2021.

[Radwan *et al.* 2019] Farid Radwan, AA Alazba, and Amr Mossad. Flood risk assessment and mapping using AHP in arid and semiarid regions. *Acta Geophysica*, 67:215–229, 2019.

[Ramírez and others 2000] Jorge A Ramírez et al. Prediction and modeling of flood hydrology and hydraulics. *Inland flood hazards: Human, riparian and aquatic communities*, page 498, 2000.

[Rasmussen and Nickisch 2010] Carl Edward Rasmussen and Hannes Nickisch. Gaussian processes for machine learning (gpml) toolbox. *The Journal of Machine Learning Research*, 11:3011–3015, 2010.

[Roy and Sarker 2016] Sadhan Kumar Roy and Subaran Chandra Sarker. Integration of remote sensing data and GIS tools for accurate mapping of flooded area of Kurigram, Bangladesh. *Journal of Geographic Information System*, 8(2):184-192, 2016.

[Sadek *et al.* 2020] Mohammed Sadek, Xuxiang Li, Eman Mostafa, Mohamed Freeshah, Ahmed Kamal, Mohamed Adou Sidi Almouctar, Fubo Zhao, and Elhadi K. Mustafa. Low-cost solutions for assessment of flash flood impacts using sentinel-1/2 data fusion and hydrologic/hydraulic modeling: Wadi el-Natrun region, Egypt. *Advances in Civil Engineering*, 2020:1039309, 2020.

[Saksena and Merwade 2015] Siddharth Saksena and Venkatesh Merwade. Incorporating the effect of DEM resolution and accuracy for improved flood inundation mapping. *Journal of Hydrology*, 530:180–194, 2015.

[Samanta *et al.* 2018] Sailesh Samanta, Dilip Kumar Pal, and Babita Palsamanta. Flood susceptibility analysis through remote sensing, GIS and frequency ratio model. *Applied Water Science*, 8:66, 2018.

[Samela *et al.* 2018] Caterina Samela, Raffaele Albano, Aurelia Sole, and Salvatore Manfreda. A GIS tool for cost-effective delineation of flood-prone areas. *Computers, Environment and Urban Systems*, 70:43–52, 2018.

[Scott *et al.* 2011] Warren Scott, Peter Frazier, and Warren Powell. The correlated knowledge gradient for simulation optimization of continuous parameters using Gaussian process regression. *SIAM Journal on Optimization*, 21(3):996–1026, 2011.

[Sensoy and Kara 2014] Huseyin Sensoy and Ömer Kara. Slope shape effect on runoff and soil erosion under natural rainfall conditions. *iForest-Biogeosciences and Forestry*, 7(2):110, 2014.

[Shafapour Tehrany *et al.* 2019] Mahyat Shafapour Tehrany, Lalit Kumar, Mustafa Neamah Jebur, and Farzin Shabani. Evaluating the application of the statistical index method in flood susceptibility mapping and its comparison with frequency ratio and logistic regression methods. *Geomatics, Natural Hazards and Risk*, 10(1):79–101, 2019.

[Shahabi *et al.* 2020] H. Shahabi, A. Shirzadi, K. Ghaderi, E. Omidvar, N. Al-Ansari, J. J. Clague, M. Geertsema, K. Khosravi, A. Amini, S. Bahrami, O. Rahmati, K. Habibi, A. Mohammadi, H. Nguyen, A. M. Melesse, B. B. Ahmad, and A. Ahmad. Flood detection and susceptibility mapping using Sentinel-1 remote sensing data and a machine learning approach: hybrid intelligence of bagging ensemble based on k-nearest neighbor classifier. *Remote Sensing*, 12:266, 2020.

[Sharif *et al.* 2014] H.O. Sharif, F.H. Al-Juaidi, A. Al-Othman, I. Al-Dousary, E. Fadda, S. Jamal-Uddeen, and A. Elhassan. Flood hazards in an urbanizing watershed in Riyadh, Saudi Arabia. *Geomatics, Natural Hazards and Risk*, 7:702–720, 2014.

[Shi *et al.* 2019] Yijun Shi, Guofang Zhai, Shutian Zhou, Yuwen Lu, Chen Wei, and Jinyang Deng. How can cities respond to flood disaster risks under multi-scenario simulation? A case study of Xiamen, China. *International Journal of Environmental Research and Public Health*, a6(4):618, 2019.

[Sivakumar and Fazel-Rastgar 2023] Venkataraman Sivakumar and Farahnaz Fazel-Rastgar. Heavy rainfall resulting from extreme weather disturbances in eastern coastal parts of South Africa: 11 April 2022. In Peiyue Li and Vetrimurugan Elumalai, editors, *Recent Advances in Environmental Sustainability*, pages 161–186, Cham, 2023. Springer International Publishing.

[Snelson and Ghahramani 2006] Edward Snelson and Zoubin Ghahramani. Sparse Gaussian processes using pseudo-inputs. *Advances in Neural Information Processing Systems*, 18:1259–1266, 2006.

[Snoek *et al.* 2012] Jasper Snoek, Hugo Larochelle, and Ryan P Adams. Practical Bayesian optimization of machine learning algorithms. *Advances in Neural Information Processing Systems*, 25, 2012.

[Sözer *et al.* 2018] Burhan Sözer, Sultan Kocaman, Hakan A. Nefeslioglu, O. Firat, and Candan Gokceoglu. Preliminary investigations on flood susceptibility mapping in Ankara (Turkey) using modified analytical hierarchy process (M-AHPp). *The International Archives of the Photogrammetry Remote Sensing and Spatial Information Sciences*, XLII-5, 2018.

[Tehrany *et al.* 2013] MS Tehrany, B Pradhan, and MN Jebur. Spatial prediction of flood susceptible areas using rule based decision tree (DT) and a novel ensemble bivariate and multivariate statistical models in GIS. *Journal of Hydrology*, 504:69–79, 2013.

[Tehrany *et al.* 2015] Mahyat Shafapour Tehrany, Biswajeet Pradhan, and Mustafa Neamah Jebur. Flood susceptibility analysis and its verification using a novel ensemble support vector machine and frequency ratio method. *Stochastic Environmental Research and Risk Assessment*, 29(4):1149–1165, 2015.

[Thanh Ngo *et al.* 2023] Huong Thi Thanh Ngo, Nguyen Duc Dam, Quynh-Anh Thi Bui, Nadhir Al-Ansari, Romulus Costache, Hang Ha, Quynh Duy Bui, Sy Hung Mai, Indra Prakash, and Binh Thai Pham. Prediction of flash flood susceptibility of hilly terrain using deep neural network: A case study of Vietnam. *Computer Modeling in Engineering & Sciences*, 135:2219-2241, 2023.

[Tsegaw *et al.* 2020] Aynalem Tassachew Tsegaw, Thomas Skaugen, Knut Alfredsen, and Tone M Muthanna. A dynamic river network method for the prediction of floods using a parsimonious rainfall-runoff model. *Hydrology Research*, 51(2):146–168, 2020.

[Tyler *et al.* 2021] Jenna Tyler, Abdul-Akeem Sadiq, Douglas S. Noonan, and Rebecca Entress. Decision making for managing community flood risks: Perspectives of United States floodplain managers. *International Journal of Disaster Risk Science*, 12:649-660, 2021.

[Ullah and Zhang 2020] Kashif Ullah and Jiquan Zhang. GIS-based flood hazard mapping using relative frequency ratio method: A case study of Panjkora River basin, eastern Hindu Kush, Pakistan. *PloS One*, 15(3):e0229153, 2020.

[Ur Tariq *et al.* 2020] Muhammad Atiq Ur Tariq, Rashid Farooq, and Nick van de Giesen. A critical review of flood risk management and the selection of suitable measures. *Applied Sciences*, 19)23):8752, 2020.

[USGS 2014] USGS, 2014.

[Verzano 2009] Kerstin Verzano. *Climate change impacts on flood related hydrological processes: Further development and application of a global scale hydrological model*. PhD thesis, University of Kassel Kassel, 2009.

[Wang *et al.* 2018a] Pengtao Wang, Liwei Zhang, Yingjie Li, Lei Jiao, Hao Wang, Junping Yan, Yihe Lü, and Bojie Fu. Spatio-temporal variations of the flood mitigation service of ecosystem under different climate scenarios in the upper reaches of Hanjiang river basin, China. *Journal of Geographical Sciences*, 28:1385–1398, 2018.

[Wang *et al.* 2018b] Yi Wang, Haoyuan Hong, Wei Chen, Shaojun Li, Dragan Pamucar, Ljubomir Gigovic, Siniša Drobnjak, Dieu Tien Bui, and Hexiang Duan. A hybrid GIS multi-criteria decision-making method for flood susceptibility mapping at Shangyou, China. *Remote Sensing*, 11(1):62, 2018.

[Wang *et al.* 2020a] Yi Wang, Zhice Fang, Haoyuan Hong, and Ling Peng. Flood susceptibility mapping using convolutional neural network frameworks. *Journal of Hydrology*, 582:124482, 2020.

[Wang *et al.* 2020b] Yi Wang, Zhice Fang, Mao Wang, Ling Peng, and Haoyuan Hong. Comparative study of landslide susceptibility mapping with different recurrent neural networks. *Computers & Geosciences*, 138:104445, 2020.

[Wedajo 2017] GK Wedajo. Lidar dem data for flood mapping and assessment; opportunities and challenges: A review. *J. Remote Sens. GIS*, 6:2015–2018, 2017.

[Wolman and Leopold 1957] Markley Gordon Wolman and Luna Bergere Leopold. *River Flood Plains: some observations on their formation*, volume 282. US Government Printing Office Washington, DC, 1957.

[Wood *et al.* 2011] Eric F. Wood, Joshua K. Roundy, Tara J. Troy, L. P. H. Beek, M. F. Bierkens, Eleanor Blyth, Ad de Roo, Petra Döll, M. B. Ek, J. S. Famiglietti, David Gochis, Nick van de Giesen, Paul R. Houser, Peter R. Jaffé, Stefan Kollet, Bernhard Lehner, Dennis P. Lettenmaier, Christa D. Peters-Lidard, Murugesu Sivapalan, Justin Sheffield, Andrew J. Wade, and Paul Whitehead. Hyperresolution global land surface modeling: Meeting a grand challenge for monitoring earth's terrestrial water. *Water Resources Research*, 47(5):W05301, 2011.

[Woodruff *et al.* 2013] Jonathan D Woodruff, Jennifer L Irish, and Suzana J Camargo. Coastal flooding by tropical cyclones and sea-level rise. *Nature*, 504(7478):44–52, 2013.

[WWA 2022] WWA. *Climate change-exacerbated rainfall causing devastating flooding in eastern South Africa*, 2022.

[Xu and Liang 2021] T. Xu and F. Liang. Machine learning for hydrologic sciences: an introductory overview. *WIREs Water*, 8:e1533, 2021.

[Yadav and Shukla 2016] Sanjay Yadav and Sanyam Shukla. Analysis of k-fold cross-validation over hold-out validation on colossal datasets for quality classification. *2016 IEEE 6th International conference on advanced computing (IACC)*, 78–83, 2016.

[Yamazaki *et al.* 2011] D. Yamazaki, S. Kanae, H. Kim, and T. Oki. A physically based description of floodplain inundation dynamics in a global river routing model. *Water Resources Research*, 47:W04501, 2011.

[Yannopoulos *et al.* 2015] Stavros Yannopoulos, Eleni Eleftheriadou, S. Mpouri, and I. S. Giannopoulou. Implementing the requirements of the European flood directive: The case of ungauged and poorly gauged watersheds. *Environmental Processes*, 2:191-207, 2015.

[Yu *et al.* 2014] Dingjun Yu, Hanli Wang, Peiqiu Chen, and Zhihua Wei. Mixed pooling for convolutional neural networks. In Duoqian Miao, Witold Pedrycz, Dominik Ślzak, Georg Peters, Qinghua Hu, and Ruizhi Wang, editors, *Rough Sets and Knowledge Technology*, pages 364–375, Cham, 2014. Springer International Publishing.

[Yu *et al.* 2015] Miaozi Yu, Lulu Zhang, Xuexuan Xu, Karl-Heinz Feger, Yanhui Wang, Wenzhao Liu, and Kai Schwärzel. Impact of land-use changes on soil hydraulic properties of Calcaric Regosols on the Loess Plateau, NW China. *Journal of Plant Nutrition and Soil Science*, 178:486–498, 2015.

[Zhao and Hendon 2009] M Zhao and HH Hendon. Representation and prediction of the Indian Ocean dipole in the Poama seasonal forecast model. *Quarterly Journal of the Royal Meteorological Society: A Journal of the Atmospheric Sciences, Applied Meteorology and Physical Oceanography*, 135(639):337–352, 2009.

[Zhou *et al.* 2021] X. Zhou, W. Ma, W. Echizenya, and D. Yamazaki. The uncertainty of flood frequency analyses in hydrodynamic model simulations. *Natural Hazards and Earth System Sciences*, 21:1071–1085, 2021.